UNIVERSITÀ DEGLI STUDI DI MILANO

Department of Biosciences

Doctoral school in Integrative Biomedical Research

Cycle XXXII

Repetitive membrane potential oscillations enhance metformin's antiproliferative effect on glioblastoma cancer stem cells

Tutor and supervisor:

Michele MAZZANTI, PhD

Author:

Ivan VERDUCI

R11794

Academic Year

Table of contents

1. Abstract

Glioblastoma (GB) is the most common brain tumor with an extremely poor prognosis. Although the current standard of care is a combination of surgery, chemo, and radiotherapy, their effectiveness remains extremely poor in terms of patients' survival. Recent publications highlight the presence of a functional subset of cells that may be responsible for tumor recurrence and resistance to conventional therapies. This subset is known as glioblastoma stem cells (GSCs). New strategies selectively targeting GSCs and/or their microenvironmental niche should be designed. The chloride intracellular channel 1 (CLIC1) represents a fruitful research topic to achieve this purpose since its functional activity was reported to be related to glioblastoma aggressiveness. CLIC1 is a peculiar protein that coexist in two isoforms. In normal condition it's mostly cytoplasmic, while in response to persistent stress translocates to the plasma membrane (tmCLIC1) determining a chloride conductance. tmCLIC1 was found to be chronically expressed in GSCs sustaining their abnormal *in vitro* proliferation rate. Given this, tmCLIC1 could be considered a promising pharmacological target to counteract glioblastoma progression.

Our laboratory has recently found tmCLIC1 protein as an extracellular target of the antidiabetic drug metformin. Despite it is well known the antineoplastic effect of metformin, the mechanism of action remains unclear. It was proposed that the binding between metformin and tmCLIC1 occurs at the level of Arg29 only when the channel is in the open state. However, metformin impairs GSCs proliferation at a millimolar range, a concentration unattainable in the brain upon metformin oral administration. The purpose is to decrease metformin's working concentration, enhancing its action on tmCLIC1. tmCLIC1 is a voltage dependent channel and its open probability increases under depolarization. We propose to enhance CLIC1-metformin interaction using repetitive membrane potential oscillations provided by field potential, optogenetics and electromagnetic field stimulations.

In this work, we confirm that metformin inhibits CLIC1 channel by binding to the R29 amino acid, which is localized inside the pore region. We show that by applying stimulation to GSCs the operative metformin concentration is reduced up to 10-fold. In addition, we demonstrate that the phenomenon is specifically confined to metformin. The combination of metformin treatment with repetitive membrane depolarizations produce an average 30% decrease of GB progression compared to metformin itself *in vitro* as well as *in vivo.* Taken together, we provide insights of a new possible therapeutic approach to face glioblastoma progression by specifically targeting GSCs.

2. Introduction

2.1 Glioblastoma: the most lethal glioma

Gliomas are the most common primary brain tumors, representing 81% of malignant brain cancers[1]. Although relatively rare, they cause significant mortality and are characterized by high malignancy and invasiveness. The yearly incidence of malignant gliomas is about 5-6 cases out of 100.000 people with a slight predominance in males. Malignant gliomas may develop at all ages, with a peak of incidence around the fifth and sixth decades of life[2].

Gliomas originate from neoplastic transformation of mature glial cells, as astrocytes, oligodendrocytes and ependymal cells, or their precursors[3]. They are divided into two main classes (low- and high-grade gliomas) on the basis of their invasiveness and progression towards more malignant forms. All gliomas are subcategorized according to World Health Organization (WHO) into grade I, II, III and IV tumors. Lower grade gliomas (I and II) are mainly benign and with a better prognosis compared to higher grade gliomas[4,5]. They are composed of cells that are histologically similar to astrocytes and oligodendrocytes. However, low-grade gliomas undergo recurrence or malignant transformation over time. Grade III and IV gliomas are more aggressive tumors, characterized by necrosis and presence of anaplastic cells that are able to hyper-proliferate and infiltrate in the brain parenchyma.

Originally, gliomas were thought to be derived solely from glial cells; however, evidence suggests that they may arise from multiple cell types with neural stem cell-like properties. These cells are at multiple stages of differentiation, from stem cell to glia, with phenotypic variations largely determined by molecular alterations in signaling pathways rather than by differences in the cell type of origin[6]. Gliomas are characterized by alterations in many different oncogenes and tumor suppressor genes. The earliest genetic modification in low-grade astrocytoma is the overexpression of the platelet- derived growth factor (PDGF) ligands and receptors that cause an autocrine growth factor stimulation loop. This altered pathway leads to the inactivation of the p53 gene that plays a key role in the cell- cycle progression. Since p53 has several functions including cell-cycle arrest, DNA repair, and apoptosis in response to genotoxic stress and DNA damages, its inactivation promotes the anaplastic transformation through genomic instability[7,8]. Uncontrolled progression of cell cycle is also due to different alterations of the retinoblastoma (pRb)- mediated cell cycle regulatory pathway.

Moreover, a characteristic of primary malignant gliomas, especially glioblastoma, is the overexpression of the epidermal growth factor (EGF) receptor that boosts a proliferative

intracellular pathway. Therefore, gliomagenesis and tumor progression are closely associated with loss of cell cycle control and increased tyrosine-kinase signaling. At a late stage of tumor progression, these pathways are mostly involved in all malignant gliomas[5,9].

Glioblastoma (GB) is the most common primary malignant brain tumor, comprising 16% of all brain and central nervous system neoplasms[10]. It is a highly heterogeneous tumor with distinctive histologic hallmarks including high cell density, intratumoral necrosis, vascular hyperplasia and invasion through brain parenchyma[11].

GB is classified by WHO as a grade IV brain tumor, the most aggressive and the fastest growing type. It is characterized by a poor prognosis and an average life expectancy of 15 months under current treatment. The rate of tumor growth is uncontrolled, to the extent that without any treatment, patients only show three months survival. The complexity of the tumor and its heterogeneity make it a great clinical challenge[12].

The current standard of care is a combination of surgery, radio- and chemotherapy, although several new approaches have been studied over the last few years. Treatment of newly diagnosed GB requires a multidisciplinary approach. Current standard therapy includes maximal safe surgical resection, followed by postoperative radiation therapy (RT) and then adjuvant chemotherapy with temozolomide (TMZ) (Temodar®), an oral alkylating agent. Extensive and complete surgical resection of GB is difficult because these tumors are frequently invasive and are often in eloquent areas of the brain, including areas that control speech, motor function, and the senses. Because of the high degree of invasiveness, radical resection of the primary tumor mass is not curative, and infiltrating tumor cells invariably remain within the surrounding brain, leading to later disease progression or recurrence[13].

Moreover, the methylation of the MGMT gene, located on chromosome 10q26, is a strong predictor of patient-related outcome of the treatment. MGMT codes for an enzyme involved in DNA repair. So, patients who have methylated (not activated) MGMT exhibit compromised DNA repair. When the MGMT enzyme is activated, it can interfere with the effects of treatment[14]. RT and alkylating chemotherapy exert their therapeutic effects by causing DNA damage and cytotoxicity and triggering apoptosis. Therefore, the presence of methylated MGMT is beneficial for patients undergoing TMZ chemotherapy and RT. For this reason, methylation of MGMT is a strong predictor of better outcomes from TMZ treatment. Concurrent with RT, TMZ is typically given at a dose of 75 mg/m2 daily for six weeks, followed by a rest period of about one month after RT is completed. When restarted, TMZ is dosed at 150 mg/m2 daily for five days for the first month (usually days 1–5 of 28). If tolerated, the dose is escalated up to 200 mg/m2 for five consecutive days per month for the

remainder of the therapy. In common practice, TMZ cycles are applied for 12–18 months. Despite maximal initial resection and multimodality therapy, about 70% of GBM patients will experience disease progression within one year of diagnosis[15], with less than 5% of patients surviving five years after diagnosis[1].

In October 2015, Optune®, the device delivering tumor-treating fields (TTFields), received approval from the U.S. Food and Drug Administration (FDA) as a treatment along-side TMZ for adults with newly diagnosed supratentorial GB, following surgery and standard-of-care treatment. Optune uses TTFields, an innovative technology that delivers low-intensity, intermediate-frequency alternating electrical fields to tumor cells. TTFields interrupt cell division, causing apoptosis, or cell death. Optune plus TMZ demonstrated superior overall survival of 20.5 months versus 15.6 months with TMZ alone[16]. Optune is indicated following histologically or radiologically confirmed recurrence in the supratentorial region of the brain after receiving chemotherapy and is intended as an alternative to standard medical therapy for GB after surgical and radiation options have been exhausted[17]. The lack of significant side effects from the device – except for scalp irritation from the electrodes – makes TTFields an attractive treatment option. In addition, patients reported improved quality-of-life indicators, such as cognitive and emotional functioning, over patients receiving chemotherapy. The use of Optune for delivery of TTFields has been included as an option in the NCCN guidelines for recurrent GB[18,19]. TTFields remains a persuasive treatment option for maintenance therapy in recurrent disease.

Despite the above-mentioned therapies, new approaches to counteract GB progression are being considered. Immune checkpoint blockade is a promising target in recurrent GB. Agents targeting programmed cell death protein 1 (PD-1) receptors, its ligand PD-L1, and cytotoxic T-lymphocyte– associated antigen 4 (CTLA4) receptors have been shown to have antitumor activity in other cancers, such as melanoma; therefore, research in patients with recurrent GB is underway. Manipulation of the blood–brain barrier to enhance targeted delivery of drug is also being studied[6].

Recent publications highlight the presence of a functional subset of stem-like cells that may be responsible for tumor recurrence and confer resistance to chemotherapy and radiotherapy. This subset is known as glioblastoma stem cells (GSCs). To successfully eradicate GB development and recurrence, new strategies selectively targeting GSCs and their microenvironmental niche should be designed[20].

2.2 Brain cancer stem cells

In 1990, Potten defined a stem cell as "undifferentiated cell capable of proliferation, self-maintenance, production of a large number of differentiated functional progeny, regenerating the tissue after injury, and flexible in the use of these options"[21]. Since then the definition of stem cells has not changed meaning. Stem cells have the potential to develop into many different types of cells in the tissue of origin (multipotency) and, at the same time, to maintain a constant pool of stem cells for the entire life of the individual (self-renewal)[21,22]. According to the canonical assessment, self-renewal is maintained by two possible ways of cellular division: asymmetrical, by which a mature progenitor and a copy of the mother cell are generated, or symmetrical, by which either two stem cells (or two mature progenitors) are generated. The self-renewal capability is crucial to guarantee the repair system to the body. Stem cells too can go through alteration of the regulatory mechanism of the self-renewal. Thus, generating cancer-initiating stem-like cells[22].

Cancer stem cells (CSCs) were first identified by John E. Dick in acute myeloid leukemia in the late 1990s and became a fruitful research topic in cancer research. Nowadays, they are recognized in several brain tumors, such as anaplastic astrocytoma, medulloblastoma, pilocytic astrocytoma, ependymoma, ganglioblastoma and glioblastoma[23-25]. As for healthy stem cells, cancer stem cells too are able to divide asymmetrically giving rise to both new malignant stem cells and/or cells belonging to the active dividing tumor mass[26]. In addition, CSCs are able to form tumors that histologically resembles the original tumors when xenotransplanted into immunodeficient mice[26]. In order to maintain self-renewal capability, cancer stem cells are cultured in serum-free conditions. By using a fine proportion of the mitogens epidermal growth factor (EGF) and fibroblast growth factor (FGF), differentiation is limited, and the culture is enriched in cancer stem cells. These mitogens act through their receptor tyrosine kinases (RTKs) and induce activation of downstream pathways such as the Phosphoinositide 3-kinase/Akt (PI3K/Akt) and Mitogen-Activated Protein Kinase (MAPK), to induce proliferation, survival and tumorigenesis. Furthermore, blocking the PI3K/Akt pathway has been shown to impair CSCs self-renewal and tumorigenesis. Finally, the knockdown of CD133 in GSCs causes downregulation of Akt phosphorylation, further highlighting the role of the PI3K/Akt pathway in GSCs biology[27].

It has been shown that Notch signaling is involved in several GB tumorigenic processes, by regulating both self-renewal and differentiation of CSCs. Originally identified in genetic screens in Drosophila as a master regulator of neurogenesis, Notch signaling plays different

roles in nervous system development, including maintenance of self-renewal and regulation of differentiation in neural and glial lineages. Upon binding to its ligands (Delta-like and Jagged), heterodimeric Notch receptors (Notch1-4) get cleaved by γ secretase in the cytoplasm, releasing the Notch intracellular domain (NICD). NICD translocates into the nucleus where it acts as co-activator for the transcription of Hes and Hey genes families. These genes are transcriptional repressors of neurogenic genes, thereby causing maintenance of stemness in activated cells[27].

At last, Transforming Growth Factor-b (TGF-b) signaling promotes GSCs self-renewal through regulation of distinct mechanisms. In particular, it was shown to act through SRY-Related HMG-Box transcription factors Sox2 and Sox4 to induce self-renewal[27].

Cancer research was previously dominated by the clonal evolution model, also known as a conventional stochastic model, a concept whereby all cells within a tumor have equal potential to propagate and maintain a tumor no matter of the presence of CSCs or other types of bulk cells[28-30]. Recently, an increasing number of studies suggest tumor as a hierarchical organization, which is the basis of the hierarchical or CSC model[31]. In the hierarchical model, only a small subset of cancer cells – CSCs – possess the ability to self-renew, differentiate, and reform a tumor. CSCs are thus considered as "roots of cancer" operating in a hierarchical fashion. The hierarchical model stands on the basis that CSCs are reliable and stable over time. As one can imagine, this "immutable" feature is subject of debates among researchers. This gave rise to a new model, known as dynamic CSC model. The dynamic model is a kind of mix of the stochastic and the hierarchical model. It suggests that the CSC phenotype is much more fluid than previously predicted and can be regulated by external signals[32,33]. In this way CSCs can self-renew and/or differentiate to non-CSCs but, importantly, the de-differentiation of non-CSCs to CSCs can also occur and thus return to the malignant growth cycle[33,34]. This latter model is consistent also with the genome instability characterizing cancer.

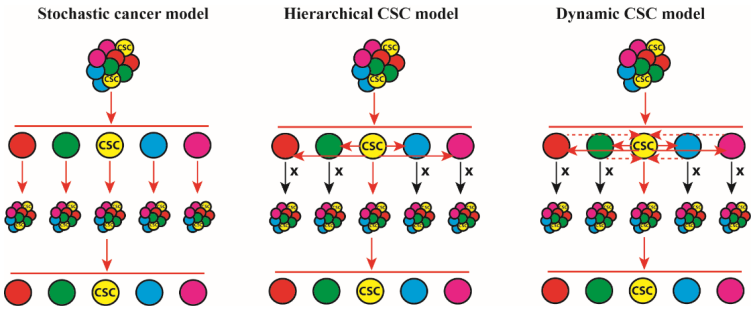

Figure 1. Stochastic and Hierarchic models.

As far as brain tumor is concerned, until the end of the 1990s, there was the belief that, in an adult brain, mature glia was the only dividing cellular population and that glioma originated solely from the neoplastic transformation of these cells. Subsequently, other cellular subtypes able to proliferate, self-renew and originate neurons and mature glia after damage were

discovered: the neural stem cells and the glial progenitors. These findings are consistent with the function of stem cells/progenitor cells existing in other parts of the body. This restricted pool of cells whose primary function is to replace any damaged adult cell types could go through genetic aberrations leading to the establishment of brain tumor stem cells[22]. These cells have been shown to be resistant to standard chemotherapy and radiotherapy, underlying their key role in tumor progression and recurrence. Therefore, GSCs knowledge is instrumental to develop new therapeutic approaches against GB. A multitude of potential cell surface markers (as CD122, CD15, integrin α6, CD44, L1CAM, and A2B5) as well as healthy stem cells markers (as SOX2, NANOG, Nestin, OCT4), have been suggested to identify cancer stem cells[35-40]. However, the presence in most tissues of stem cell populations characterized by the same markers can lead to high false-positive rate. Studying GSCs could permit to find out new specific diagnostic markers that are characteristic for the pathology.

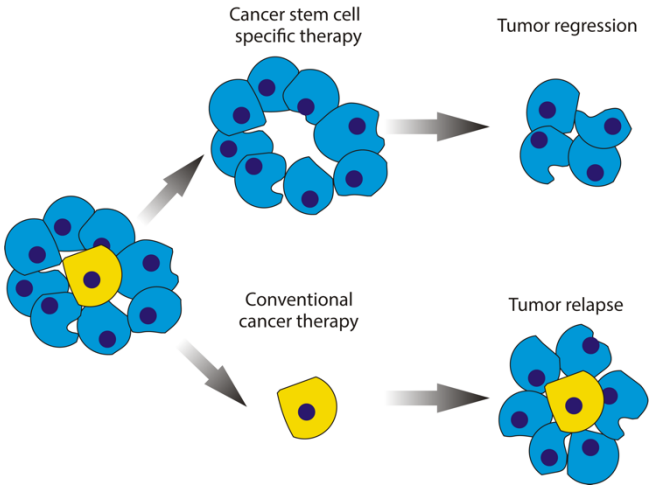

Figure 2. Comparison between a conventional antitumoral therapy and one directed against cancer stem cells.

Importantly, GSCs are usually not targeted by classical approaches like surgery or chemotherapy, which are normally directed against high proliferating cells (Figure 2). GSCs are believed to be resistant to chemotherapy through several distinct mechanisms. One mechanism involves the active transport of chemotherapeutic agents to the extracellular space via ABC-type transporters on the cell surface. Secondary, chemo-resistance relies in the cell cycle profiles of GSCs. Most chemotherapeutic agents target actively cycling cells. However, GSCs are slow-cycling cells, thereby resisting such therapies[40]. In addition, GSCs are also radiation resistant. Notch and TGF-b signaling pathways increase DNA repair capacity of GSCs, making them less susceptible to radiation-induced apoptosis[40]. GSCs can be isolated and expanded in serum-free medium enriched with Epidermal Growth Factor (EGF) and Fibroblast Growth Factor 2 (FGF2). In this selective medium partially differentiated cell are negatively selected, while cancer stem cells rapidly grow in response to mitogen stimuli, forming neurospheres. Neurospheres formation has been recognized as an identifying sign to assess GSCs presence[25]. These aggregates grow in suspension and can be dissociated and plated in order to generate secondary spheres. Upon

mitogen removal, cells differentiate into the heterogenic cellular population that compose the tumor. In this way, GSCs can be cultured and studied *in vitro*.

2.3 Chloride Intracellular Channel 1 (CLIC1)

2.3.1 CLIC1 biophysical properties

During the last twenty years an important role for ion channels in tumors has been defined and the scientific community began to focus its effort into the study of them as putative targets in oncology.

Ion channel expression is often altered in tumor cells. This may be due to the genetic alteration occurring during the transition from the homeostatic state towards the allostatic state in which tumor relies. The alteration, for this reason, could reflect also to ion channel expression or function[41]. The implication of ionic permeabilities has been confirmed in many aspects of cancer pathology, including uncontrolled growth, decreased apoptosis, disorganized angiogenesis, aggressive migration, invasion and metastasis[42]. In particular, in recent times chloride channels have become a topic of study for the regulation of tumor development and progression[43].

Chloride channels exerts different functions in every stage of cellular physiology, from cellular maturation to adult cells. They are involved in ion homeostasis, fluid transportation, regulation of cell volume, cytoskeletal rearrangement, cellular motility, excitability. Several of the just mentioned functions play an important role in tumor biology[44,45]. In addition, it has been found that some Cl- channels show cell cycle-dependent expression[46]. Recently, it has been also demonstrated that chloride fluxes are needed during the G1/S phase transition[47] of GSCs.

Recently, the Chloride Intracellular Channel 1 (CLIC1) became a fruitful research topic as its functional expression was found to be related to the progression and development of several solid tumors[47-52], including glioblastoma. CLIC1 is a member of

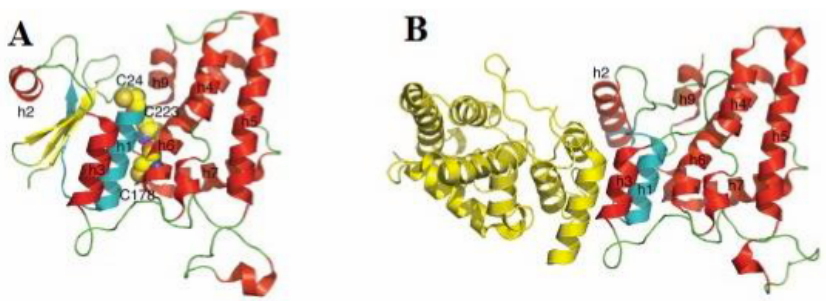

Figure 3. Structure of CLIC1 protein. A) The structure of soluble, reduced monomeric form colored by secondary structure (helices in red, strands in yellow, loops in green). The putative TM region is shown in cyan (residues 25–46). B) The crystal structu

the CLICs family which includes 6 different protein named from CLIC1 to CLIC6. CLICs proteins are highly conserved in vertebrates and several proteins resembling their structure were found also in metazoans[53]. CLICs proteins have both soluble and integral membrane forms, a peculiarity that distinguishes them from most ion channels. In particular, CLIC1 plasma membrane insertion is modulated by different stress stimuli like cellular oxidation and pH alkalization[54-56]. Persistent oxidation and cytoplasm alkalization are hallmarks of cancer cells[57,58], resulting in the mostly chronic accumulation of CLIC1 protein in the plasma membrane of these cells[59]. The peculiar feature to colonize specifically the plasma membrane of cancer cells makes CLIC1 an interesting pharmacological target. Transmembrane CLIC1 (tmCLIC1) works as a chloride-selective ion channel[23,60]. The structure of the soluble configuration of CLIC1 has been determined in two crystal forms at 1.4 A° and 1.75 A° resolution (Figure 3A)[61]. Its structure indicates that it belongs to the Glutathione S- transferases (GST) superfamily of proteins. The N-domain (residues 1–90) has a thioredoxin fold that consists of a four-stranded mixed b-sheet plus three α-helices, with a well conserved glutaredoxin-like site for covalent interaction with glutathione GSH. GSH appears to be covalently attached to Cys-24, indicating that CLIC1 is likely to be regulated by redox processes. The C-terminal domain is helical, closely resembling the Ω class GST[61].

On the contrary, the crystal structure of the transmembrane form is not yet solved. It has been suggested that the region between Cys-24 and Val-46 of CLIC1 sequence may constitute a transmembrane helix with Arg-29 and Lys-37 lining one face of the helix[61]. The modality by which CLIC1 protein forms a transmembrane chloride ion channel remains speculative. In the transition from the hydrophilic soluble form to the membrane-associated protein, many structural rearrangements occur involving the N-domain of CLIC1 and disrupting the glutathione-binding site[61]. In oxidizing conditions, GSH detaches from its binding site causing a reversible transition from a monomeric to a non-covalent dimeric state due to the formation of an intramolecular disulphide bond (Cys-24–Cys-59) (Figure 3B). This state may represent the membrane docking form of CLIC1. Probably, an additional structural change is then required to integrate the transmembrane domain into the membrane[53]. In addition, a further oligomerization step is likely to be required to form the active ion channel (Figure 4). However, it is still unknown how and how many CLIC1 monomers subunits form the functionally active channel once inserted into the membrane. Different hypotheses propose the association of several subunits, ranging from two to eight oligomers to constitute one single ion channel. Anyway, single CLIC1 proteins were proven to act as ion channels

too[23,53,56,60-62]. When inserted into the membrane, CLIC1 exposes its N-domain to the extracellular side, leaving the C-domain facing the cytoplasm.

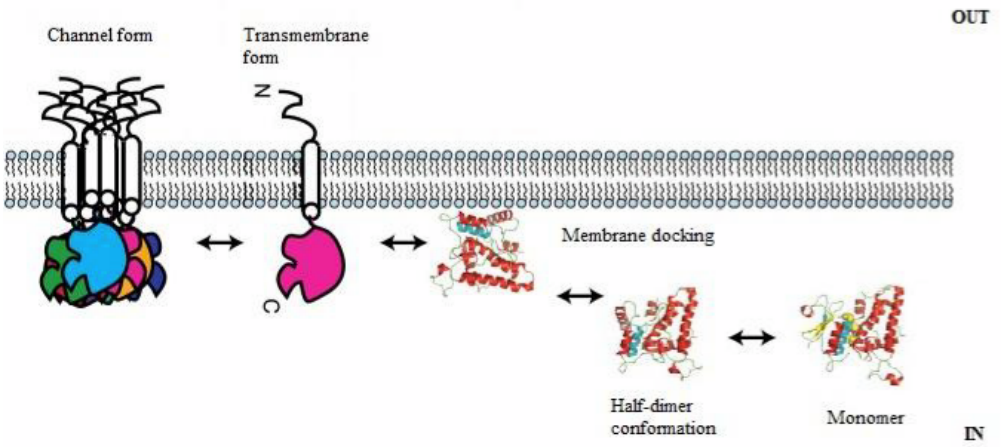

Figure 4. A proposed model for the transition between the soluble form of CLIC1 and the integral membrane ion channel form,

As mentioned above the intracellular pH also plays a role in the regulation of CLIC1 membrane insertion. It has been demonstrated that in artificial lipid bilayers CLIC1 channel activity is dependent on proton concentration, being minimal at pH 7, and reaching the maximum rate at ± 2 pH units[63]. It has been shown also that two histidine residues are fundamental for this pH-dependency of tmCLIC1 activity[64]. In physiological conditions, when the membrane voltage of the cells is more positive than the chloride reversal potential, CLIC1 mediates an outward current (inward chloride) that rectifies at +40/+50 mV[65]. It has also been shown that CLIC1 is voltage-dependent[56]. Patch clamp experiments in cell attached configuration displayed that CLIC1 open probability increases linearly with the membrane potential depolarization, going from -40 mV to +40 mV[66]. CLIC1-mediated current is completely and reversely blocked by the inhibitor IAA94 (Indanyloxyacetic acid 94), while the most common chloride channels inhibitor DIDS (4,4'- Diisothiocyano-2,2'-stilbenedisulfonic acid) does not have any effect on CLIC1 conductance[67]. Recently, the antidiabetic drug metformin has been proposed as a selective blocker of CLIC1 channel activity[68].

2.3.2 CLIC1 role in tumor biology

CLIC1 protein levels are reportedly increased in human breast ductal carcinoma[69], gastric cancer[70], gallbladder metastasis[71], colorectal cancer[72], nasopharyngeal carcinoma[73], ovarian cancer[74] hepatocellular carcinoma[75], and high- grade gliomas[76]. In 2004, Huang proposed that the overexpression of CLIC1 in liver cancer might alter cell division rate and/or antiapoptotic

signaling, resulting in cellular transformation[77]. In mouse hepatocarcinoma cells, CLIC1 is overexpressed and contributes in promoting migration and invasion[77]. Moreover, two recent studies suggested that CLIC1 expression is related to the metastatic potential of colon cancer cells[78,79]. The role of CLIC1 as an ion channel has been analyzed by suppressing its current with IAA94 or by knocking-down CLIC1 expression. In both cases, migration and invasion of colon cancer cells were inhibited. This effect was attributed to the drop of RVD (regulatory volume decrease) capacity.

As previously said, oxidation is one of the main stimuli responsible for CLIC1 insertion in the cell membrane. Reactive Oxygen Species (ROS) normally act as second messengers in many cellular processes involving cell replication and migration – two primary features of tumor development. In physiological conditions ROS production is balanced by the release of antioxidant molecules, allowing a fine cellular control of the mechanisms requiring ROS[80]. When the ratio between ROS production and antioxidants is unbalanced towards ROS, a microenvironment encouraging the development of several pathological states is established. The most known pathological states related to ROS overproduction are degenerative processes, inflammation, and cancer[57,81,82]. It is established that changes in ROS levels are fundamental for the progression of the cell cycle[83]. CLIC1 and ROS crosstalk can possibly be involved in tumors development: the hypothesis is that ROS increase could regulate CLIC1 membrane insertion or, conversely, the boost of CLIC1 chloride current could sustain ROS production necessary for the progression through the cell cycle[47]. Increased CLIC1 expression and activity could lead to an increase of proliferation, migration, and invasiveness of tumor cells.

An important role of CLIC1 as a chloride channel is specifically associated with the development of glioblastoma, the most aggressive and frequent brain tumor. As said above, in these tumors the core of malignant cells is generated by a rare fraction of self-renewing, multipotent cancer stem cells responsible for tumor origin, progression, and recurrence. CLIC1 is highly expressed in glioblastoma and both mRNA and protein levels were found to be increased in high grade brain tumors in comparison to low grade ones or healthy brain tissue[59,76]. The silencing of CLIC1 protein is able to impair both proliferation and self-renewal properties *in vitro*. In addition, the injection into the mice brain of CLIC1-silenced GSCs was able to reduce the progression of the tumor *in vivo* compared to non-silenced GSCs[59]. To address the ability of tmCLIC1 in sustaining the high proliferation rate of the tumor, Setti and co-workers[59] showed not that the IAA94-sensitive membrane current was drastically reduced

in CLIC1 silenced human GSCs. In addition, they proved also that GSC neurospheres treated for 48 hours with NH_2-CLIC1 antibody – as a channel blocker – compromised cancer development in injected mice. Electrophysiological experiments on GSCs isolated from different patients showed that CLIC1-mediated current is related with glioblastoma aggressiveness[48]. These data suggest that the presence of CLIC1 in the membrane could be assumed to be a feature of cells having undergone – or undergoing – transition to a hyperactivated state. It should be pointed out that a transient insertion to the plasma membrane could be a feature required for the physiology of healthy cells. On the contrary, only when the phenomenon becomes irreversible – with a chronic expression of tmCLIC1 – one can consider CLIC1 functional activity instrumental to the development of the pathological state. Given the exclusive feature to enrich the plasma membrane of GSCs, tmCLIC1 could be considered a privileged therapeutic target in glioblastoma.

Recent studies from our laboratory strongly support this hypothesis showing that CLIC1 activity can be pharmacologically regulated, discriminating among GSCs and normal stem cells. The inhibitory effect of IAA94, NH_2-CLIC1 antibody, and metformin on proliferation was shown to be evident in GSC-enriched cultures but not in differentiated GSCs in which CLIC1 localization was mainly confined to the cytosol[68]. The same insensitivity to the above-mentioned treatments and CLIC1 cytosolic localization were also evident in umbilical cord-derived mesenchymal stem cells (uc-MSCs) used as a negative control. In addition, it has been also demonstrated that the inhibition of CLIC1 current leads to significant accumulation of GSCs in G1 phase of the cell cycle. In particular, Peretti and colleagues have shown that CLIC1 takes part in the regulation of the transition from G1 to S phase of the cell cycle. tmCLIC1 is functionally expressed in the membrane in accordance with the G1/S transition which occurs from 4 to 10 hours after the synchronization in G1 phase. CLIC1 mediated current was found to increase after 4 hours from the G1 synchronization, reaching a peak at 8 hours. In the time interval following the G1/S transition (12 hours) the current was found to be decreased[47].

All these reports propose CLIC1 as a possible tumor marker. It is known that oxidative level oscillations in the intracellular compartment contribute to the regulation of cell cycle progression through the different phases[80] and that alterations in the oxidative basal level of the cells are typical conditions for many tumorigenic processes. It is not surprising that the activity of CLIC1 channel – induced by oxidation – is higher in tumor cells. In this scenario, cancer cells could take advantage of a feed-forward mechanisms between CLIC1 channel activity and ROS production. The fact that, in prolonged stress conditions, CLIC1 membrane

expression becomes chronic makes the channel a very interesting potential pharmacological target, making possible to hit specifically cancer cells. This would limit the off-targets toxicity of the conventional antitumor therapies.

2.4 Metformin in cancer treatment

According to national and international guidelines, metformin is the recommended first-line oral therapy for the treatment of type 2 diabetes (T2D)[84-86]. This is due to several factors, including the impressive safety record of the drug, having been in clinical use for over 50 years, and the fact that metformin treatment is weight neutral. In addition, there are likely to be other beneficial effects, including a reduction in cardiovascular disease and mortality compared with non-intensive treatment[87] and a possible reduction in cancer incidence, which will be later detailed. As metformin was discovered before the era of modern target-based drug discovery, the molecular details of its mechanism of action were not established before it was used clinically, and these continue to be an area of vigorous research.

The history of biguanides can be traced from the use of Galega officinalis (Goat's Rue or French Lilac) as a treatment for diabetes in medieval Europe[88]. Guanidine, the active component of galega, was used to synthesize several antidiabetic compounds in the 1920s; metformin and phenformin, the two main biguanides, were introduced in the late 1950s[89]. Phenformin was withdrawn from clinical use in many countries in the late 1970s when an association with lactic acidosis was recognized[90]. Lactic acidosis is not a major problem with metformin, and metformin is now used in more than 90 countries.

Chemically, biguanides such as metformin are composed of two guanidine groups joined together with the loss of ammonia. Anti-hyperglycemic effects have been observed in response to many, but not all, guanidine-containing compounds. Metformin has an absolute oral bioavailability of 40-60%, and gastrointestinal absorption is apparently complete within 6 hours of ingestion. An inverse relationship was observed between the dose ingested and the relative absorption with therapeutic doses ranging from 05 to 2.5g, suggesting the involvement of an active, saturable absorption process[91].

To date, there is not a well-defined mechanism of action of metformin. The large amount of drug required (up to 2.5 g per day) for therapeutic effects led early investigators to hypothesize that it might not depend on a conventional single/specific protein target[92]. Different works found that biguanides reduce mitochondrial oxygen consumption, suggesting this organelle as an important site of action of guanidine-based agents[93-95]. The preferential action of metformin

would occur in hepatocytes and it is due to the predominant expression of the organic cation transporter 1 (OCT1), which has been shown to facilitate cellular uptake of metformin[96]. Deletion of the OCT1 gene in mouse dramatically reduces metformin uptake in hepatocytes and human individuals carrying polymorphisms of the gene (SLC22A1) display an impaired effect of metformin in lowering blood glucose levels[96]. Although the exact mechanism(s) by which metformin acts at the molecular level remain(s) unknown, it has been shown that the drug inhibits mitochondrial respiratory-chain specifically at the complex 1 level without affecting any other steps of the mitochondrial machinery[97]. This unique property of the drug induces a decrease in NADH oxidation, proton pumping across the inner mitochondrial membrane and oxygen consumption rate, leading to lowering of the proton gradient and ultimately to a reduction in proton-driven synthesis of ATP from ADP and inorganic phosphate (Pi). Metformin was observed to activate also the AMPK pathway which results in shutting down the ATP-consuming synthetic pathways and restoring energy balance[98]. Metformin most likely does not directly activate AMPK as the drug does not influence the phosphorylation of AMPK. The activation of AMPK by metformin in the liver, and probably in other tissues, is the direct consequence of a transient reduction in cellular energy. The demonstration that the AMPK is not one of the direct targets of metformin was recently strengthened by showing that the metabolic effect of the drug is preserved in liver-specific AMPK-deficient mice[99].

Although the idea that anti-diabetic biguanides might be promising as anticancer drugs dates back to the early 1970s, metformin has attracted increasing attention over the past few years for its repositioning in oncology. Drug repositioning represents a smart way to exploit new molecular targets of a known drug or target promiscuity among diverse diseases. Epidemiologic studies in patients with T2D highlighted a positive association between the chronic intake of metformin and a decrease in the incidence of several types of cancer[100]. Metformin effects have been evaluated in preclinical studies on different solid tumor models, such as breast, lung, prostate and glioblastoma. Several papers reported the selective antitumoral activity of metformin on cancer stem cells isolated from different cancers. Cancer stem cells have been reported to be highly dependent on glycolysis[101] for growth and survival and this would not explain their sensitivity to metformin – which it was found to targets oxidative phosphorylation (OXPHOS) pathway to produce energy. In addition, glioblastoma stem cells have been reported to rely on both glycolysis and OXPHOS energetic pathways[102,103]. For this reason, the hypothetic blockade of one metabolic way should not impair cellular proliferation since it would be compensated by the other pathway.

Recently, Gritti and colleagues[68] demonstrated that metformin effects on GB cells are directed *also* to an "extracellular" pathway which involves CLIC1 blockage. In particular, metformin would act on Arg29 located inside the channel pore; on the contrary the IAA94 binding site was identified on the external Cys24[61]. Electrophysiology experiments show that metformin perfusion decreases the whole-cell current that is not further reduced by the perfusion of the specific CLIC1 inhibitor IAA94. Current/voltage (I/V) relationships show that the current amplitudes, at different membrane potentials, are superimposed, suggesting that the two drugs converge on the same molecular target. Metformin treatment causes GSCs arrest in the G1 phase of the cell cycle, while the proliferation of differentiated GSCs and MSCs was unaffected by metformin treatment. However, the presence of an alternative "metabolic" way is not clear. These results suggest the preferential interaction between metformin and tmCLIC1 in glioblastoma stem cells.

2.5 Stimulation: inducing membrane potential oscillations (MPOs)

Brain and nervous system stimulation techniques have generated renewed interest in recent decades as promising tools to explore human neuronal functions and to treat neurological disorders.

Thanks to their low cost, non-invasiveness and painless behaviors, these techniques have driven interest in potential clinical application[104,105]. Currently, at least 13 forms of brain stimulation are undergoing development and evaluation as interventions for neurological and psychiatric disorders. Stimulation techniques are a unique form of treatment distinctly different from pharmacology, psychotherapy, or physical therapy. They are based on two different kinds of stimuli: direct current electric field (DCEF) stimulation and electromagnetic field (EMF) stimulation.

2.5.1 Direct current electric field (DCEF) stimulation

In DCEF techniques, cells are stimulated by applying a weak current to the environment using metal electrodes connected to a direct current (DC) power supply. Both anode and cathode electrodes can be used to stimulate the cells. DCEF is recognized to influence excitability of neuronal cells. Moreover, it also influences phenotypic and functional parameters such as the morphology, orientation, migration, growth, and metabolism of several mammalian cells, including neurons, glial cells and neural stem cells[106]. The relationship

between the stimulation and responses of cells is not only dependent on the electrode type, but also on the length and strength of the electric field applied. Moreover, it depends on the orientation of the cells in the DCEF. However, little is known about the mechanisms of action that govern these effects.

Among all existing brain stimulation therapies, transcranial direct current stimulation (tDCS) is the main technique that uses DCEF to stimulate cells. Current is conveyed via electrodes positioned on the scalp of the patient; the stimulation electrode above the region of interest and the reference electrode placed elsewhere on the body. Approximately 50% of the applied current enters in the brain through the skull.

The promising clinical outcomes obtained in various conditions coupled with the evidences that this approach is safe, well tolerated, inexpensive and simple to administer has catalyzed the popularity of tDCS and its potential use in routine clinical practice[104]. To date, it has been tested to treat aspects of stroke[107], Alzheimer's disease[108], Parkinson's disease[109] schizophrenia[110] and depression[111]. Despite much evidence supporting the efficacy of tDCS as a treatment option for these conditions, there are few Phase III clinical trials currently taking place. All previous trials have been conducted to confirm safety and targeted endpoints in small cohorts. Further studies will thus be critical to confirm its true effectiveness for specific disorders[104].

In order to better understand the molecular mechanism of DCEF-induced effects, studies focused on neuronal membranes and their behavior with changing membrane potentials are needed[112]. The plasma membrane lipid bilayer of nerve or glial cells is almost impermeable to ions and it acts as an insulator, separating cytoplasm from extracellular fluid. Ions cross the membrane only through specialized proteins such as ion channels. Transmembrane crossing of ions is essential for establishing the resting membrane potential. Ion channels recognize, select, and conduct specific ions, and open and close in response to specific electrical, mechanical or chemical signals.

Many different signals depend on rapid changes in the electrical potential difference across cell membranes. DCEF presumably targets cell signaling by influencing ion channels or by modifying electrical gradients. This influences the electrical balance of charges inside and outside of the membrane, shifting the membrane potential[112]. It has been proposed that DCEF affects primarily voltage-gated channels that are mostly closed when the membrane is at resting potential. Their probability of opening is regulated by changes in membrane potential and it is associated with the reorientation of a set of fixed charges (or dipoles) in the transmembrane domain. Thus, they may become involved in DCEF effects after altering the resting membrane potential[112]. The rate of transition between open and closed state of a voltage-gated channel

depends strongly on the membrane potential, with time scales varying from several microseconds to a minute. Furthermore, many but not all voltage-gated channels can enter in a refractory state after activation[112]. In general, anodal direct current stimulation (aDCS) results in a subthreshold depolarization that can increase the voltage-dependent ion channels opening. On the contrary, cathodal direct current stimulation (cDCS) leads to a subthreshold hyperpolarization that inactivates these channels[104].

In neuronal cells, electrical excitability derived from voltage-dependent ion channels is a fundamental biological phenomenon that is responsible for initiation of action potentials and graded membrane potential changes in response to synaptic input and other physiological stimuli. Thus, anodal stimulation leads to an increase in neuronal excitability, while cathodal stimulation leads to neuronal inhibition. However, DCS does not trigger action potentials but most likely affects the spike timing of individual neurons. Moreover, DCS can modify neuronal excitability by modulating neurotransmitter release-probability either through effects on action potential propagation or vesicle release probability[105].

The hypothesis that membrane potential changes are involved in the effects of DCEF has been tested by blocking voltage-dependent Na^{+} channels and Ca^{++} channels with carbamazepine (CBZ)[113] and flunarizine (FLU) respectively, during tDCS experiments[114]. Blocking voltage-dependent sodium channels completely eliminates the excitability enhancement that is observed during anodal stimulation, while blocking calcium channels diminishes it. On the other hand, the reduction in excitability caused by cDCS is not changed by voltage-gated ion channel blockade. This is probably due to the cathodal hyperpolarization effect that inactivates the respective sodium and calcium channels. Thus, administration blockers CBZ and FLU do not have any effect.

Another DCEF effect is the increase of intracellular Ca^{++} concentration. Studies on animals indicate that aDCS can open voltage-sensitive Ca^{++} channels. Furthermore, higher intensity and longer duration aDCS has a greater effect on Ca^{++} accumulation[105]. In neuronal cells, the increase of both intracellular calcium level and cAMP concentration leads to long-term modulation of neuronal activity. This is due to protein synthesis-dependent pathway controlled by these two elements. Moreover, intracellular Ca^{++} concentration is involved in many biological processes such as metabolism, growth and migration in different cell types. Different data suggest that changes in orientation and speed of cell migration are partially due to the intracellular Ca^{++} and its localized shift inside the cytoplasm. Linked to this is the asymmetrical delocalization of receptors within the membrane brought about by DCEF[104]. In many cell types, different membrane receptors move and accumulate at one end of the

electrical field to cause an electrotaxis. In glial cells, greater intracellular Ca^{++} concentration also leads to increased energy metabolism[104,114].

DCEF techniques appear to enhance adaptive patterns of brain activity, suppress maladaptive forms of activity and restore equilibrium in imbalanced neural networks. Moreover, they are able to modulate cell migration and proliferation in many different tissues. Therefore, DCS has been examined as a potential therapeutic intervention in multiple clinical disorders, including nerve tissue lesions, stroke, Alzheimer's disease and cancer.

Nerve tissue lesions DCEF is able to support the regeneration of nerve tissue by affecting different phenomena. Firstly, DCEF has been shown to reduce apoptotic processes by both decreasing caspase-3 activity and upregulating many anti-apoptotic proteins[104]. Secondary, DCEF increases the number of proliferating cells and neuronal stem cells within the stimulated region. In addition, weak DCEF applied to neurons can increase the neurite growth and modulate their orientation. At last, DCEF can accelerate the migration of endothelial cells to the stimulated area. Cultured endothelial cells secrete higher levels of vascular endothelial growth factor, nitric oxide and interleukin-8 that are all critical players in anagenesis. All these effects lead to a better recovery of the damaged tissue[104].

DCEF shows immune responses and has significant effects on the inflammatory response both in the central and peripheral nervous systems. *In vitro*, DCEF can accelerate and polarize the migration of several types of peripheral immune cells, including lymphocytes, monocytes, neutrophils and macrophages. Moreover, cultured astrocytic cell lines align perpendicularly to the EF and have increased energy metabolism when stimulated by DCEF. It has been demonstrated that high-voltage EFs may provoke an inflammatory response in quiescent BV2 microglial cells[114]. At the same time, it has been shown that DCEF is able to reduce inflammation in nerve tissues affected by ischemic stroke by decreasing chronic activation of microglia cells and necrosis factor-α secretion. These data suggest that DCEF can induce both anti-inflammatory and pro-inflammatory effects[104].

Stroke

Stroke is a leading cause of disability in United States. Restitution of post-stroke motor function is frequently incomplete, with the majority of stroke patients unable to perform professional duties and activities of daily living. The better understanding of plastic changes or brain remodeling following stroke have contributed to the development of novel targeted therapies. Several studies show the influence of maladaptive plasticity in sustaining behavioral deficits in stroke. Neuroimaging analyses of stoke subjects have noted critical increase in cortical excitability in the intact primary motor cortex of the unaffected hemisphere. In

addition, the level of cortical excitability of the intact hemisphere correlates with the level of inhibition in the affected hemisphere. tDCS can be used in order to modulate excitability of unaffected region and, on the other hand, facilitatory stimulation may be provided to the affected hemisphere to enhance beneficial plasticity and to improve motor outcomes[107]. Besides motor function in stroke, language recovery has also been explored with tDCS. Anodal tDCS over perilesional areas improves language function, but the effect was found to persist over time only when tDCS was coupled with language training[107].

Alzheimer's disease

Neurodegenerative cognitive disorders, also referred to as dementias, affect more than 46 million people worldwide. To date, there are no interventions to prevent, cure, or even slow down these disorders. tDCS has been tested for its effects in patients with neurodegenerative disorders, especially patients with Alzheimer's dementia. In one study, repetitive tDCS with ten 20-minutes sessions delivered daily over 2 weeks to the frontal cortex of rat models of AD has been shown to reduce spatial learning and memory deficits. It also resulted in histological changes suggestive a protective effect of tDCS against Ab induced neurotoxicity. In Ferruci et al.[115], ten participants with AD received three 15-minutes tDCS sessions in a random order and 1 week apart: anodal tDCS, cathodal tDCS, and sham tDCS. This study has shown that anodal tDCS can improve word recognition and discrimination assessed 30 minutes after stimulation. Furthermore, in Boggio et al.[108] ten 70–92 years old patients with AD received two 30-minutes sessions of unilateral anodal tDCS. Anodal tDCS improved performance on a visual recognition memory task assessed during stimulation. At last, Penolazzi et al[116] treated one AD patient (age 60), with one course of anodal tDCS, daily for 20 minutes for 10 days. Each tDCS was followed by 45 minutes of cognitive training. Following the course, the patient experienced improvement in global cognitive function and it persisted for 1 month. Taken together, these studies suggested both a positive effect of tDCS in AD but also a persistence of these effects several weeks following the end of the intervention. The mechanism underlying any pro-cognitive effect of tDCS in patients with AD is largely unknown.

Cancer

As expressed above, ion channels and transporters undergo a fine modulation in the expression and/or activity. Their correct function is highly required for the regulation and maintenance of membrane potential (Vm). Membrane potential (Vm) is a key biophysical signal in non-excitable cells, modulating important cellular activities, such as proliferation and differentiation[117]. Cancer cells show distinct bioelectrical properties, above all a depolarized Vm that favors cell proliferation[117]. Emerging data also raise the hypothesis that membrane

potential influences the migration of tumor cells. Consequently, this could impact on tumor growth. It has been shown that low-frequency, low-intensity, alternating current (AC) directly affects cell proliferation without a significant deleterious contribution to cell survival by directly modifying ion fluxes. Brain stimulators currently used for the treatment of neurological disorders may thus also be used for the treatment of brain (or other) tumors.

2.5.2 Transcranial magnetic stimulation (TMS)

TMS was introduced nearly 40 years ago and has developed as a sophisticated tool for neuroscience research. TMS is a non-invasive and effective methodology with potential diagnostic and therapeutic uses.

TMS, as currently used, was introduced by Anthony Barker (University of Sheffield, UK) in 1985[118]. TMS provided, for the first time, a non-invasive, safe, and, unlike transcranial electrical stimulation (TES), painless[119] method of activating the human motor cortex and assessing the integrity of the central motor pathways (Figure 5). Since its introduction, the use of TMS in clinical neurophysiology, neurology, neuroscience, and psychiatry has spread widely, mostly in research applications, but with increasing usage in clinics[120].

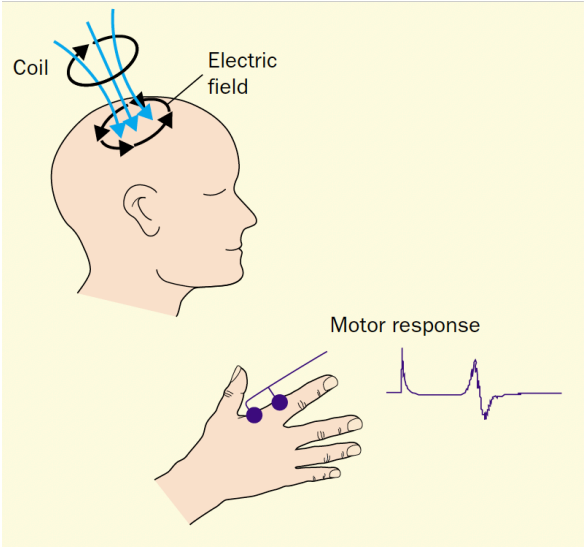

Figure 5. Principle of TMS: the current flowing briefly in the coil generates a changing magnetic field that induces an electric current in the tissue, in the opposite direction. In case of proper intensity of the stimulus, a motor response is generated.

TMS is based on the principle of electromagnetic induction, as discovered by Michael Faraday in 1838. If a pulse of current passing through a coil placed over a person's head has sufficient strength and short enough duration, rapidly changing magnetic pulses are generated that penetrate scalp and skull to reach the brain with negligible attenuation. These pulses induce a secondary ionic current in the brain. The site of stimulation of a nerve fiber is the point along its length at which sufficient current to cause depolarization passes through its membrane. The capacity of TMS to depolarize neurons depends on the "activating function", which causes transmembrane current to flow and can be described mathematically as the spatial derivative of the electric field along the nerve. Thus, stimulation will take place at the point where the spatial derivative of induced electric field is maximum.

During TMS, the operator can control the intensity of the stimuli by changing the intensity of current flowing in the coil, thus changing the magnitude of the induced magnetic field and of the secondarily induced electrical field. The focus of the magnetic field depends on the shape of the stimulation coil. Two different shapes of coils are most commonly used: a figure-of-eight shaped coil and a circular coil. The former provides a more focal stimulation, allowing fairly detailed mapping of cortical representation. The latter induces a more widely distributed electric field allowing for bihemispheric stimulation, which is particularly desirable in the study of central motor conduction times[121]. In addition to its intensity and focus, operators can also control the frequency of the delivered stimuli, which will critically determine the effects of TMS on the targeted region of the brain. Of course, the location of a stimulation coil is also dependent on the operator: different brain regions can be stimulated to evoke different behavioral effects. Anatomically precise localization of stimulation can be achieved by use of a frameless stereotactic system[122-124].

When TMS is applied to the motor cortex at appropriate stimulation intensity, motor evoked potentials (MEPs) can be recorded from contralateral extremity muscles. Motor threshold refers to the lowest TMS intensity necessary to evoke MEPs in the target muscle when single-pulse stimuli are applied to the motor cortex[125]. Motor threshold is believed to reflect membrane excitability of corticospinal neurons and interneurons projecting onto these neurons in the motor cortex, as well as the excitability of motor neurons in the spinal cord, neuromuscular junctions and muscle[126]. Ultimately, motor threshold provides insights into the efficacy of a chain of synapses from presynaptic cortical neurons to muscles. Motor threshold is often increased in diseases that can affect the corticospinal tract, such as multiple sclerosis, stroke, and brain or spinal-cord injury[127-130]. A train of TMS pulses of the same intensity applied to a single brain area at a given frequency that can range from one stimulus per second to 20 or more is known as repetitive TMS (rTMS). The higher the stimulation frequency and intensity, the greater is the disruption of cortical function during the train of stimulation.

However, after such immediate effects during the TMS train itself, a train of repetitive stimulation can also induce a modulation of cortical excitability. This effect may range from inhibition to facilitation, depending on the stimulation variables (particularly frequency of stimulation[131-133]. Lower frequencies of rTMS, in the 1 Hz range, can suppress excitability of the motor cortex[134] while 20 Hz stimulation trains seem to lead to a temporary increase in cortical excitability[135,136]. While these effects vary among individuals[135-137], the effect of low

frequency rTMS is robust and long lasting[134,135] and can be applied to the motor cortex and to other cortical regions to study brain–behavior relations.

Several studies in human beings that combine rTMS and functional neuroimaging techniques (eg, MRI and PET) have detected suppressed or increased cerebral blood flow and metabolism in the stimulated area after slow (1 Hz) or rapid (10–20 Hz) rTMS of the motor cortex, respectively[132,138,139]. Similar phenomena have been observed after TMS to other cortical areas, such as frontal eye field and dorsolateral prefrontal cortex[140,141]. However, even when TMS is delivered at low intensity (below the motor threshold intensity), spinal reafferences accounting for or contributing to the detected neuroimaging results cannot be ruled out. Nevertheless, the combination of TMS and neuroimaging can be most helpful in the investigation of functional connectivity between regions in the living human brain[139,140,142]. Furthermore, the combination of rTMS with tracer PET[143] or magnetic resonance spectroscopy may become a novel tool to investigate neurochemical functional anatomy in health and disease.

The mechanisms of the modulation of cortical excitability beyond the duration of the rTMS train are still unclear. Long-term potentiation[144] and depression[145] of cortical synapses or closely related neuronal mechanisms have been suggested as possible mechanisms to explain the effect of high and low-frequency rTMS, respectively. Animal studies suggest that modulation of neurotransmitters[146,147] and gene induction[148] may contribute to these long-lasting modulatory effects of rTMS. Further work in animal models with appropriately sized TMS coils is needed to shed light on this issue.

The lasting modulation of cortical activity by rTMS is not limited to motor cortical areas. There is also evidence that these long-lasting effects of rTMS can be induced in areas outside the motor cortex and be associated with measurable behavioral effects, including visual[149], prefrontal[150], parietal cortex[151], as well as cerebellar[152]. This finding raises the possibility of therapeutic applications of rTMS to normalize pathologically decreased or increased levels of cortical activity. Several studies of various neurological disorders are providing results on such uses of rTMS. However, even with such favorable results, there might not be a causal link between improvement and the effect of TMS. More insights into the physiological basis for the behavioral effects of this technique are needed. In addition, to establish a clinical therapeutic indication for rTMS, well- controlled multicenter randomized clinical trials with high numbers of patients are required.

Depression

Treatment of depression is the most thoroughly studied of the potential clinical applications of rTMS. Lasting beneficial effects have been seen in about 40% of patients with medication-resistant depression in recent studies[153-156]. Both high frequency repetitive TMS of the left dorsolateral prefrontal cortex and low frequency stimulation of the right side can improve depression. Kimbrell and colleagues[141] suggested that patients with decreased cerebral metabolism might respond better to high frequency and those with hypermetabolism may respond better to low frequency stimulation, which is in line with the frequency-dependent effects of rTMS on the motor cortical excitability.

Parkinson's disease

Pascual-Leone and co-workers[157] first reported that in five patients with Parkinson's disease submotor-threshold rTMS at high frequency (5 Hz) to the motor cortex improved contralateral hand function. There are two rationales for trials of this method in Parkinson's disease: first, increasing cortical excitability to thalamocortical drive, which is believed to be lacking in this disease; and second, modifying catecholamine metabolism subcortically through cortical stimulation[158]. The mild benefits were reproduced by the other groups[159] and Strafella and colleagues[143] recently have shown that rTMS of the prefrontal cortex can increase dopamine in the caudate nucleus. However, other careful and systematic studies have not shown any favorable effects[160,161]. These contradictory results for rTMS in patients with Parkinson's disease draw attention to the difficulty of proving a clinical therapeutic effect, the likely variability of TMS effects across individuals, and the importance not to extrapolate from an acute, symptomatic change in very few patients to a claim of therapeutic applicability.

Other pathologies

After physiological studies of task-specific dystonia suggested hyperexcitability of the motor cortex or a failure of intracortical inhibition[162], rTMS of the motor cortex at 1 Hz has been used to treat patients with writer's cramp[163]. The improvement of deficient intracortical inhibition and handwriting lasted at the most 3 h after application of a 30 min train of TMS but resulted in clinical benefits in only 2 of 16 patients studied. In tic disorder, a similarly abnormal increase of cortical excitability is reported[164], and 1 Hz rTMS of the motor cortex can reduce the frequency of tics. These effects are transient, but the data support the concept of impaired inhibitory mechanisms in the motor cortex. Several other studies have tried to use low frequency rTMS to treat other diseases, for example intractable seizures[165,166] and showed successful reduction in the frequency of seizures or abnormal movements, but in very few

patients. Similar logic might be applicable to spasticity, intractable neurogenic pain, or schizophrenia, where suppression of abnormally increased cortical excitability might achieve desirable symptomatic relief.

Outcome after stroke may be favorably influenced by rTMS suppressing maladaptive cortical plasticity and improving adaptive cortical activity to promote neurorehabilitation. Functional imaging studies after stroke show increased activity in undamaged brain areas[167,168], but the role of these areas is controversial[169]. Some activation in the uninjured brain could reflect adaptive cortical reorganization that promotes functional recovery, but some changes may be maladaptive and generate the emergence of behaviors, suppression of which would improve functional outcome. The symptoms after a brain damage are as much due to the damage as to the changes in activity across the undamaged brain. Contralesional neglect after stroke is not due to the lesion itself but primarily due to the hyperactivity of the intact hemisphere, and 1 Hz rTMS of the unaffected parietal lobe to suppress excitability of the intact hemisphere can improve contralesional visuospatial neglect after stroke[170]. Naeser and co-workers[171] have shown that patients with Broca's aphasia may improve their naming ability after 1 Hz rTMS of the right Brodmann's area[166] that is supposed to be overactivated in patients with unrecovered, non-fluent aphasia. These observations are transient, and it is premature to propose them as realistic therapeutic applications. Nevertheless, rTMS of the region of interest detected in functional images could highlight the property of plastic changes of the cortical circuitry and hint at future novel clinical interventions.

Studies to date have not provided enough data to establish the clinical indication for a systematic application of TMS as a diagnostic or therapeutic tool in any neurological or psychiatric disease. Nevertheless, the ability of TMS to measure and modify cortical activity offers exciting capabilities that warrant carefully designed clinical trials. Combined with neurophysiological studies in animals and human beings that expand our understanding on the mechanisms of action of TMS, future work promises to provide valuable advances in our understanding of the pathophysiology of a wide range of neuropsychiatric conditions, generate widely applicable diagnostic tools for clinical neurophysiology, and perhaps establish neuromodulation as a viable therapeutic option in neurology, neurorehabilitation, and psychiatry.

2.5.3 Optogenetics

Optogenetics is a biological technique which involves the use of light-sensitive microbial proteins to control cell physiology. Nowadays, it is one of the most useful technologies employed in neuroscience and physiology fields. Classical techniques, as electrical and physical techniques, are not spatially precise and can cause perturbation of surrounding cells and biological processes. Pharmacological and genetic methods have an improved spatial selectivity but lack temporal resolution at the scale of millisecond. Optogenetics overcomes these problems providing a precise control of cellular functions *in vitro* and *in vivo* by using specific probes activated by light ("opto-") and genetically encoded ("-genetics")[172]. The possibility to control cell behavior by using flash of light was first hypothesized by Francis Crick in 1999 at the University of California San Diego[173]. Only in 2005 the accurate control of neural activity became possible by using Channelrhodopsin-2 (ChR2), an opsin identified in the unicellular green alga *Chlamydomonas reinhardtii*[174]. When ChR2-expressing neurons are illuminated by light of the proper wavelength they depolarize evoking action potentials with a precise duration and amplitude, which is proportional to the duration and intensity of the light stimulus. The *in vitro* manipulation of neuronal activity allowed the *in vivo* investigation of neural circuits and behavior[175]. Indeed, the most important optogenetics application fields are retinal degeneration, Parkinson's disease, sleep/wake circuitry, epilepsy, and memory mechanisms. Recently optogenetics has been employed also to study intracellular signaling pathways[176], such as the ROS signaling, by using the photo-inducible genetically-encoded ROS-generating proteins (RGPs)[177], and also in cancer research[178,179].

Optogenetic actuators are specific proteins that respond to the light stimulus when applied on the cells in which they are expressed, allowing the passage of ions through the membrane. These actuators can induce action potentials, suppress or enhance neural activity or modify biochemical pathways with millisecond timescale control. The most widely used actuators are opsins (Figure 6). Opsins are light-sensitive transmembrane proteins found in a great range of organisms, from microbes to primates[180]. They can be engineered and inserted into cell genomes by transfection or by lentiviral infection[174]. Opsins are organized into two classes: microbial opsins (Type I) or vertebrate opsins (Type II)[180]. Type I opsins, which are the first used opsins in optogenetics experiments, are found in eukaryotic and prokaryotic organisms and are composed of a single protein bound to membrane that has either pump or channel functions. Type II opsins are found in animal cells and are implied in vision and in modulation

of circadian rhythms. These opsins are G-protein coupled receptors and produce slower changes in cellular activity compared to Type I opsins. Actually, the Type I opsin are used to control cellular functions due to their faster kinetics.

Among the opsins, Channelrhodopsin is the most commonly used. Channelrhodopsin was first discovered in green algae *Chlamydomonas Reinhardtii* in which mediates phototaxis and photophobic responses[181]. Studies on *C. Reinhardtii* genome revealed two opsin-coding sequences, Channerhodopsin-1, highly selective for protons and mediates the high intensity-responses, and Channelrhodopsin-2, selective for different cations and responsible for low-intensity photocurrents[181].

ChR2 was the first used opsin to control the spiking activity of neurons[174]. It presents an all-trans retinal chromophore that induces a conformational change when photons are absorbed (Figure 7). This change allows the opening of the channel and the passage of cations, resulting in cell depolarization. A single flash of blue light can induce an action potential in ChR2-expressing neurons with a precise temporal control. This allowed the development of new investigation techniques based on the ChR2 use. In particular *in vitro* experiments are performed on primary neuronal cultures, cancer cells, and virtually all kind of cell that need to be studied; whereas, *in vivo* approaches were first performed on *Caenorhabditis elegans*[182] and nowadays on transgenic mice[183]. After the discovery of channelrhodopsins a great variety of opsins with a different spectral, temporal and conductive properties have been discovered or engineered. These opsins are used to control cell activity in different ways.

The need of faster temporal control of cellular activity led to the creation of a new class of opsins (ChETA) with faster temporal kinetics. They were obtained by accelerating deactivation through point mutations or chimera design such as ChEF/ChIEF opsins. Due to their

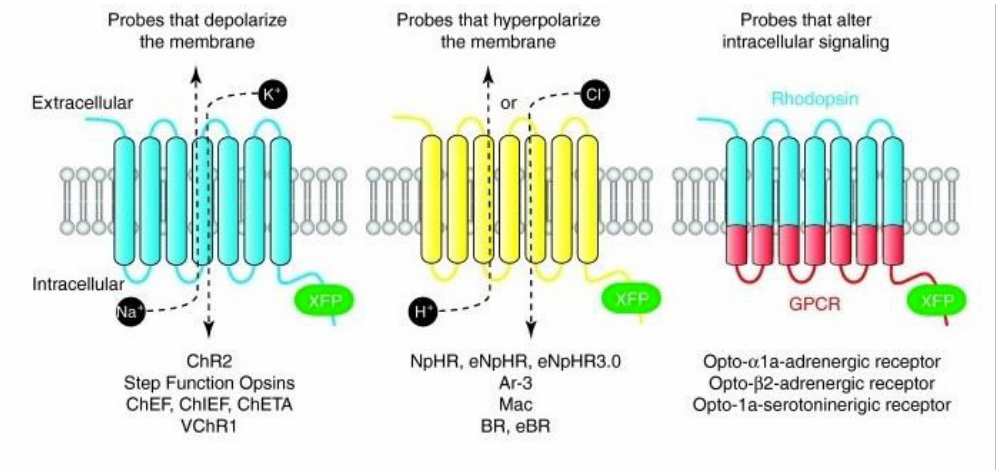

Figure 6. Different type of opsins. From left to right: excitatory opsins (depolarization), inhibitory opsins (hyperpolarization) and opsins coupled with G-protein coupled receptor (activation of intracellular pathways).

characteristics these tools are suitable to perform a high neural firing[180]. Furthermore, the fast kinetic reduces the extra-spike events resulting from single light pulse frequents when using ChR2.

In contrast to the Ultrafast Opsins, the Step-Function Opsins (SFOs) have a long deactivation time. SFOs were generated by introducing a point mutation in C128 position[184] that prolongs the channel opening time by inducing a long-time depolarization after the light pulse[180]. These opsins have a wide range of deactivation timescale that depends on mutations in their sequences. In particular ChR2/D156A variant has a deactivation timescale of minutes[185] and SFO-ChR2 (C128/D156A) variant has a spontaneous deactivation timescale of half an hour[186]. These opsins can be controlled by different wavelength light. Photocurrents are stimulated by a blue light pulse and terminated by a yellow light pulse allowing a precise temporal control on depolarization onset and offset[180].

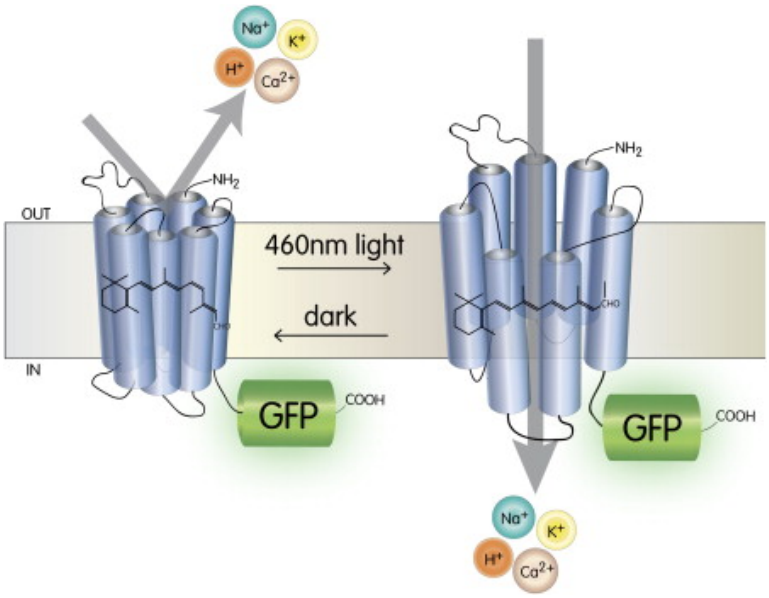

Figure 7. Channelrhodopsin-2 molecular structure and mechanism of action. The photon induces the conformational change leading to the channel opening. In the open state the opsin drives a nonselective flux of cations through the membrane.

Two main technical problems arise with the use of ChR2: the first derives from the spectral overlap in systems with two or more opsins; the second one is related to the low penetrance of blue light that does not reach the deepest areas of tissues. In order to overcome these problems, spectrally shifted opsins (SSOs) were developed. A long wavelength-sensitive opsin would enable a deep penetration of light into tissue allowing a non-invasive light delivery[180]. The first identified red-shifted opsin, VChR1, was found in *Volvox carteri* and it is excited with a 535 nm wavelength light, significantly red-shifted compared to ChR2 which is excited at 460 nm[187]. A variant of VChR1, the red-activated channelrhodopsin (ReaChR), is redder-shifted than ChR2, with an excitation range from 590 to 630 nm. It has been improved membrane trafficking of the opsin with higher photocurrent and faster kinetics, it also enables transcranial optical activation of specific neurons through the intact skull preventing the implantation of optical fibers[188]. These opsins have a red-shifted activation peak, but they also

exhibit a residual absorption of blue light. Two recently discovered opsins called Chrimson and Chronos avoid this problem[189]. Chrimson has an excitation spectrum 45 nm red-shifted and Chronos is a blue and green light sensitive opsin with a high light sensitivity and fast kinetic. The combination of these opsins offers two different wavelengths of light to activate independent neuronal populations without any crosstalk between neurons.

The inhibition of cellular functions is performed using different types of opsins such as chloride pumps and the new discovered Luminopsin. One of the most efficient and used inhibitory opsin is NpHR, a halorhodopsin from archaeon *Natronomonas pharaonic*[190]. NpHR allows the flux of chloride ions into the cell upon a flash of light resulting in hyperpolarization[180]. Recently, by enhancing the NpHR functioning it has been engineered eNpHR3.0, an opsin with improved surface membrane localization and a large photocurrent[191]. It has an excitation peak at 590 nm thus it can be activated by green, yellow or red wavelengths of light. Another chloride pump discovered in the last few years is the chloride-conducting ChRs (ChloCs) inhibitory opsins that present a replacement of E90 in the central gate of ChR with positively charged residues that generate a high-affinity Cl- binding site near the gate[192]. Also, proton pumps can be used to inhibit neurons through hyperpolarization by pumping protons out of the cell. They are useful alternatives to chloride pumps because of a faster recovery from inactivation and a higher light-driven currents[180]. The most widely used proton pumps are Arch (archaerhodopsin-3 from *Halorubrum sodomense*), Mac (from the fungus *Leptosphaeria maculans)*, ArchT (an archaerhodopsin from *Halorubrum* strain TP009) and eBR (an enhanced version of bacteriorhodopsin from *Halobacterium salinarum)*[180]. These opsins are also spectrally red-shifted with the excitation maximum between 520 nm and 590 nm.

Recently new inhibitory opsins with a redder shifted excitation maximum have been discovered. One of them is a red-shifted cruxhalorhodopsin, Jaws, which is a chloride pump isolated from *Haloarcula salinarum*[193]. It has a photocurrent three times higher compared to those of elder silencers thus becoming a non-invasive tool for neuronal inhibition of deep brain areas. Unfortunately, these inhibitory opsins have two limitations: First, these pumps move only one ion per absorbed photon, which makes them less efficient than excitatory opsins; second, light sensitivity and long-term photocurrent stability cannot be increased because of the pore size[180]. Recently two new light- activated chloride pumps were developed to solve these problems[192].

Luminopsins (LMOs) are the latest opsins class discovered. They were developed by directly coupling a bioluminescent light source (a genetically encoded luciferase) to an opsin. In this way the luciferase provides the light source to stimulate opsin activation without requiring an external light source. The two first LMOs created were LMO1 and LMO2[194] both of them are excitatory: LMO1 was obtained by the fusion of ChR2 and a luciferase from the marine copepod *Gaussia princeps* (GLuc); LMO2 derived by the fusion of *Volvox* Channelrhodopsin 1 (VChR1) and GLuc. VChR1 is redder shifted compared to ChR2 and its mediated photocurrents have slower kinetics. More recently a new inhibitory Luminopsin (iLMO) has been developed combining *Renilla* luciferase (Rluc) and *Natronomonas* halorhodopsin (NpHR)[195]. In particular two iLMOs were created coupling NpHR with two different luciferases, iLMO1 (red- shifted *Renilla* luciferase TagRFP- RLuc+NpHR) and iLMO2 (firefly luciferase FLuc+NPhR). Both iLMO1 and iLMO2 are redder shifted than ChR2 and both effectively suppress neural activity.

Correct opsin illumination is fundamental to their activation that requires a proper beam of light at the proper wavelength. The two main light sources used in optogenetics are lasers and light-emitting diodes (LEDs).

Laser is a linear beam of light produced by an amplifier that has maximum power of 100 mW with a high precision. It is mostly used coupled with optical fibers for *in vivo* stimulation of specific deep brain areas. Small diameter of optical fibers (approximately 200 μm) minimizes tissue damage and they can be fixed directly on the skull or inserted into the brain of the animals using a cannula[180]. Laser systems have several drawbacks[196]. They are extremely expensive, fragile and require long warm- up times. Laser light sources are also bulky and can require specialized optical components to couple light to the fiber. Finally, millisecond-width pulses can be generated with lasers of some precise wavelengths, for example yellow lasers cannot be modulated on this timescale.

LEDs are less expensive, smaller, more stable and reliable than lasers. LEDs have only one great disadvantage: The difficulty to couple the light source with the optical fiber that does not generates light powers high enough to effectively perform *in vivo* stimulation[196]. Recent improvements have increased LEDs power. In particular blue leds are more powerful, delivering ~25 mW. However, some LEDs continue to emit low powers, as yellow LEDs that currently deliver little more than 3 mW. This light power may be enough to perform some experiments but is too low to perform more complex experiments in which the light must run through multiple coupling stages or be split for bilateral illumination.

Due to the possibility to precisely control the cell functions, optogenetics has imposed as one of the most interesting tools used in medical research in recent years. It has been applied in a wide range of pathologies from neural disorders to the treatment of spinal cord injury.

Epilepsy

Seizures are the main and most serious symptom in epilepsy. Actual treatments for drug-resistant epilepsy have limited success. Optogenetics has been proposed as a novel method to control seizures[197]. In particular the research has been focused on two different approaches: The first is to express an inhibitory opsin, such as halorhodopsin, in excitatory neurons to suppress excitability and reduce epileptic events. The second way provides the expression of excitatory opsins in interneurons in order to enhance inhibition of neurons in the neighborhood. In the first case, it has been shown that the expression of *Natronomonas pharaonis* (NpHR) in excitatory neurons and the subsequently light stimulation is sufficient to inhibit excessive hyperexcitability and reduce paroxysmal activity in hippocampal brain slices, a pharmaco-resistant epilepsy model system[198]. In the second case the activation of a subpopulation of GABAergic cells, representing <5% of hippocampal neurons, by using ChR2 stops seizures rapidly upon light application[199].

Parkinson's disease

Optogenetics are also used to investigate the neural circuits underlying the Parkinson's disease-related pathology[200] and the effectiveness of novel treatments. For example, halorhodopsin is used to reveal how transplanted dopaminergic neurons work to restore motor functions in Parkinson's disease models[201]. Dopamine neurons engineered to express halorhodopsin release dopamine, which binds to D1 receptors and regulates glutamatergic inputs to GABA neurons, thereby restoring the motor function of grafted mice.

Depression

Optogenetics have been applied to reveal the neurological causes of depression. Recently it has been shown using different optogenetic approaches on two models of depression that the phasic activation of ChR2 expressed in dopaminergic neurons in the ventral tegmental area (VTA) can mediate important effects[202,203]: It modulates multiple independent depression symptoms caused by chronic stress and induces a susceptible phenotype in previously resilient mice that had been subjected to repeated social defeat stress.

Alzheimer's disease

Experimental evidences indicate that acute neuronal activation increase Aβ release from presynaptic terminals however the effects of chronic synaptic activation on Aβ release are not clear. To investigate this issue a recent study has used the SFO to stimulate the hippocampal

perforant pathway[204]. After five months of chronic optogenetic stimulation the amount of Aβ of the stimulated side was 2.5-fold higher compared to that in the contralateral side.

Retinal disorders

Due to the high similarity between optogenetic opsins and mammalian visual opsins the possibility to use these opsins as an optogenetic actuator to restore the vision in some models of retinal disorders, such as the retinis pigmentosa (RP),[205] has been investigated. The first opsin used was melanopsin because of its presence in human retina. Unfortunately, this opsin conducts very slow photocurrents thus it was not useful for RP treatment. Subsequently another opsins class was used, the halorhodopsin, however its low sensitivity and its tendency to hyperpolarize cells made it unsuitable for RP treatment. Several successful studies have used ChR2 in retinal bipolar cells to drive upstream signaling in mouse models of RP[206] but it lacks sufficient photon capture efficacy to be used under normal lighting conditions. More recently a genetically and chemically engineered light-gated ionotropic glutamate receptor (LiGluR) has been developed [207]. When expressed in retinal ganglion cells (RGCs) of a model of retinal degeneration it restores light sensitivity to these cells, increases light responsiveness to the primary visual cortex and restores both pupillary reflex and natural light-avoidance behavior.

Spinal cord injury

During spinal cord injury (SCI) motor neurons are disrupted leading to a motor impairment such as a loss of function of a body part. Actual therapies are based on surgical decompression, use of therapeutic agents and stem cells transplantation. However, none of them seems to be an effective treatment. New hypotheses are based on the coupling between stem cell therapy and optogenetic approaches[208]. In particular, ChR2 is expressed in damaged motor neuron and its stimulation in the presence of stem cells could restore functional networks. The main targets are the restoration of respiratory function, recovery of the body function using both ChR2 and NpHR, restoration of muscle function using embryonic stem cells (ESCs) and optogenetic actuators.

Cancer

Recent experiments investigated the effect of optogenetic stimulation on cancer cells, in particular on human glioblastoma cells. Regulating polarization status of cell membrane and ion channels could exert effects on the activities of malignant glioma, including proliferation, migration, and metabolism. Optogenetic techniques can be used to achieve gain- or loss-of-function in a cell- or tissue-specific manner. In particular, using engineered opsin ChETA into

primary human glioma cells, it decreases cell proliferation and increases mitochondria-dependent apoptosis, upon light stimulation[179].

3. Aims of the work

To date glioblastoma represent a great clinical challenge, being a tumor with a miserable prognosis once diagnosed. Every discovery able to understand tumor physiology and its molecular mechanisms would represent a success in the development of a therapy aimed to increase life quality and expectancy. Glioblastoma's resistance to therapy and tumor relapses are attributed to a restricted pool of slow-dividing self-renewing cells known as glioblastoma stem cells (GSCs). The transmembrane form of CLIC1 (tmCLIC1) plays an exclusive role in the proliferation of glioblastoma stem cells *in vitro* representing a promising pharmacological target. Recently, our lab demonstrated that the antidiabetic drug metformin is able to slow down the progression of GSCs through the impairment of tmCLIC1 function.

The first aim of this thesis work is to demonstrate unambiguously that the transmembrane form of CLIC1 protein is the one and only molecular target of metformin in patient derived stem cell enriched primary cultures.

Once the specific interaction has been demonstrated, the second aim to pursue is to find the specific amino acid to which metformin binds. This was identified as the Arg29 located in the inner portion of tmCLIC1 pore.

Given the biophysical properties of tmCLIC1 as a voltage dependent channel our third and final aim is to develop a strategy aimed to increase the ability of metformin to reach its state-dependent binding site. Repetitive membrane potential oscillations delivered to GSCs increase tmCLIC1 open probability and thus diminish the amount of drug needed to exert its antitumoral properties. This last aspect of the study is instrumental to circumvent the obstacle represented by the small amount of bioactive molecule able to reach the tumor microenvironment.

The broad purpose of the following work is to provide new approaches for the development of an adjuvant therapy aimed to glioblastoma stem cells.

4. Materials and Methods

4.1 Cell cultures

Human glioblastoma cancer stem cells (GSCs)

GB primary cell lines, already tested for stem cells properties and tumorigenicity, were kindly provided by professor T. Florio's laboratory from University of Genova (Genova, Italy). They were obtained from surgical specimens at the Neurosurgery Department of IRCCS-AOU San Marino IST (Genova, Italy) from patients who did not received therapies before intervention. Samples were histologically classified as GB grade IV (referring to WHO classification) and were used after patients' informed consent and Institutional Ethical Committee (IEC) approval.

In particular, we used for our experiments two different primary GSCs named as GBM1 and GBM2.

GSCs cultures were maintained in a humidified incubator at 37°C in 5% CO2. Cells were grown in permissive stem cells medium composed by Dulbecco's Modified Eagle's Medium (DMEM) and F12-GlutaMAX in a ratio 1:1, supplemented with 1X B27 (Thermo Fisher Scientific), 10 μg/μL basic fibroblast growth factor (FGF, Miltenyi Biotec), 20 μg/μL human epidermal growth factor (EGF, Miltenyi Biotec) and Penicillin/Streptomycin (Pen/Strep, 100 U/L) (Thermo Fisher Scientific).

GBM1 GSCs grow in suspension as spheroid aggregates called neurospheres. Twice a week neurospheres were mechanically dissociated into single-cell suspension to form secondary neurospheres. This procedure allows cells at the core of neurospheres to get in touch with selective medium and growth factors, preventing differentiation. For routinely culture, collected cells are centrifuged at 120 x g for 8 minutes and re-plated in fresh medium.

GBM2 GSCs grow in adhesion on plastic supports. Cultured GBM2 cells were detached from the plate twice a week by using Tryple (Thermo Fisher Scientific), collected in a tube and centrifuged at 180 x g for 6 minutes and re-plated in fresh medium.

For some experiments GSCs were also grown on plates coated with growth factor reduced Matrigel (BD Biosciences). The coating was prepared diluting 1:80 Matrigel stock solution (9-12 mg/mL) in DMEM and letting polymerize it on the plate for at least 30 minutes at 37°C. Once polymerized, the excess of Matrigel solution was removed and cells were directly seeded.

Murine glioma cell line

GL261 mouse glioma cells were cultured in DMEM, 10% FBS, 1% PenStrep. 37°C, 5% CO2.

4.2 Reagents

Indanyloxyacetic acid 94 (IAA94) (Sigma-Aldrich) was used to specifically inhibit CLIC1 activity. It was dissolved in absolute ethanol to make a 50 mM stock solution and used at 100 µM working concentration in complete medium or external solution for electrophysiology experiments.

1,1-Dimethylbiguanide hydrochloride (Metformin) (Sigma-Aldrich) is a biguanide compound used, in this case, as an alternative CLIC1 inhibitor. It was dissolved in ultrapure deionized water at 1M concentration and mostly used at 1-5 mM.

Temozolomide (Sigma-Aldrich) is a DNA methylating agent, anti-tumor and anti-angiogenic commonly used to treat glioblastoma multiforme patients. It was dissolved in DMSO to make a 100 mM stock solution and used at 5 µM working concentration in complete medium.

Rapamycin (Sigma-Aldrich) is the inhibitor of mammalian target of rapamycin (mTOR). It was used to evaluate possible effects of stimulation on the intracellular pathway in which metformin is involved. It was used at a concentration of 0.7 and 7 nM (depending on the cell culture) starting from 1 mM stock solution in DMSO.

PD033 isethionate (Sigma-Aldrich); is an inhibitor of cyclin-dependent kinase (CDK) 4 and 6. It was used to synchronize cells in G1 phase of the cell cycle at a concentration of 2.5 µg/ml.

4.3 Clic1$^{-/-}$ mutant generation by CRISPR-Cas9 technology

GBM1 cell line was transfected with transEDIT lentiviral gRNA plus Cas9 expression (pCLIP-All- hCMV-ZsGreen V66) lentiviral vectors according to the protocol from manufacturer (Transomic). Two plasmids were used, a gRNA targeting a specific region of *Clic1* coding sequence (see table below) and one targeting GFP as negative control (NC). Plasmids carry ZsGreen fluorophore as a selection marker.

Gene	Clone ID	Target seq.	Target location	Strand	Amino acid position
CLIC1	TEVH-1165427	TGAGTGCCCCTAT ACC TGGG	NM_001288.4	antisense	272

Plasmids were provided as bacterial glycerol stocks and were extracted using GenElute HP Plasmid Midiprep kit (see section 7 of Materials and Methods).

Once extracted, the procedure to transfect plasmid DNA into mammalian cells in a 6-well format was the following:

One day prior to transfection, GBM1 cells were plated in 2 ml of growth medium so that cells were 70–95% confluent at the time of transfection. Cells were kept in adhesion using Matrigel coating.

Transfection was performed using Lipofectamine LTX, following the indicated protocol (see section 8 of Materials and Methods). Cells were incubated overnight at 37°C in a CO2 incubator. Transfected cells were then selected by fluorescent protein expression through sorting at FACS (BD Facs Aria III, BD Bioscience) and single cells for each type of plasmid were plated in 96-well plates (one cell per well, one multiwell per gRNA clone). Using FACS analysis to select for cells with highest fluorescent protein expression allows to enrich for the population of cells with the highest frequency of genome editing.

During growth, cells were gradually transferred from 96-well to 48-well, 24-well and 6-well up to get to a proper number of cells.

4.4 Protein extraction and Western Blot analysis

Cells were seeded into 35 petri dishes ($4x10^5$ cells/well) and directly lysed through the addition of hot Lysis Buffer (LB) composed by 0.25M Tris-HCl pH 6.8, 4% SDS, 20% Glycerol in water. Samples were then sonicated for 30 minutes, syringed and boiled for 10 minutes at 95°C to achieve complete protein denaturation. Samples were later centrifuged at 4,000 x g for fifteen minutes and supernatants were collected and stored at -20°C.

Protein concentration in the whole-cell lysates was evaluated through BCA assay (Thermo Fisher Scientific). For this purpose, a known amount of each cell lysate (5 µl) was added to water (45 µl) and to 500 µl of BCA reagent A+B (1:50). Samples were boiled at 60°C for 30 minutes and the absorbance at 562 nm was read using EnSight Multimode Plate Reader (PerkinElmer's).

Protein concentration in whole cell lysates was determined through normalization with standard BSA (2 µg/ml) linear fit.

For each sample, equal amount of protein extracts (30-40 µg) were combined with a certain volume of 4X LDS Sample buffer (Thermo Fisher Scientific), in order to obtain 1X final concentration, and boiled 5 minutes at 95°C. Samples were loaded onto 12% SDS-polyacrilamide electrophoresis gel (PAGE) and run at constant voltage (100 V) for 1-2 h RT

in running buffer. Separated proteins were transferred to a nitrocellulose membrane (Amersham Protran, GE Healtcare) with of 0.45 µm pore size at 100 V constant for 1 h on ice in transfer buffer.

At the end of the transfer process, membranes were colored with Ponceau solution 0.1 % (w/v) in 5% acetic acid (Sigma-Aldrich), and cut in the correspondence of the molecular weight of interest. Membranes were blocked for 1 h RT to saturate the non-specific antibodies' binding site.

After blocking, membranes were incubated in primary antibody solutions overnight at 4°C. Membranes were washed three times with washing solution to remove the excess of primary antibodies and incubated 1 h RT with secondary antibody solutions.

After washing, membranes were incubated with SuperSignal® West Femto Maxium Sensitivity Substrate (Thermo Fisher Scientific) 1 minute in the dark. Immunoreactive protein bands were detected using *ChemiDoc Touch*® imaging system (BioRad). Intensity of the bands corresponds to the protein expression levels. Images were analyzed using ImageLab software (BioRad). Values are then normalized to the levels of housekeeping control signal.

Solutions used for western blot assay are the following:

- Separating buffer 4X: 1.5 M Tris-HCl, 0.4% SDS pH 8.8 in H2O
- Stacking buffer 4X: 0.5 M Tris-HCl, 0.4% SDS pH 6.8 in H2O
- 12% SDS-polyacrilamide gel: 30% Acrylamide, 10% APS, TEMED, 1X separating/ stacking

  buffer in H2O:

- Running buffer 10X: 25 mM Tris-HCl, 192 mM glycine, 0.1% SDS in H2O
- Transfer buffer 10X: 0.02M Tris-HCl, 1% glycine in H2O
- Blocking solution: 5% w/v BSA in PBS 0.1% Tween® 20
- Staining solution: 5% w/v BSA in PBS 0.1% Tween® 20
- Washing solution: PBS 0.1% Tween® 20
- Secondary antibody solution: anti-mouse and anti-rabbit horseradish peroxidase (HRP)-conjugated (Sigma Aldrich) diluted 1:10000 in staining solution

  Primary Antibody solutions used are the following:

1. Mouse monoclonal anti-Vinculin (Sigma-Aldrich) diluted 1:2000 in staining solution

2. Mouse monoclonal anti-CLIC1 (Santa Cruz Biotechnology) diluted 1:750 in staining solution.

3. Rabbit monoclonal anti-Cyclin E (Cell Signaling) diluted 1:1000 in staining solution.

4.5 Fluorescence intensity assay

Fluorescence intensity assay was performed to evaluate the total amount of tmCLIC1 staining in *Clic1*$^{-/-}$ cells, negative control and rescued cells.
Cells1x10^6 cells/well) were washed three times and incubated in blocking solution 30 minutes on ice.
Primary antibody solutions were directly added to samples without removal of blocking solution and incubated for additional 2h on ice.
After washes, samples were incubated with secondary antibody solution 1h on ice in the dark.
Samples were washed again for three times and distributed onto a black 96-well plate.
All the washes and staining steps were performed maintaining cells in suspension.
Samples were analysed at *Ensight Multimode Plate Reader* (PerkinElmer's) using appropriate filter to visualize fluorescence intensity emitted by Alexa Fluor 488 conjugated antibody (Em=488 nm; Ex=350 nm).
Fluorescence intensity values of samples incubated with anti-NH_2-CLIC1 are proportional to the amount of tmCLIC1 and were normalized to values of samples incubated only with secondary antibody.
Solutions used are:

- Washing solution: 1% w/v BSA in PBS, 0.1% sodium azide
- Blocking solution: 5% w/v BSA in PBS, 0.1% sodium azide
- Staining solution: 3% w/v BSA in PBS, 0.1% sodium azide
- Primary antibody solution: monoclonal mouse anti-NH_2 (PRIMM s.r.l) 1:140 in staining solution
- Secondary antibody solution: Donkey anti-mouse conjugated to Alexa Fluor 488 (Thermo Fisher Scientific) 1:400 in staining solution

4.6 Field potential, optogenetics and electromagnetic stimulation apparatus

Field potential stimulation was performed on human GBM1 cells. The custom-made instrument is made up by 20 electrode couples fixed onto two 24-wells plates cover. Electrodes are dipped into the medium and connected to an amplifier which enhances by 10-fold the impulse received by a generator. A symmetrical biphasic current stimulus of 80V at 1 Hz frequency (800 µs per second) was applied for 72 hours.

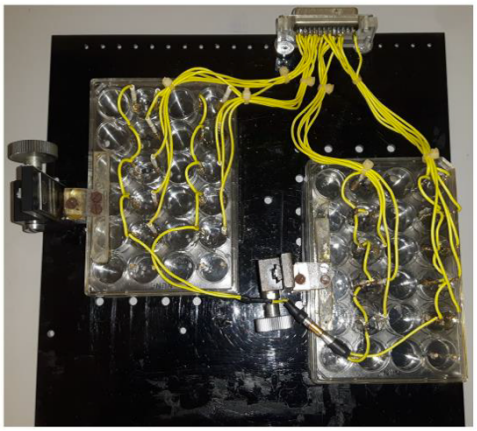

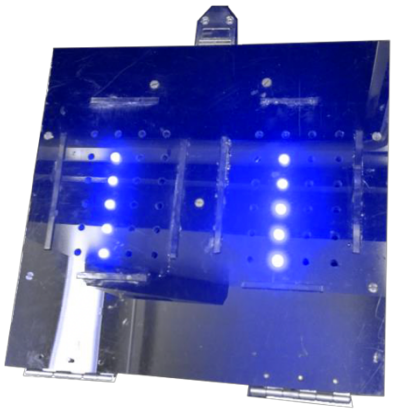

Optogenetic stimulation was performed on human GBM2 infected (see section 9 of Materials and Methods) with pLenti- EF1a-hChR2(H134R)-EYFP-WPRE, a gift from Karl Deisseroth (Addgene plasmid #20942). The stimulus was delivered for 96 hours by a custom-made apparatus consisting of 10 LEDs fixed under two 24-well plates hollows. The stimulus frequency was 0.1 Hz (10 ms of light impulse every 10 seconds).

Electromagnetic field stimulation was performed on GBM1 and GBM2. The custom-made instrument consists of 12 coils placed under two 24-well plates. The device delivers a 3.5 mT stimulus at 1Hz frequency (5ms stimulus per second).

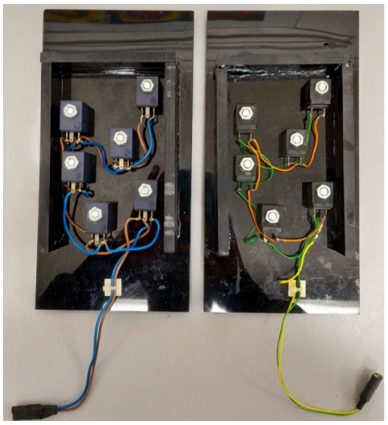

4.7 Growth curves, dose-response and cell count analysis

For all this kind of experiments, $2x10^4$ GBM1 cells or $7x10^3$ GBM2 cells were plated in 700 µL of growth medium per well (eventually supplemented with treatment) in a 24-well plate. For each experimental condition and time point cells were plated in triplicates.

Growth Curves

Cells were plated in 24-multiwell plates and counted after 24, 48, 72 and 96 hours to build up the growth curve. Cells were collected and centrifuged, and the resuspended pellet was diluted 1:1 with Trypan Blue. Countess II FL automated cell counter (Thermo Fisher Scientific) was used to count them. All data were normalized to their controls.

Dose-response curves

Cells were plated in 24-well support with increasing concentrations of metformin in a range between 0 mM (control) and 10 mM. After 72 hours (GBM1) or 96 hours (GBM2) cells were collected, centrifuged, resuspended in a known volume, diluted in Trypan Blue (1:1) and counted with Countess II FL automated cell counter (Thermo Fisher Scientific). Data were normalized on their controls, plotted using a logarithmic X-scale and completed with a fitting curve.

Cell count analysis

For stimulation experiments, GBM1, GBM2 and GL261 cells were counted at given time points (72 or 96 hours) after a chronic exposure to the specific stimulus.
Cells were plated in 24-multiwell plates and positioned over the stimulation machinery. After stimulation, cells were collected and centrifuged. The resuspended pellet was diluted 1:1 with Trypan Blue and counted using a Countess II FL automated cell counter (Thermo Fisher Scientific). All data were normalized to their controls.

4.8 3D Cultures

GBM1 cells (NC, *Clic1*$^{-/-}$, *Clic1*$^{-/-}$+*Clic1* WT, and *Clic1*$^{-/-}$+*Clic1* R29A) were plated in 24-well plates at a density of $2x10^4$ cells. After the formation of a solid 3D structure (24 to 48 hours after plating) single spheroids were transferred to a new 24-well plate in fresh medium with or without metformin (1-5mM) and the first photos were captured to measure their initial area. Spheroids were then incubated for 72 hours.
For EMF experiments incubated cells underwent stimulation at 1Hz frequency for the whole experimental procedure.
After 72 hours photos were captured, and the final area was normalized on the initial area of every 3D structure.
The area of spheroids was measured using ImageJ software (Freehand selection).

4.9 Plasmids

CLIC1wt-pIRES2-EGFP or CLIC1R29A-pIRES2-EGFP plasmids were used to rescue CLIC1$^{-/-}$ cells.

To generate GBM2 stably expressing ChR2 we used pLenti-EF1a-hChR2(H134R)-EYFP-WPRE. It was a gift from Karl Deisseroth.

(Addgene plasmid # 20942 http://n2t.net/addgene:20942; RRID: Addgene_20942)

4.10 Transfection

CLIC1-KO cells were rescued through CLIC1wt-pIRES2-EGFP or CLIC1R29A-pIRES2-EGFP.

GBM1 cells were seeded in two wells of a 6-well plate the day before transfection in order to get to 70-90% confluency. Lipofectamine was diluted in OptiMem. 3ug of both plasmid DNAs (WT and R29A) were separately diluted in OptiMem as well. Each DNA solution was then mixed with lipofectamine in 1:1 ratio and incubated 5 minutes to allow DNA-lipid complex formation. Then, lipid-DNA complex was added to cells.

After three days cells were examined under a fluorescence microscope to see if they were expressing the reporter GFP and to evaluate that an apropriate transfection efficiency was reached.

At this point cells were ready to be detached and plated for both growth curves and cell count experiments.

4.11 Lentivirus production and infection

Viral infection was used to produce a stable line of GBM2-ChR2 for optogenetics experiments.

Plasmids encoding different parts of the viral structure, together with ChR2 plasmid, were transfected in HEK293T cells using a Calcium Phosphate precipitation based method. On Day 1, HEK293T cells were seeded in a p100 Petri dish to reach 40% confluence on the next day. On Day 2, the medium was changed to an antibiotic free one three hours before transfection began. Then, all viral plasmids (3.9 µg ENV; 2.72 µg REV; 5.4 µg MDL; 6.5 µg pADVANTAGE) were mixed together with 13 µg pLenti-EF1a-hChR2(H134R)-EYFP-WPRE plasmid in ddH2O + 0.1% TE (10 mM Tris-HCl; 0.1 mM EDTA; pH 8) and 54 µl of CaCl2 2.5M solution, to a final volume of 540 µL. The same volume of HBS 2X phosphate

buffer (50 mM HEPES; 280 mM NaCl; 1.5 mM Na2HPO4; pH 7.05) was added with a pipettor at max power making bubbles for 30 seconds. The mix was immediately distributed dropwise, and cells incubated until the next day. On Day 3, about 14 hours later, the medium was gently changed to a fresh antibiotic-containing one. Here the viral particles containing ChR2 DNA were released from HEK293T cells. Note that this last medium needed to be compatible for the cells to be infected.

On Day 4, medium containing the viral particles was harvested and directly used on the cells to infect or kept at -80°C.

Once Lentivirus was made, infection could be performed.

GBM2 cells were plated in p35 Petri dish to reach 50% confluence the day of infection. Just before infection, Polybrene was added to viral medium at a final concentration of 8 μg/mL. Cell growth medium was substituted with the viral one and incubated for 18-20 hours. After incubation, the medium was substituted with a fresh one and the cells were checked if they were already expressing the construct of interest by looking at the YFP reporter.

4.12 Patch clamp experiments

The patch electrodes (BB150F-8P with filament, Science Products) with a diameter of 1.5 mm, were pulled from hard borosilicate glass on a Brown-Flaming P-97 puller (Sutter Instruments, Novato, CA) and fire-polished to a tip diameter of 1-1.5 μm and an electrical resistance of 5-8 MΩ. The cells were voltage-clamped using an Axopatch 200 B amplifier (Axon Instruments).

For whole-cell experiments the perforated patch configuration was used. The antibiotic used was Gramicidin (final concentration in the pipette 5 μg/ml) that forms pore in the membrane permeable only to monovalent cations; in this way, the internal chloride concentration of the cells was preserved. Ionic currents were digitized at 5 kHz and filtered at 1 kHz. Clampex 9.2 was used as the interface acquisition program.

In time-course experiments, the holding potential was set according to the resting potential of the single cell and every 5 seconds a +60 mV voltage step was applied. The current was measured at the end of the 800 ms voltage step. Once the current amplitude reached a constant value metformin (5mM) and/or (IAA94) were perfused.

The voltage step protocol used to isolate current/voltage relationships consisted of 800 ms pulses from -60 mV to +60 mV (20 mV voltage steps). The holding potential was set according to the resting potential of the single cell (between 0 and -80 mV). CLIC1-mediated chloride

currents were isolated from other ionic currents by perfusing IAA94 100 μM dissolved in the bath solution.

I=0 current clamp mode experiments were performed on single cells to measure the depolarization induced by optogenetics, field potential and electromagnetic field stimulation.

In optogenetics and EMF time-course experiments, the acute stimulus was delivered at 2Hz frequency.

The solutions used are the following:

Bath solution: NaCl 140 mM, KCl 5 mM, Hepes 10 mM, MgCl2 1 mM, CaCl2 2 mM, glucose 5 mM.

Pipette solution: KCl 135 mM, NaCl 5 mM, hepes 10 mM, MgCl2 1 mM, CaCl2 2 mM, Gramicidin 2.5 μg/ml.

Analysis was performed using Clampfit 10.2 (Molecular Devices) and OriginPro 9.1.

4.13 In vivo experiments

Glioblastoma murine models

C57bl6/j mice were injected with GL261 tumor cells expressing ChR2.

All the animals received the injection in the forelimb primary motor cortex (Caudal Forelimb Area, CFA). In the same operation, an access chamber to the brain for optogenetic stimulation was created and covered with gentamicin, agarose and silicone and a metal post was cemented to the skull for head fixation. Once recovered from the operation, animals were randomly assigned to four experimental groups.

Each animal was accustomed to the locking system for longer periods of time and rewarded with concentrated milk. Starting from day 9 after injection, metformin was administered in the drinking water (1.5 mg/kg/day) of the selected groups. Two weeks after the injection, the stimulated groups were blocked on the stimulation platform and the brain tissue access chamber opened. An optical fiber was brought closer to the brain tissue immediately above the injection site. A stimulation consisting of 1 ms blue light pulses at a frequency of 1 Hz was applied directly above the GB development site. Each animal was stimulated daily for 2 hours for 5 consecutive days, rewarding it constantly with concentrated milk and keeping it in an isolated environment to limit discomfort. At the end of each stimulation session, the access room was covered again with gentamicin, agarose and silicone. The control groups were also blocked for the same amount of time and the recording room was open daily but no light stimulation was provided. At the end of the last treatment session (day 5), a solution of Bromo-

deoxy Uridine (BrdU, 500 µl/100g) was injected intraperitoneally to all 4 experimental groups and two hours later the entire cohort was perfused with paraformaldehyde 4%. The brains was extracted and cryoprotected with 30% sucrose and cut with a microtome to obtain 45 µm slices comprising the entire rostro-caudal extension of the tumor mass. The sections were processed for immunostaining with antibodies against BrdU and Ki67.

4.14 Statistical analysis

All data were plotted using GraphPad Prism 7 software (GraphPad Software Inc., San Diego, California), by which we calculated all mean values and standard errors. Statistical analysis on these data were performed on the same software.

To compare data between two different conditions, we used unpaired t-test analysis. One-way ANOVA test was used to compare more than two groups within the same experimental condition, while for multiple groups comparison within different conditions we used two-way ANOVA test. Each condition of any experiment was supported by at least 3 independent replicates (n=3). A cutoff value of p value < 0.05 was considered statistically significant.

5. Results

5.1 Generating a Clic1 Knockout of patient-derived glioblastoma stem cells using CRISPR-Cas9 technology

So far, tmCLIC1 implication in the cell cycle progression of patient-derived glioblastoma stem cells and its interaction with metformin was assumed on the basis of strong but indirect evidences[68]. These data involve several types of electrophysiological and pharmacological approaches as well as shRNA targeting CLIC1. The ideal background to study both the phenomena would be the knockout (KO) of the protein in glioblastoma stem cells and the investigation of the phenotypic effect linked to *Clic1* gene removal. Such a system would provide definitive information about the implication of *Clic1* in GB development *in vitro*. Importantly, this would finally highlight the possible interaction between metformin and tmCLIC1 taking into account the possibility to perform total rescue experiments. For this reason, the first step was to generate a population of *Clic1* KO GSCs using Crispr-Cas9 technology. After the initial stage of selection from single cell to population, and a series of

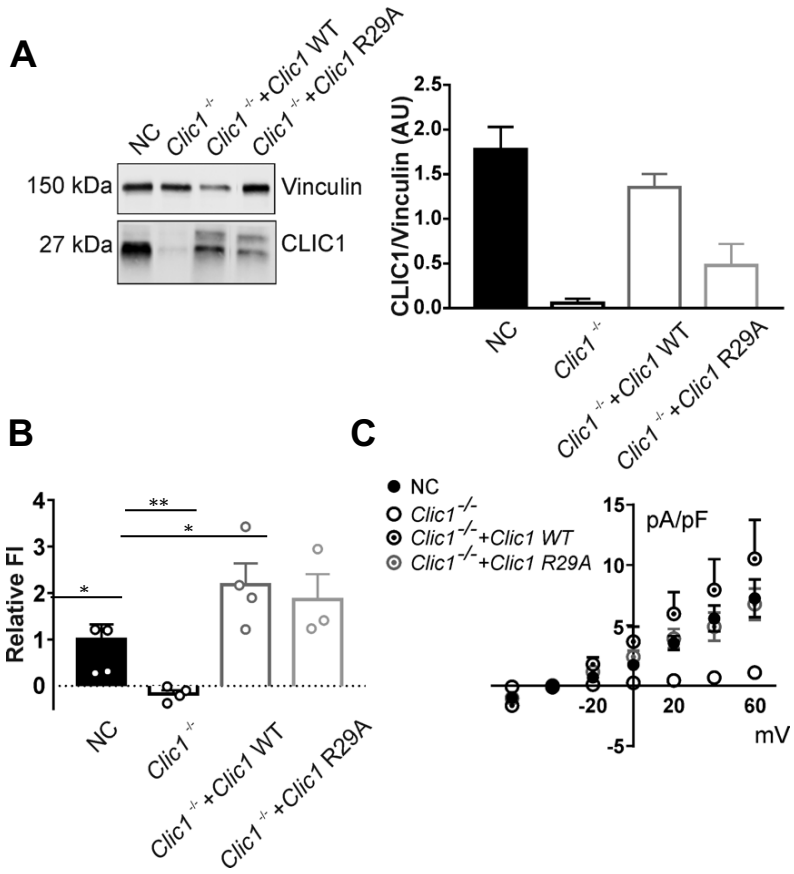

*Figure 1. A) Representative Western Blot analyses of lysates of NC, Clic1$^{-/-}$, and rescued GSCs populations (left panel). In the right panel, quantification of CLIC1 protein expression in the samples (n=3). B) Relative fluorescence intensity of tmCLIC1 in the four cell types. Although the differential protein expression level among Clic1$^{-/-}$+Clic1 WT and Clic1$^{-/-}$+Clic1 R29A observed in panel A, the localization of the protein is predominantly confined to the plasma membrane (NC n=5; Clic1$^{-/-}$ n=4; Clic1$^{-/-}$+Clic1 WT n=4; Clic1$^{-/-}$+Clic1 R29A n=3; one-way ANOVA; NC vs Clic1$^{-/-}$ **p=0,0020; Clic1$^{-/-}$+Clic1 WT vs Clic1$^{-/-}$ ***p=0,0007; Clic1$^{-/-}$+Clic1 R29A vs Clic1$^{-/-}$ **p=0,0040). C) Electrophysiology recording in perforated patch clamp of the whole cell current of single glioblastoma stem cells in the four experimental conditions. As expected, tmCLIC1 function is almost zeroed in KO cells while it's maintained in rescued cells in a similar manner among all the four populations. The results are consistent with the ones observed in panel B (NC n=7; Clic1$^{-/-}$ n=7; Clic1$^{-/-}$+Clic1 WT n=5; Clic1$^{-/-}$+Clic1 R29A n=4).*

Western Blot (WB) analyses to carefully select the clone, we focused on the effect of *Clic1* absence in one glioblastoma stem cells primary culture. In particular, our investigation involved the rescue of the *Clic1* KO background with two different CLIC1 forms (i) the wild type (WT) and (ii) the Arginine 29 (R29A) mutant. The rescue through the wild type form would be crucial to define the interdependence between the antiproliferative effect of metformin and tmCLIC1. The R29A mutant, on the contrary, would be useful to deeply understand the specific interaction that would occur. Figure 1 depicts the presence, the localization and the quantification in the plasma membrane of CLIC1 in the negative control (NC) CLIC1 KO (*Clic1*$^{-/-}$) and the WT/R29A rescue. In figure 1A we show a WB analysis demonstrating the absence of CLIC1 protein and its rescued expression after transient transfection of the two CLIC1 forms in GSCs. CLIC1 localization in living cells was then investigated at the population level using fluorescence intensity assay (for details, see Materials and Methods section) as shown in figure 1, panel B. The experiment was instrumental to assess the amount of protein at the membrane level. The results argue that although the differential expression among the two rescued populations - due to different transfection efficiency - the localization of CLIC1 protein is confined to the membrane in a similar manner. This suggests the importance of CLIC1 localization regardless of the total protein levels. The last technique used to fully validate the four cellular populations was patch clamp. The patch-clamp technique allows one to quantify tmCLIC1 and test the functional activity of the two CLIC1 mutants as well. CLIC1-mediated current has been obtained by subtraction of IAA94-sensitive current from the whole-cell current recorded. The results are plotted in figure 1, panel C. *Clic1*$^{-/-}$ cells display almost zeroed CLIC1-mediated current in contrast to NC and rescued cells which show a similar CLIC1 functional activity.

5.2 Metformin's effect on proliferation and cell cycle progression of Clic1$^{-/-}$ *and rescued GSCs*

After the validation of the whole system, we tested the proliferation of the mentioned cell populations performing a growth curve over 96 hours in the absence or presence of metformin. The concentration used in this set of experiments was 5 mM since it is the concentration that exerts the maximum antiproliferative effect on the given cells. This experiment was instrumental to test and compare the proliferation rate of the four cell populations. This would provide details about the effect of *Clic1* knockout and rescue on the proliferation of GSCs at first. In addition, the experiment would clearly show how metformin affects the growth rate of the given cells.

Figure 2 shows that after 96 hours 5 mM of metformin reduced the proliferation of Crispr-Cas9 negative control GBM1 stem cells of approximately 50% a trend almost superimposable to previous results observed in WT GSCs[68]. *Clic1*$^{-/-}$ cells show a slowed-down proliferation rate which is similar to metformin treated NC cells. The same population is insensitive to metformin treatment as well. *Clic1*$^{-/-}$ cells rescued with both WT and R29A CLIC1 plasmids are able to fully recover the phenotype similarly to NC cells. Importantly, they show a different response to metformin treatment. WT rescued cells are sensitive to metformin in a similar manner as observed in NC cells. In contrast, R29A rescued cells show an opposite behavior compared to WT rescued cells. An impressive result is the total insensitivity that these cells displays towards metformin. This suggests not only that the hypothesized metformin binding site with tmCLIC1 protein is the arginine 29 but also that CLIC1 could be the only metformin target in these cells.

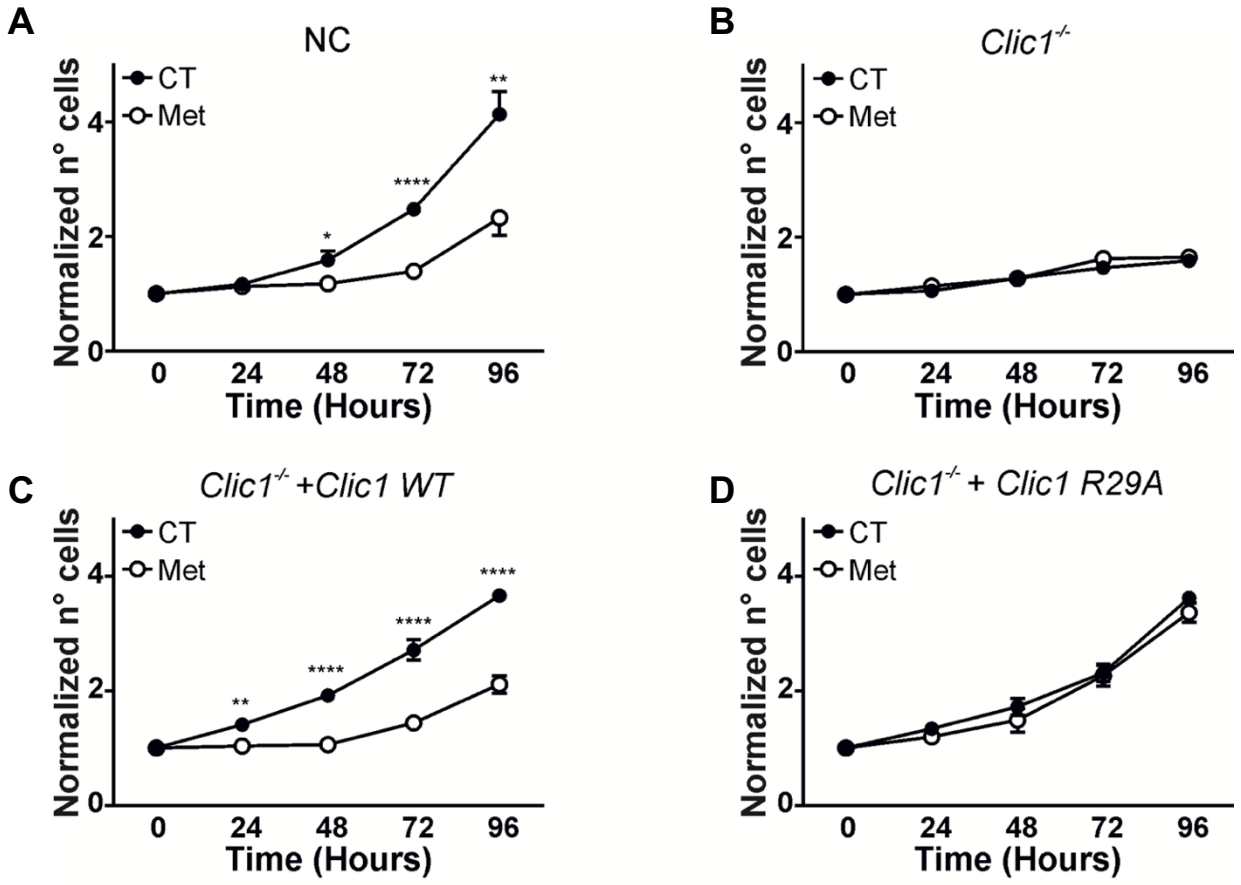

Figure 2. A) Growth curve of NC (A), Clic1$^{-/-}$ *(B), Clic1*$^{-/-}$*+Clic1 WT (C), and Clic1*$^{-/-}$*+Clic1 R29A (D) glioblastoma stem cells over 96 hours in the absence (black circles) or presence (empty circles) of 5 mM metformin treatment. Clic1*$^{-/-}$*+Clic1 WT show a trend similar to what observed in NC cells (NC metformin t-test: 48 hours (n=7) *p= 0,0110; 72 hours (n=7) ****p<0,0001; 96 hours (n=7) **p= 0,0060; Clic1*$^{-/-}$*+Clic1 WT metformin t-test: 24 hours (n=8) **p=0,0018; 48 hours (n=8) ****p<0,0001; 72 hours (n=8) ****p<0,0001; 96 hours (n=8) ****p<0,0001). KO cells show a dramatic slowdown of the proliferation without further effect under metformin exposure. Clic1*$^{-/-}$*+Clic1 R29A show an increase of the proliferation rate which is not impaired after the incubation with the drug.*

Transmembrane CLIC1 implication in cell cycle progression of glioblastoma stem cells (GSCs) has been well determined in previous works. In particular, in our recent publication we demonstrated that its functional activity is subject to the timing of signals that control membrane insertion (ROS) and removal (pH alkalization)[47]. CLIC1 insertion to the plasma membrane occurs approximately after 8 hours from G1 synchronization. Such a subtle tuning underlines a crucial role of the protein in sustaining the high rate of proliferation of glioblastoma *in vitro*. As a matter of fact, knockdown and knockout of the protein resulted in a slow-down of the cell cycle, showing a proliferation rate comparable to what was observed by incubating GSCs with both IAA-94 and the antibody targeting the tmCLIC1 N-terminus region.

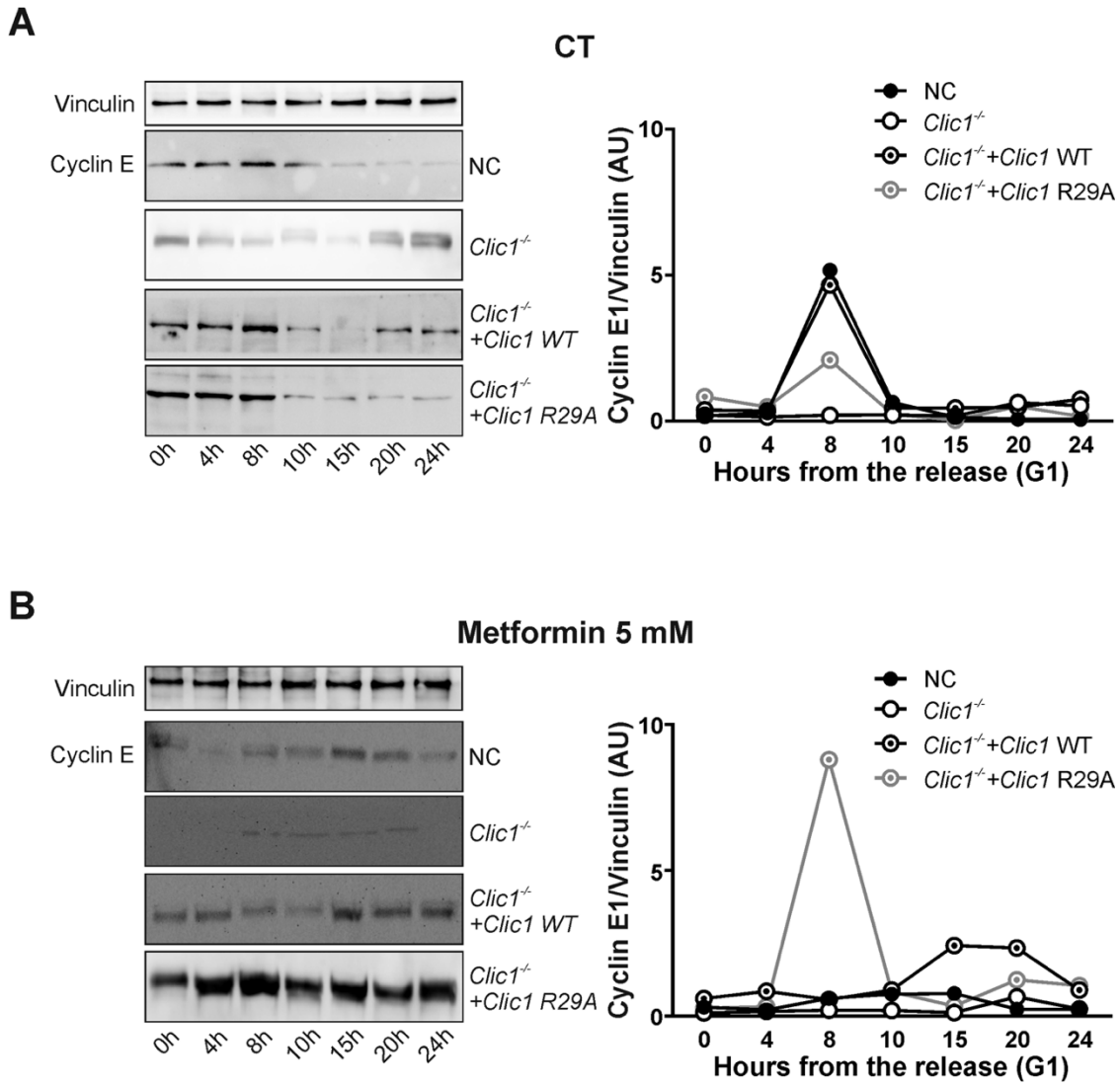

Figure 3. A – B left panel) Cyclin E1 representative Western Blot analyses of lysates of NC, Clic1$^{-/-}$, and rescued GSCs populations at different time points after the release from G1 synchronization in absence (top) or presence (bottom) of 5mM metformin treatment. In the right panel, quantification of cyclin E1 protein expression in the samples. Rescued cells undergo a peak of cyclin E1 mostly synchronous with that of NC cells. Metformin treatment delays cyclin E1 peak up to overlap with Clic1$^{-/-}$ cells timing of all clones except for R29A rescued cells.

Given this premise, we investigated also the timing of G1/S transition of our four clones looking at the expression levels of Cyclin E1. Cyclin E1 forms a complex with and functions as a regulatory subunit of CDK2, whose activity is required for cell cycle G1/S transition. This protein accumulates at the G1-S phase boundary and is degraded as cells progress through the S phase. As a result, the expression of the protein follows a trend which peaks during the G1/S transition and dramatically drops when cells enter S phase. Cells were synchronized in early G1 by incubating them with PD0332991 (for details, see Materials and Methods section) for 24 hours and released for the appropriate time in the absence or presence of 5 mM metformin. PD0332991 is a CDK4/6 inhibitor effective at arresting cells in the early G1 phase. Panel A of figure 3 depicts the timing of G1/S progression in absence of metformin. It is evident that all the clones follow the same trend, except from *Clic1*$^{-/-}$. In particular, each clone is subject to a peak of cyclin E1 at 8 hours from G1 synchronization despite the efficiency of transfection. *Clic1*$^{-/-}$ cells show a delayed cell cycle progression consistent with growth curves (figure 2) with a rising of cyclin E1 levels approximately after 20 hours from synchronization. Cells treated with metformin (figure 3B) produced an outcome similar to what observed in figure 2. Specifically, NC and *Clic1*$^{-/-}$*+ Clic1 WT* rescued cells show a delayed peak of cyclin E1 occurring from 15 to 20 hours after G1 synchronization and nearly synchronous to what was observed in *Clic1*$^{-/-}$ cells. As expected, *Clic1*$^{-/-}$*+ Clic1 R29A* cells don't show any timing alteration in cyclin E1 levels highlighting that these cells are almost insensitive to metformin treatment.

5.3 Investigating metformin effect in 3D models

A useful way to test the response of the tumor to a specific treatment is to mimicry what realistically could occur *in vivo*. Tumors don't spread in two dimensions, but the mass is a three-dimensional structure expanding over time. This feature is one of the tumor ways to elude pharmacological treatments since they are confined to mass edges. For this reason, a way to determine how a drug affects tumor spread is to culture cells in order to have a 3D structure. For this purpose, we performed the spheroids assay, a valuable model to test metformin treatments on glioblastoma stem cells. After spheroid's formation (for details, see Materials and Methods section), cells were incubated in absence or presence of 5mM metformin and observed after 72 hours. Figure 4 shows a behavior superimposable to what observed previously in 2D (figure 2). Metformin treatment is able to reduce spheroids' development on NC and WT rescued cells. On the contrary, metformin doesn't exert any effect on KO and the R29A rescued populations. Interestingly, KO cells show an average

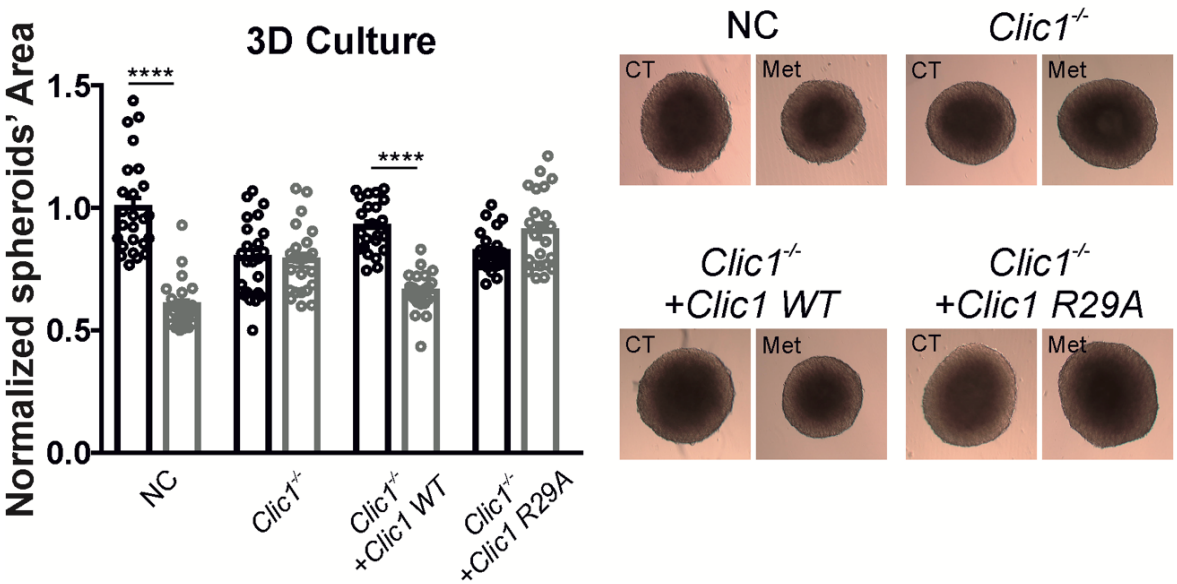

*Figure 4. (left) Spheroids' area measured at 72 hours post 3D structures formation in absence (black) or presence (grey) of 5 mM metformin treatment. (right) Representative pictures showing the trend plotted in the scatter plot on the right. Metformin exert an antiproliferative effect both in NC and WT rescued cells (NC and Clic1-/-+Clic1 WT (n=24), one-way ANOVA, ****p<0,0001). KO and R29A rescued cells show no alterations under metformin exposure.*

spheroids' area greater than NC treated cells. This effect could be explained taking into account that the spheroid *in vitro* lacks the vascularization useful to provide nutrients to the whole tumor. As a result, the core of the spheroid begins to be necrotic over time, impairing the whole structure. This finally reflects on the total measured area. For this reason, KO cells are only subjected to the necrotic effect. NC treated cells on the contrary could undergo metformin inhibition and core necrosis simultaneously, showing a smaller total area.

5.4 Effect of metformin on tmCLIC1 functional activity

Figures 2-4 provide valid information about tmCLIC1 implication in proliferation itself as well as the relationship between metformin and CLIC1. In order to elucidate the effect of metformin in the four above-mentioned cellular backgrounds from a functional point of view we performed electrophysiological recording in perforated patch clamp using a time course protocol. NC and both WT/R29A rescued cells were acutely perfused first with 10mM of metformin and then with 100µM IAA94 in order to completely zero tmCLIC1 mediated current. The two drugs were also perfused in the reverse order to test for the possibility that they could converge on different targets. As figure 5 suggests, metformin and IAA94 both converge on the same molecular target. Particularly, the effect on the whole cell current is similar in NC and *Clic1*$^{-/-}$+*Clic1* WT cells in terms of current inhibition amplitude and kinetics of inhibition. As expected, *Clic1*$^{-/-}$+*Clic1* R29A show no metformin sensitive current while acutely respond to IAA94 (as also shown in figure 1, panel C) in a similar manner to the other

cellular populations. This result confirms that the functional activity of the R29A rescued mutant is unaltered and show at the same time that IAA94 and metformin block tmCLIC1 ion flux by targeting two different binding sites.

After having clarified the direct interaction between metformin and the transmembrane CLIC1 isoform, efforts were made to find a strategy to reduce metformin working concentration. The reason of such a strategy is that metformin is able to impair GSCs primary cultures but at a concentration ranging between 5-10 mM. Such a dose is quite impossible to be reached in tissues and even more difficult to be reached in the brain. Furthermore, the blood brain barrier filter would add an additional limitation. To find a possible solution we took advantages of two crucial pieces of information: (i) metformin binds to tmCLIC1 in its open conformation; (ii) tmCLIC1 shows voltage dependent kinetics of opening with depolarization. These pieces of evidence led us to hypothesize that inducing a cyclic opening of tmCLIC1 would increase metformin's probability to bind to tmCLIC1 and block, thus reducing the drug's working concentration.

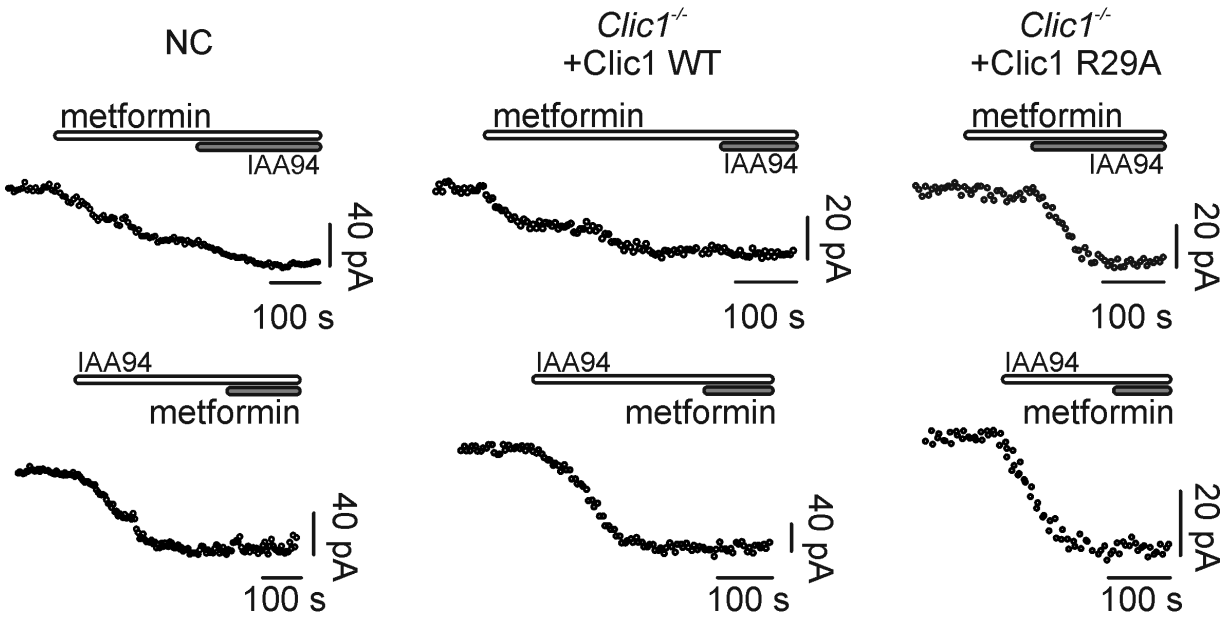

Figure 5. Representative time-course of whole cell currents in NC and WT/R29A rescued cells. Cells were stimulated every 5 seconds with a 800 ms, +60 mV test potential from the resting potential. Each point represents the average current of the last 100 ms of a single current trace. Once the current amplitude reached a constant value, metformin 5mM and IAA94 100μM (top) and vice versa (bottom) were perfused. WT rescued cells show a behavior similar to what observed in NC cells. R29A cells show no current inhibition after metformin perfusion while a IAA94 sensitive current similar to that of both NC and WT rescued cells, supporting the hypothesis of Arg29 as metformin binding site in glioblastoma stem cells primary cultures.

5.5 Development of the artificial system to induce repetitive membrane potential oscillations

To artificially induce the repetitive close to open transition of tmCLIC1, we developed three systems to be used *in vitro* (for details, see Materials and Methods section): (i) field potential stimulation (FP) consists of two electrodes directly dipped into the medium with GSCs. The electrodes deliver a biphasic current which destabilize cell surface charges, inducing a depolarization. (ii) optogenetic stimulation involving GSCs infected with Channelrhodopsin-2 (ChR2). ChR2 is a green algae-derived protein that function as a light-gated ion channel. ChR2 absorbs blue light at a maximum spectrum of 480 nm. When the protein absorbs a photon, this causes a conformational change that opens the pore allowing a non-specific inward cation flux, causing membrane depolarization. (iii) electromagnetic field stimulation (EMF) consists of a coil placed close to seeded cells. The current flowing through the wires generates an

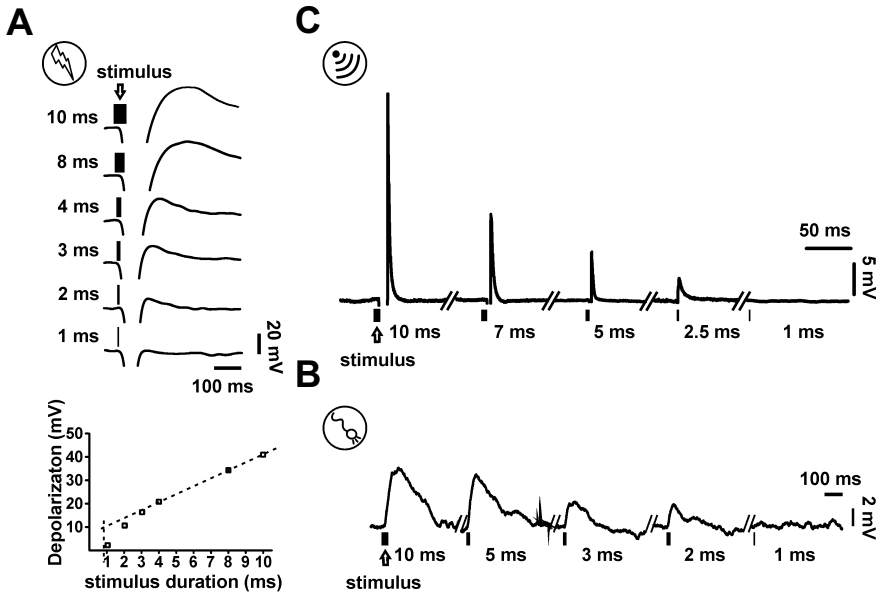

Figure 6. A) *Current clamp representative traces of the depolarization induced by the field stimulation at different impulse durations (upper panel). The depolarization induced by stimuli shorter than 4 ms was masked by the capacitive transient of the patch pipette and was derived through a linear fit regression of the experimental data obtained at longer stimulus duration. A stimulus of 800 µs (vertical dashed line) was sufficient to trigger an average depolarization of 10 mV (bottom panel). B) Depolarization induced by optogenetic stimulation at different impulse durations. An impulse of 10 ms produces an average depolarization of 7 mV. C) Depolarizations induced by EMF on GSCs. A 5 ms stimulus was able to trigger approximately 7 mV depolarization.*

electromagnetic field that induces an oscillation of the membrane potential due to the displacement of the cell surface charges.

To examine the ability of the three systems to induce an oscillation of the membrane potential they were all tested on single cells using the patch -lamp technique. In particular, the chosen configuration was I=0 current clamp perforated patch. Figure 6 shows the ability of each of the three systems to produce a depolarization. In particular, the depolarization

increases as the time of the stimulus increases. For every stimulation technique the stimulus duration was set to induce a membrane potential fluctuation of about 10 mV. The frequency of stimulation was carefully chosen in order to allow cells to recover their original condition after each stimulus, preventing a putative accumulation of calcium and/or a constant cell membrane depolarization. The stimulus frequency was set at 1 Hz for FP and EMF stimulations and 0.1 Hz for optogenetic stimulation. The goal was to couple the stimulation with metformin treatment to strengthen metformin's inhibitory action on tmCLIC1 function.

Once determined the ability of the systems to cause a depolarization of the cell membrane we evaluated the proliferation of two patient-derived GSCs primary cultures after 72 or 96 hours in a dose-response manner with increasing metformin concentrations and in the absence or presence of stimulation (figure 7). In all the cases stimulation was able to enhance the effect

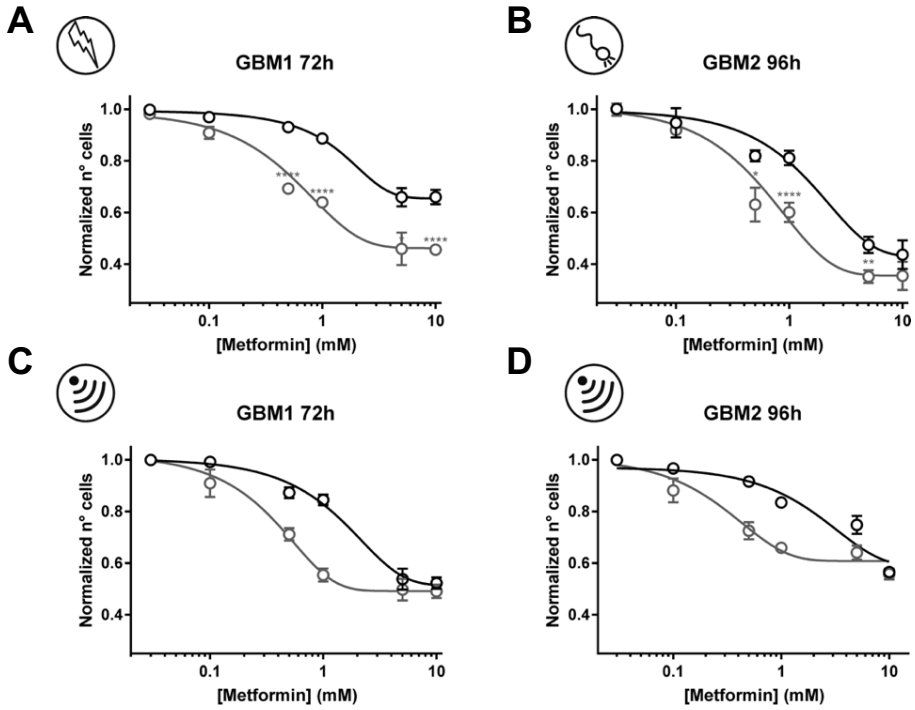

*Figure 7. A) Number of cells after 72 hours incubation with increasing metformin concentrations in absence (black) or presence (grey) of field potential stimulation (t-test metformin 1 mM: n=19, ****p<0,0001). B) Number of cells after 96 hours incubation with the same metformin concentrations as above in absence (black) or presence (grey) of optogenetic stimulation (t-test metformin 1 mM: n=19, ****p<0,0001). C-D) Effect on GSCs proliferation of increasing concentration of metformin in absence (black) or presence (grey) of EMF stimulation (t-test metformin 1 mM: GBM1 n=13, ****p<0,0001; GBM2 n=21, ****p<0,0001). In all conditions, at concentration ranging from 0,1 to 10 mM, the stimulation produces an improvement of metformin effect. We identified 1 mM as the optimal working concentration to work with, exerting the maximum divergency compared to non-stimulated conditions.*

of metformin compared to non-stimulated conditions. In particular, we identified 1 mM as the optimal working concentration to work with as it shows a relatively low anti-proliferative effect in control conditions while exerts the maximum effect – comparable to 10 mM in non-stimulated cells - when combined with stimulation. For this reason, the following experiment involving stimulation were all performed at 1 mM metformin concentration.

5.6 Testing the ability of the technique to specifically enhance the antiproliferative effect of metformin

To test whether metformin is the only compound whose effect is enhanced by stimulation we investigated a series of anti-proliferative compounds in combination with stimulation. The drugs tested were: IAA94 (CLIC1 specific inhibitor), rapamycin (mTOR inhibitor which is canonically considered to be involved in metformin intracellular pathway) and temozolomide (glioblastoma standard of care to date). Each compound was first tested in a dose-response manner in order to find the optimal anti-proliferative concentration exerted on the two GSCs cultures (figure 8).

The concentration was set as the IC50 observed after 72 or 96 hours on the targeted cells. Working with a non-saturating concentration would allow to observe the effect of stimulation on the given compound - if any - and at the same time mimics the approach used with

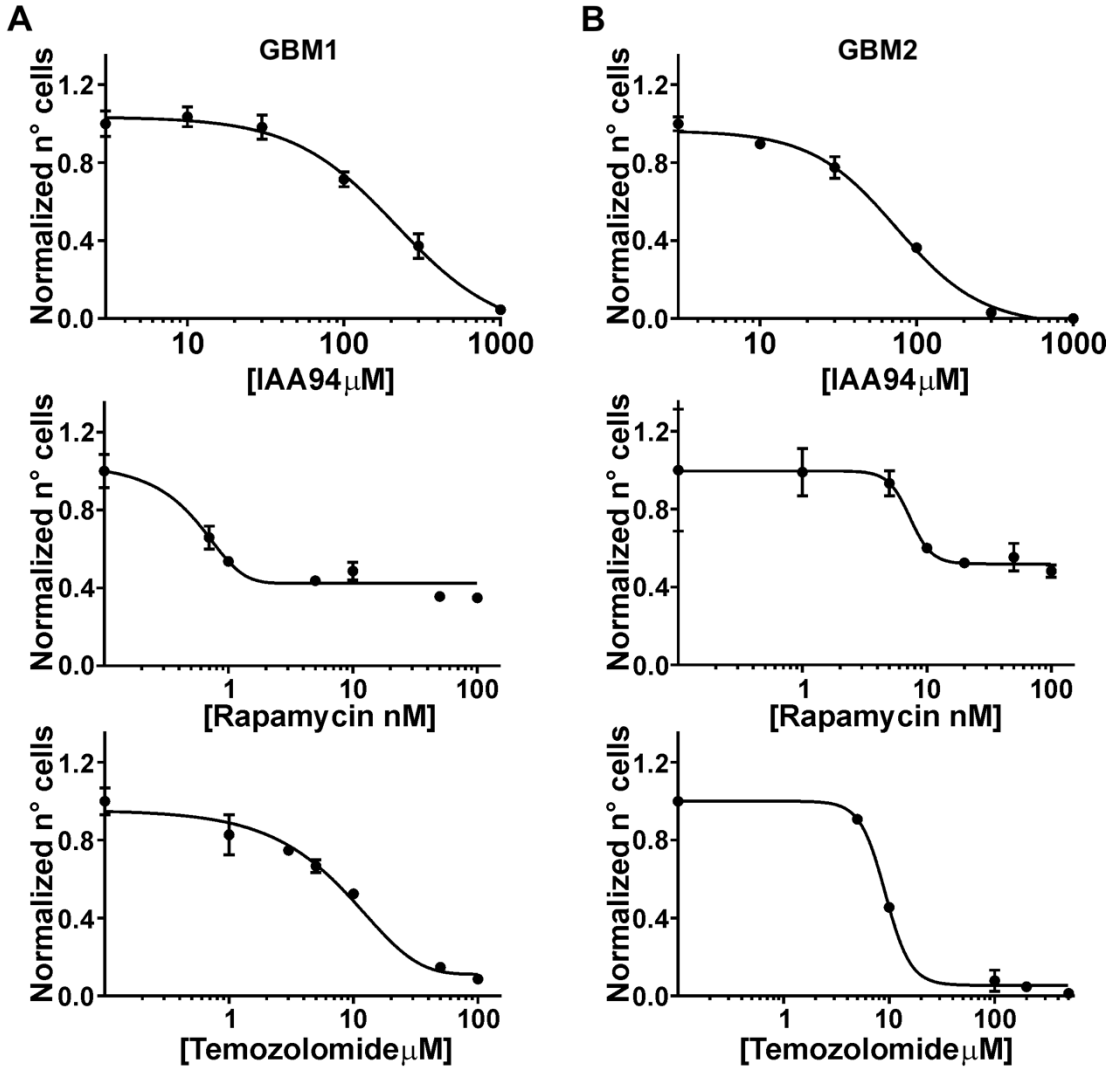

Figure 8. A) Number of cells after 72 hours incubation with increasing dose of IAA94, rapamycin and temozolomide in GBM1 cells. B) Number of cells after 96 hours incubation with increasing dose of IAA94, rapamycin and temozolomide in GBM2 cells. The same concentration of every compound exerted a similar effect except for rapamycin which was found to have a 10 times stronger effect on GBM1 compared to GBM2 cells.

metformin. The results plotted in figure 9 show that metformin is the only drug whose effect is enhanced by stimulation. Since IAA94 didn't show a behavior similar to that of metformin we hypothesized that this outcome is strictly dependent on the increased CLIC1 open probability which enhances the interaction between the drug and its target. Acting from the external side IAA94 doesn't need any tmCLIC1 conformational change. A further confirmation comes from the lack of the same effect on rapamycin-treated cells. This result allowed us to exclude the involvement of the putative canonical intracellular pathway in the investigated mechanism.

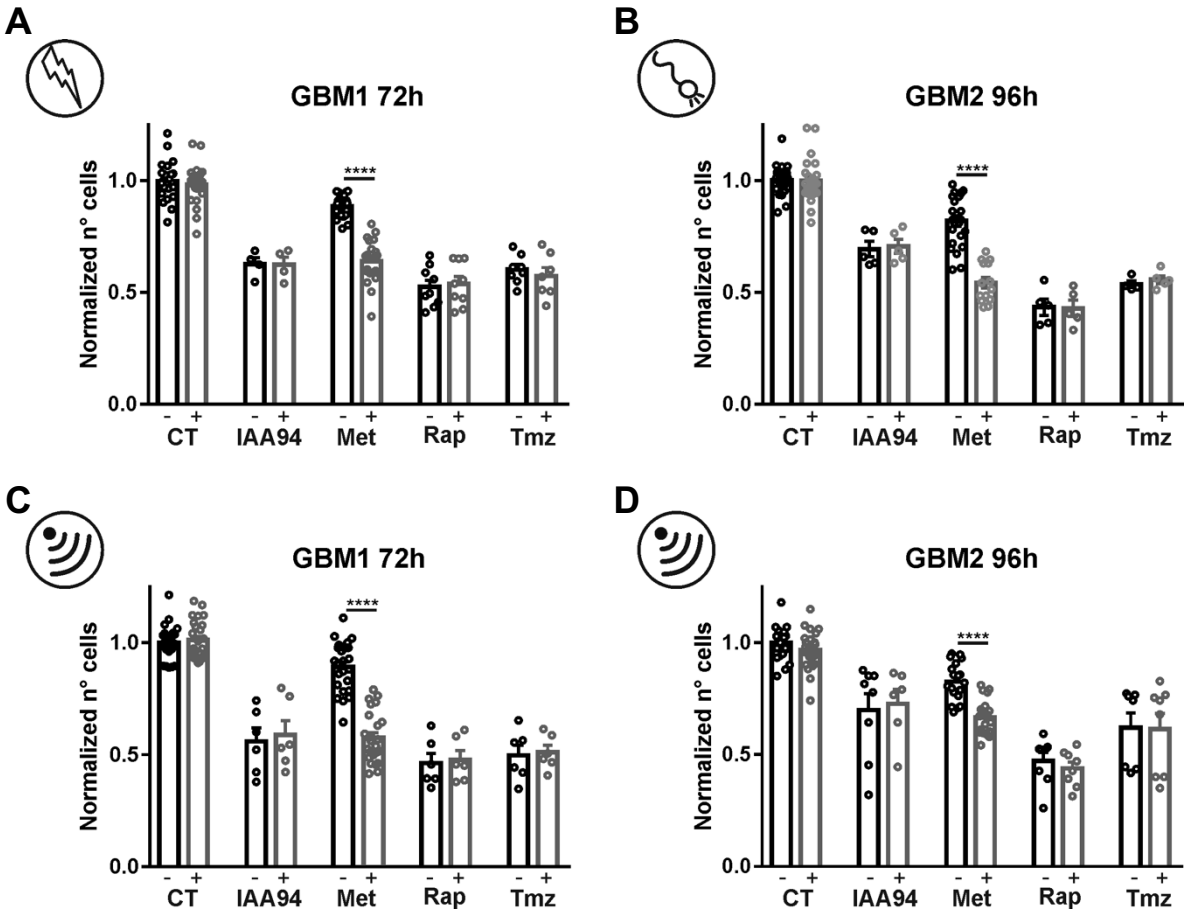

*Figure 9. A) Number of cells after 72 hours incubation with IAA94, metformin, rapamycin and temozolomide in absence (black) or presence (grey) of field potential stimulation (t-test metformin: n=24, ****p<0,0001). B) Number of cells after 96 hours incubation with the same compounds as above in absence (black) or presence (grey) of optogenetic stimulation (t-test metformin: n=18, ****p<0,0001). C-D) Number of cells after 72/96 hours incubation with the same compounds in absence (black) or presence (grey) of EMF stimulation (t-test metformin: GBM1 n=24; GBM2 n=19 ****p<0,0001).*

5.7 Investigating the effect of repetitive membrane potential oscillations on metformin's inhibition kinetics

Besides having observed the phenomenon in terms of tumor proliferation the study on stimulation-coupled metformin treatment was carried out at a mechanistic level as well. To deeply investigate the effect of stimulation on metformin-tmCLIC1 interaction, we performed patch clamp experiments using a time-course protocol. This kind of experimental procedure provides information about the kinetics of inhibition of metformin. The rationale behind this approach stands on the assumption that inducing repetitive membrane depolarizations should expose more metformin's binding sites – since it should increase tmCLIC1 open probability - resulting in faster kinetics of inhibition under stimulation conditions. The experiments were performed using both optogenetics and EMF stimulation systems on two patient derived GSCs primary cultures. The left panel of figure 10 shows representative traces displaying that stimulation is able to speed up metformin's kinetics of inhibition compared to control condition. The numerical values of the slope of the fitting red line which interpolates the decreasing current of each individual experiment were plotted in the right panel. As shown, the measured slope values under stimulation are increased significantly compared to control

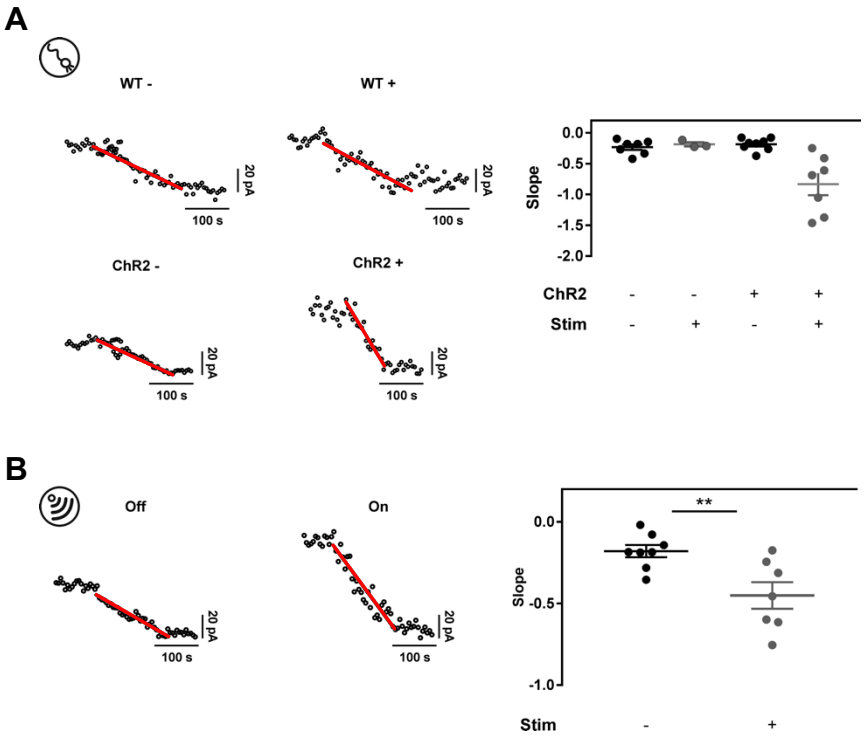

*Figure 10. A) Representative time-course of whole-cell currents in WT and Chr2-transfected GSCs in the absence (-) or presence (+) of the blue light stimulus. Cells were stimulated every 5 seconds with 800 ms, +60 mV test potential from resting potential. Each point represents the average current of the last 100 ms of a single current trace. Once the current amplitude reached a constant value, metformin 5mM was added to investigate the kinetic of the current inhibition (red line). On the right, the the slopes calculated in each single experiment (Two-way ANOVA: n=7, ***p=0,0002) are plotted for each experimental condition. B) Representative time-course of whole-cell currents in presence or absence of EMF stimulation. In the right panel, all the slope values measured (t-test: n=7, **p=0,0075) are plotted.*

conditions, demonstrating that the kinetics of inhibition are markedly influenced by repetitive membrane potential oscillations

5.8 Repetitive membrane potential oscillations enhance metformin antiproliferative effect by interacting with the Arg29 inside CLIC1 pore region

The results collected strongly support the hypothesis that in GSCs primary cultures metformin binds to tmCLIC1 through a specific amino acid, the positively charged arginine 29, located inside the pore region of the transmembrane CLIC1 isoform. This evidence is consistent with the rationale behind the stimulation approach: inducing repetitive membrane potential oscillations to increase tmCLIC1 open probability and, consequently, metformin efficiency. This is because an increase in tmCLIC1 close to open transition would increase the

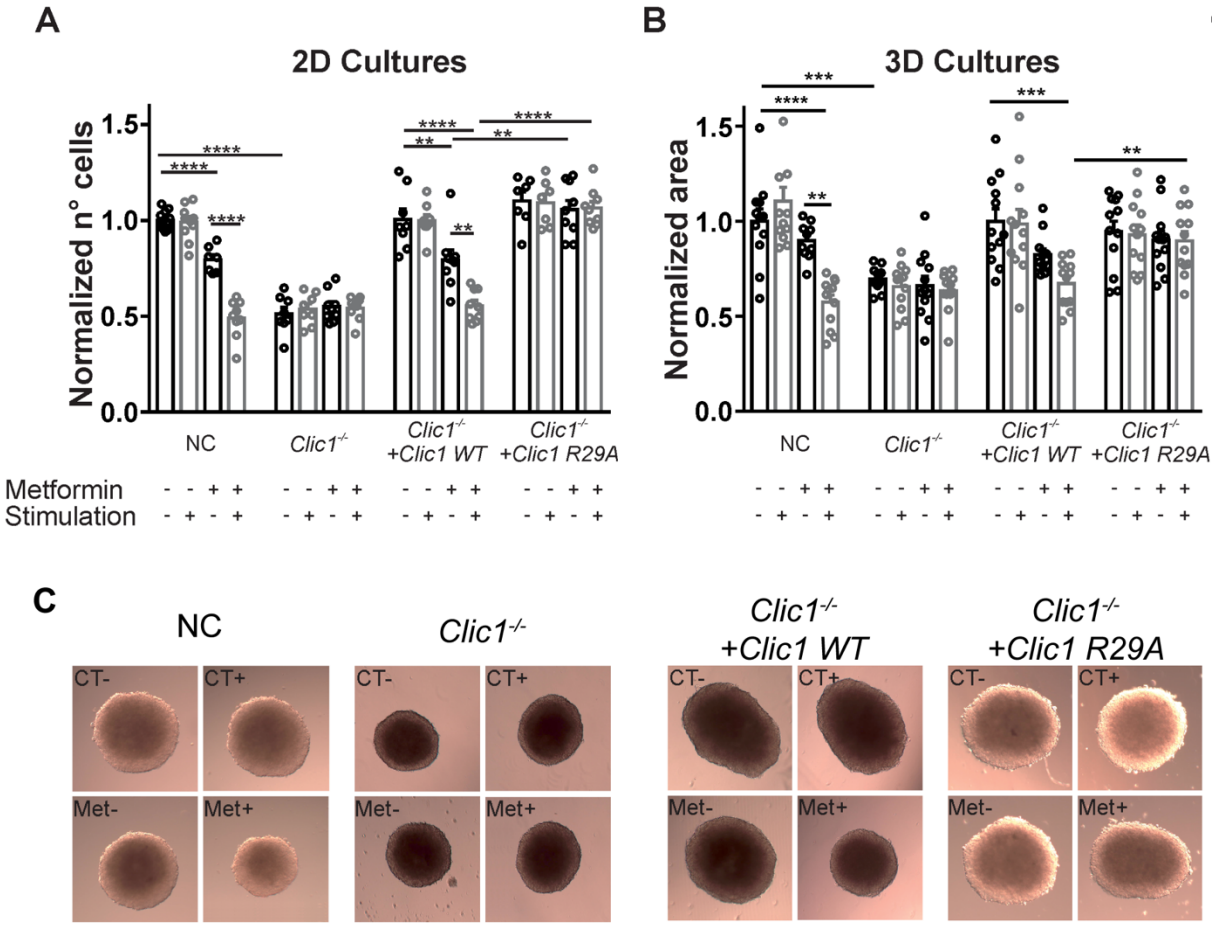

*Figure 11. A) Number of cells after 72 hours in the absence (black) or presence (grey) of EMF stimulation. Cells were incubated with 1mM metformin as indicated in the bottom part of the graph. EMF is able to significantly increase the metformin effect on proliferation both on NC and WT rescued cells, while showing no effect on KO and R29A rescued cells (NC: CT- (n=12) vs Met- (n=7) and Met- vs Met+ (n=9), two-way ANOVA, ****p<0,0001; Clic1-/-+Clic1 WT: two-way ANOVA; CT- (n=8) vs Met- (n=9) and Met- vs Met+ (n=9), ****p<0,0001; NC vs Clic1-/- (n=7): CT-, t-test, ****p<0,0001; Clic1-/-+Clic1 WT vs Clic1-/-+Clic1 R29A: Met- (n=9), t-test, **p=0,0017; Met+ (n=9), t-test, ****p<0,0001). B) Spheroids' area measured at 72 hours post 3D structures formation in the absence (black) or presence (grey) of EMF stimulation. Cells were incubated with 1mM metformin as indicated in the bottom part of the graph. EMF is able to produce an outcome similar to what was observed in 2D cultures (NC (n=12): two-way ANOVA, CT- vs Met+, ****p<0,0001; Met- vs Met+ **p=0,0018; Clic1-/-+Clic1 WT (n=12): two-way ANOVA; CT- vs Met+, ***p=0,0009; NC vs Clic1-/- (n=12): CT-, t-test, ***p=0,0002; Clic1-/-+Clic1 WT vs Clic1-/-+Clic1 R29A: Met+ (n=12), t-test, **p=0,0012).*

number of metformin available binding sites and the probability of the drug to bind to its target. The best way to test the correlation between stimulation-coupled metformin treatment and CLIC1 is the same genetic background used in previous experiments. In particular, the cellular population which would be crucial to link stimulation-metformin effect to CLIC1 would be the R29A rescue. The reason depends on the insensitivity of this cellular population towards metformin still maintaining tmCLIC1 functional activity. For this reason, if we would see no effect of the stimulation-coupled metformin treatment on these cells we could finally assert that the whole procedure works by increasing the availability of metformin binding sites through the increase of tmCLIC1 open probability. We tested this phenomenon using only EMF stimulation since the effect of all the three systems was shown to produce similar outcomes.

In figure 11 we show the results collected in 2D and in 3D in the four cellular background in thw absence or presence of stimulation, with or without incubation with 1 mM metformin. As expected, the effect on proliferation previously observed in Figure 2 and 4 is similar in NC cells as well as in WT rescued cells. Since KO cells previously showed no alteration of the proliferation (Figures 2-4) at 5 mM metformin concentration we also expected the same results at 1 mM as well. For the same reason we expected that EMF would not enhance metformin effect in any way. R29A rescued cells didn't show any alteration of the proliferation when exposed to metformin alone or coupled with stimulation as well. This outcome strongly supports the initial hypothesis that repetitive membrane potential oscillations enhance metformin's antiproliferative effect on glioblastoma stem cells through the increase of tmCLIC1 open probability.

5.9 In Vivo

The solid results obtained *in vitro* allowed the transition to the mouse model in order to have the possibility to better validate the whole strategy. The experimental procedure was conducted in Pisa CNR in collaboration with the group of Professor Matteo Caleo. The experiments were performed on immunocompetent mice stereotactically injected with a Channelrhodopsin-infected murine glioblastoma cell line (GL261) and stimulated through the optic fiber. Preliminary electrophysiological experiments performed on GL261 have shown a significant tmCLIC1-mediated current (Figure 12A). In addition, experiments performed at different time-points from G1 synchronization have shown a tmCLIC1 activity timing similar to what observed in human GSCs[47]. The *in vivo* experimental procedure consists of a daily two-hours (intermittent) stimulation carried out for five consecutive days (for details, see

Materials and Methods section). For this reason, the switch from chronic stimulation to the intermittent one was supported by previously *in vitro* experiments performed on GL261 cells

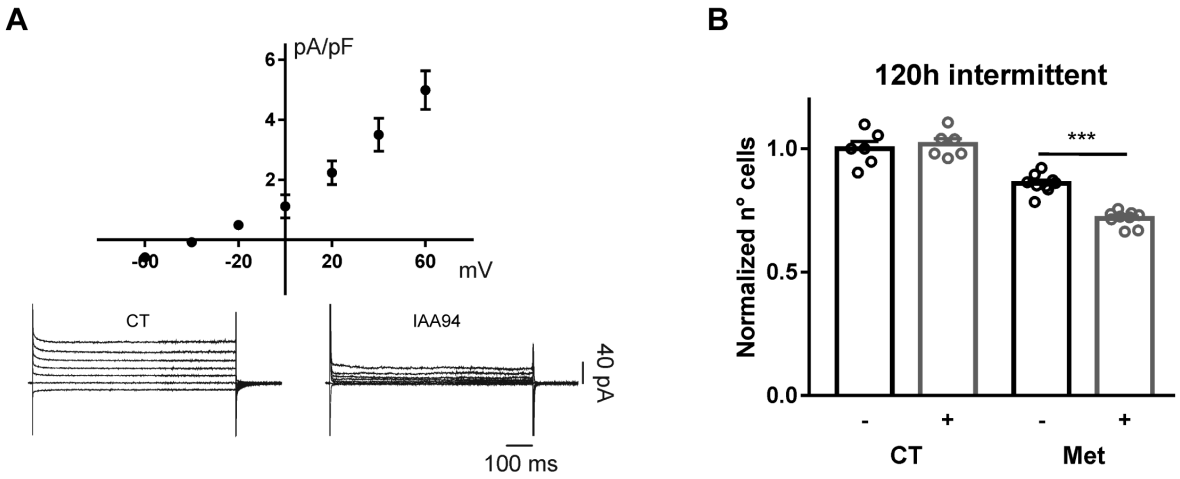

*Figure 12. A) Current density/voltage relationship of CLIC1 mediated current (top) in GL261 cells obtained from the subtraction of IAA94 sensitive current from the total whole cell current (bottom). B) Number of cells after 120 hours in absence (black) or presence (grey) of daily 2 hours optogenetic stimulation. Cells were incubated with 1mM metformin as indicated in the bottom part of the graph. Stimulation is effective in enhancing metformin antiproliferative effect even if delivered only 2 hours per day (Met- vs Met+ (n=9), two-way ANOVA, ***p=0,0001.*

following the same protocol. Figure 12B shows that the effect of intermittent-optogenetic stimulation in combination with 1mM metformin treatment was consistent with the results observed in patient-derived glioblastoma stem cells primary cultures (Figure 7B and 9B).

To measure the expansion of the implanted tumor Ki67 nuclear protein levels and BrdU incorporation were measured in mouse brain tumor slices at the end of the experimental procedure. The results depicted in figure 13 are coherent to what observed *in vitro* and point out that optogenetic stimulation is able to strengthen metformin efficiency in impairing tumor growth. These solid preliminary data are extremely encouraging and represent a solid starting point for future investigations.

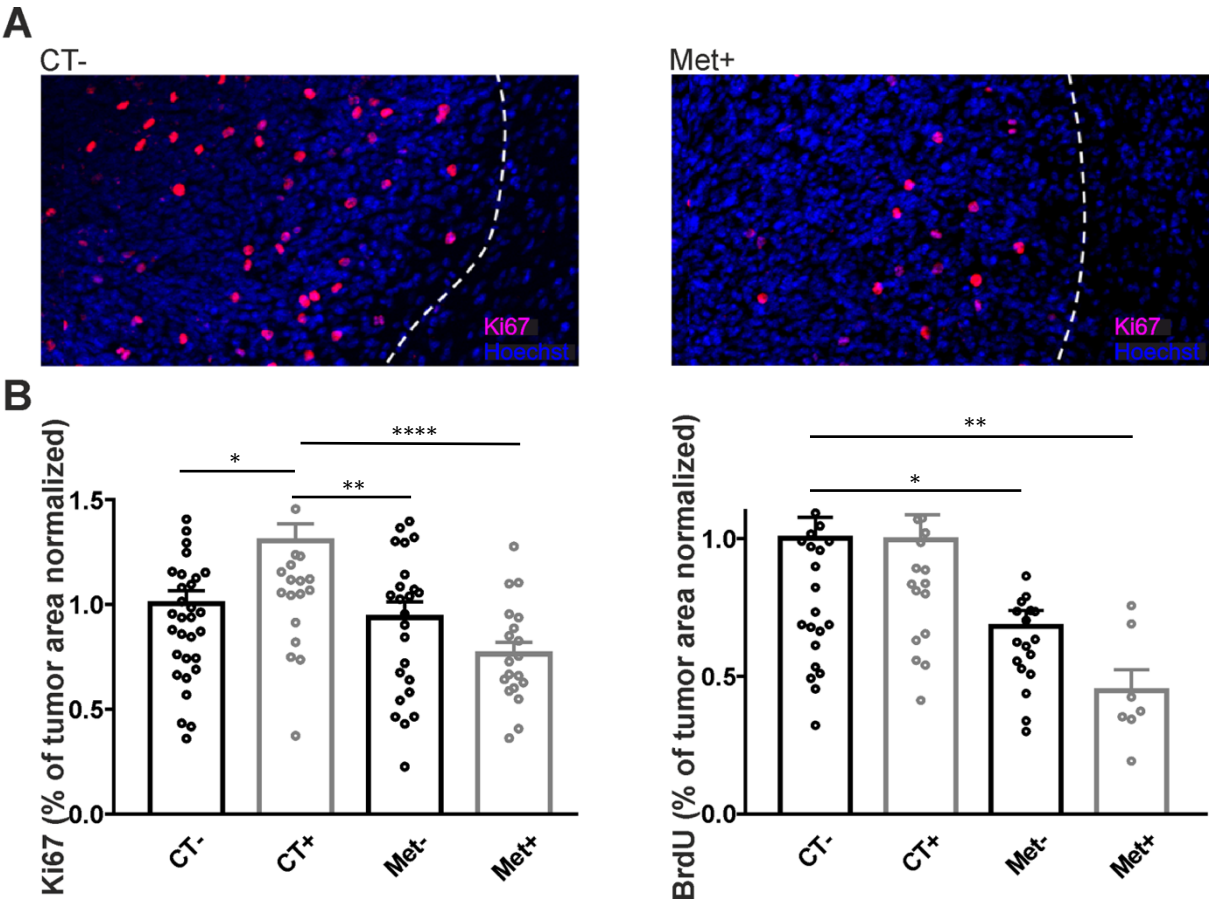

*Figure 13. A) Representative graph of Ki67 staining positive cells in mouse brain tumor slices untreated or treated with metformin + stimulation. B) Preliminary results of Ki67 expression (left) and BrdU incorporation levels (right) measured in mouse brain tumor slices after treatment in absence (black) or presence (blue) of optogenetic stimulation. Metformin administration combined with intermittent optogenetic stimulation reduces active tumor expansion compared to metformin treatment itself (Ki67: two-way ANOVA; Ct- (n=34) vs Ct+ (n=28) *p=0,0113; Ct+ vs Met- (n=25) **p=0,0029; Ct+ vs Met+ (n=19) ****p<0,0001. BrdU: two-way ANOVA; Ct- (n=30) vs Met- (n=19) *p=0,0129; Ct- vs Met+ (n=7) **p=0,0017).*

6. Discussion

So far glioblastoma (GB) represents one of the most challenging tumors to clinically cope with. The reason could be sought within primary aspects of this disease. First of all, the tumor originates in the most critical area of human body. The presence of the skull represents a mechanical constraint responsible for increased intracranial pressure which can further exasperate the effects of cancer itself. In addition, approaches pursued to hit cancer cells are limited by the blood brain barrier acting as a filter towards the tumor. Advances in knowledge and technology have been able to extend life expectancy to an average of 15 months after diagnosis. In the perspective to set a more effective therapy, it is important to develop new strategies to counteract the progression of glioblastoma. It is now well established that one of the causes making GB the deadliest glioma can be attributed to a pool of slow proliferating asymmetrically dividing cells. This cellular pool is known as glioblastoma stem cells (GSCs). GSCs are able to generate both other stem cells as well as fast proliferating cells constituting the tumor mass. This specific feature gives rise to a self-sustaining mechanism, which favors tumor development. The opportunity to target preferentially CSCs would be instrumental mainly to hit the "fuel" of the tumor, being the cause of GB resistance to conventional therapy and tumor relapse. In this scenario the transmembrane form of CLIC1 protein (tmCLIC1) represents a promising pharmacological target.

An important aspect to be considered is the peculiar feature of tmCLIC1. The chronic expression of CLIC1 on the plasma membrane is symptomatic of cells in a hyperactivated state. We extensively elucidated this feature in glioblastoma stem cells in previous investigations[59, 68, 47]. Besides the fact that tmCLIC1 has a functional role in the progression of GB *in vitro* as well as *in vivo,* it could also work as a sensor of alteration of cellular homeostasis. Chronic cellular stress stimuli act as a trigger for CLIC1 insertion into the plasma membrane. This would mean not only that tmCLIC1 plays an active role in GB progression, but also that its localization could be considered a marker of allostatic conditions like cancer. In addition, GSCs appears to show significantly higher levels of tmCLIC1 compared to tumor bulk cells. Though aiming at tmCLIC1 would mean to have the opportunity to discriminate and hit preferentially glioblastoma stem cells.

Unfortunately, the only compound to date known to impair tmCLIC1 function is IAA94 which has shown to be unusable due to kidney toxicity *in vivo.* Recent investigations have shown that in patient derived GSCs tmCLIC1 is a preferential target of the anti-diabetic drug metformin[68, 47209]. Several positive aspects need to be considered. First of all, the drug is already on the pharmaceutical markets. This would mean that no drug development and/or clinical

trials are required. For this reason, metformin usage would allow considerable savings in terms of time and money. Secondly, metformin treatment has proven to be well tolerated. According to current type-2 diabetes standard of care the daily administered doses of metformin spans between 2550 and 3000 mg with acceptable side effects. The downside is that metformin operative concentration to fully impair tmCLIC1 function stands between 5 and 10 mM. Such concentration is unattainable in patients' tissues where the measured drug concentration has shown to be in the order of μM. This picture is further undermined by the fact that the brain is more difficult to be pharmacologically reached. Consequently, the only way to reason about a putative metformin-based therapy would be to lower metformin operative concentration. Starting from this premise the approach pursued in my thesis work was to develop a strategy aimed to lower metformin operative concentration.

First, the experiments performed in a cellular background deprived of *Clic1* were instrumental to relate metformin treatment to CLIC1 function. GSCs *Clic1*$^{-/-}$ treated with different metformin concentration show that the knockout of the gene prevents the anti-proliferative effect of metformin both in 2D cultures as in 3D models (Figures 2-4). Metformin chronic incubation (5mM) was not able to produce any outcome in *Clic1*$^{-/-}$ GSCs nor was able to affect the proliferation and/or functional activity in R29A rescued cells (Figure 5). These results highlight simultaneously two pieces of evidence. The first information is that the Arg29 amino acid is responsible for metformin's binding to tmCLIC1 protein. The second and unexpected evidence is that *Clic1* impairment is sufficient to affect totally metformin antitumoral effect on patient derived glioblastoma stem cells. Although the latter aspect will be carefully validated upon several other patient derived GSCs, this suggests that tmCLIC1 can operate as the only receptor of metformin action within glioblastoma stem cells. This would explain the unusual behavior of these cells under metformin exposure. Glioblastoma stem cells have been reported to rely on both glycolysis and OXPHOS energetic pathways. Therefore, the blockade of one metabolic pathway should not affect the ability of cells to produce energy since they would fall back on the other one. This doesn't fit with the fact that GSCs exposed to metformin show a delayed cell cycle progression (Figure 3). Conversely, the inhibition exerted by metformin is in accordance with the pharmacological inhibition of tmCLIC1 and/or the KO of the gene. This reasoning suggests that tmCLIC1 could be the solely responsible for metformin's anti-proliferative effect in GSCs. Such a behavior would not exclude a putative ultimate cytoplasmic effect. In this scenario tmCLIC1 would appear as a metformin receptor, triggering downstream responses. An alternative but possible mechanism would consider tmCLIC1 as a metformin transporter. Metformin would bind to tmCLIC1 impairing its function. This would reflect in an internalization of metformin due to the

turnover of the CLIC1 membrane proteins. Once in the cytoplasm, metformin would exert its anti-proliferative function maybe targeting mitochondria or other secondary targets.

After validating the interdependence between metformin and tmCLIC1 in GSCs the strategy was to increase the affinity between metformin and its target. Since we were able to conclude that the drug binds tmCLIC1 only when the channel is in its open state (Figure 11), we took advantage of its specific biophysical properties. tmCLIC1 voltage-dependency allowed us to induce extremely low-frequency repetitive membrane potential depolarizations to increase the number of drug's binding sites in a given time. The strategy demonstrated to be functional to our purpose, producing a 10-fold decrease of metformin dose to exert the maximum effect in patient derived cancer stem cells primary cultures (Figures 7, 9, 11). Unfortunately, although stimulation strengthens up to 10-fold the effect of metformin, 1 mM is a concentration impossible to reach in the brain area. In particular, the drug's concentration measured in homogenates of the whole brain of stimulated GB mice drinking metformin is approximately 0.3 mM. However, the data depicted in Figure 13 show that optogenetic stimulation of the same murine glioblastoma model produces a reduction of the tumor mass in accordance with *in vitro* experiments. This outcome opens up several hypotheses. It is possible that (i) the continuous supply of metformin in the drinking water provides constant fresh drug circulation; (ii) metformin accumulates in the brain tissue; (iii) the tumor vascularization conveys a sufficient amount of drug able to interact with tmCLIC1 in the presence of stimulation. We take into account that the three proposed mechanisms may work together. In addition, Figure 12B shows that the two hours of stimulation per day produces *in vitro* an effect consistent to what observed exposing cells to a chronic session. This result raised the hypothesis that metformin binding with tmCLIC1 may be irreversible. Therefore, it would be sufficient to expose all the binding sites to metformin even in a limited timeframe, to impair cellular proliferation. Taking into account that metformin presence in the human body was measured to last approximately 2 days the drug could have the possibility to interact also with new tmCLIC1 proteins shuttled in the membrane to compensate the impaired ones. To test *in vitro* a putative irreversible interaction, we exposed cells to 5 mM metformin for 10 minutes, 1 hour and chronically, for 72 hours. Figure 14 shows that 10 minutes exposure to metformin saturating concentration is sufficient to have the same antiproliferative

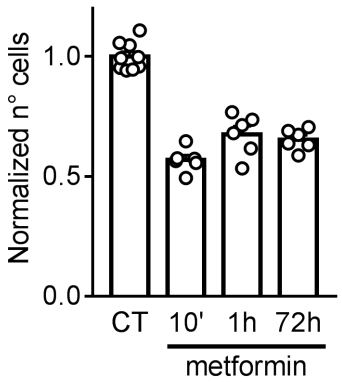

*Figure14. Normalized number of cells after 10', 1 hours and 72 hours exposure to 5 mM metformin. Each time of exposure has shown to be significantly different compared to control ****p0,0001 one-way ANOVA*

effect compared to a chronic treatment. This result strengthens the hypothesis that metformin binds irreversibly to tmCLIC1.

Observing Ki67 protein expression depicted in panel B of Figure 13 it is evident that stimulation alone causes an increased proliferation in tumor area. This effect could be seen also in the former *in vitro* experiments, although it appears as a not relevant trend. To test the effect of stimulation *in vitro* we exposed GL261 cells to optogenetic stimulation and we measured the pERK/ERK ratio as a predictor of activated cellular proliferation. The results shown in Figure 15 suggest that stimulation alone tends to promote cellular proliferation also *in vitro.* This behavior could be explained considering at least two hypotheses. The first one take into account that optogenetic stimulation produces a non-selective cationic inward current including - among the different cations – Ca^{++} flow. Calcium intake has been widely demonstrated to be a signal of cellular proliferation. The second hypothesis involves tmCLIC1 functional activity. Depolarizing stimuli would trigger tmCLIC1 function, encouraging the proliferation of cancer cells. The latter hypothesis is consistent with the rationale on which our proposed strategy stands. The effect may be exacerbated by the possibility that *in vivo* the tumor can get more nutrients.

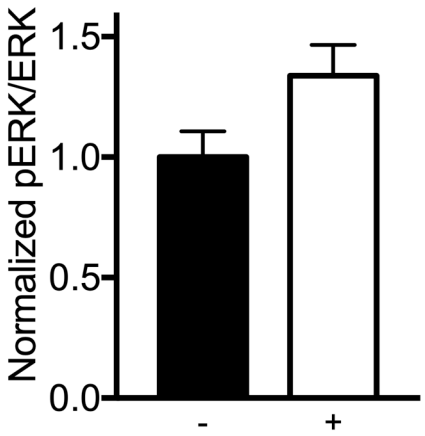

Figure 15. pERK/ERK ratio measured in GL261 cells in absence (filled histogram) or presence (empty histogram) of optogenetic stimulation. Stimulation tends to promote (not significantly) cellular proliferation.

The advantage of optogenetic stimulation is represented by the possibility to directly target cells expressing ChR2. This is functional to our purpose in order to strengthen our hypotheses limiting the phenomenon to a restricted subset of cells. The drawback is represented by the impossibility to use such a strategy on humans. Our translational strategy to GB patients would be to mimic the effect produced by optogenetic stimulation on murine models. Therefore, we propose pulsed electromagnetic stimulation in combination with metformin administration. The strategy is known *in vivo* as repetitive transcranial magnetic stimulation (rTMS), a non-invasive technique able to cause an electric current to a targeted brain area. The current is generated through a coil placed near the scalp. A changing magnetic field applied to the coil is able, in turn, to generate a sub-threshold current in the specific site. The procedure is safe and approved by the Food and Drug Administration. We are currently testing the procedure on GB mice to compare the results obtained with optogenetic stimulation.

According to our preliminary studies, the technique should enhance metformin's action on tmCLIC1 causing an impairment of tumor growth. In addition, the literature reports

transcranial stimulation to be able to exert an activating effect of microglia in murine models. This could be helpful in order to recruit the immune response towards the tumor.

An alternative strategy to target tmCLIC1 would be to find a molecule similar to metformin but with an increased affinity for tmCLIC1. Such a molecule would exert the same effect of metformin but at lower dosage. In addition, it could benefit by repetitive membrane potential oscillations to further increase its effect. Although this approach would be extremely helpful, the downside stands on the fact that such a molecule would undergo drug development and clinical trials, reflecting on a large investment in time. We are currently testing a series of synthetic biguanide compounds. We identified, among all, a compound able to impair tmCLIC1 functional activity and GSCs proliferation at 100-fold less concentration compared to metformin.

In a broad view, metformin dietary administration together with rTMS could represent a potential adjuvant therapy for glioblastoma. Taking advantage of tmCLIC1 peculiar localization into the membrane of glioblastoma cancer stem cells this therapeutic approach may potentiate the effects of the traditional GB standard of care, targeting those cells able to escape the canonical therapies.

7. References

1 Ostrom, Q. T. *et al.* The epidemiology of glioma in adults: a "state of the science" review. *Neuro Oncol* **16**, 896-913, doi:10.1093/neuonc/nou087 (2014).

2 Stupp, R. *et al.* High-grade glioma: ESMO Clinical Practice Guidelines for diagnosis, treatment and follow-up. *Ann Oncol* **25 Suppl 3**, iii93-101, doi:10.1093/annonc/mdu050 (2014).

3 Sanai, N., Alvarez-Buylla, A. & Berger, M. S. Neural stem cells and the origin of gliomas. *N Engl J Med* **353**, 811-822, doi:10.1056/NEJMra043666 (2005).

4 Jones, T. S. & Holland, E. C. Molecular pathogenesis of malignant glial tumors. *Toxicol Pathol* **39**, 158-166, doi:10.1177/0192623310387617 (2011).

5 Behin, A., Hoang-Xuan, K., Carpentier, A. F. & Delattre, J. Y. Primary brain tumours in adults. *Lancet* **361**, 323-331, doi:10.1016/S0140-6736(03)12328-8 (2003).

6 Davis, M. E. Glioblastoma: Overview of Disease and Treatment. *Clin J Oncol Nurs* **20**, S2-8, doi:10.1188/16.CJON.S1.2-8 (2016).

7 Plate, K. H., Breier, G., Farrell, C. L. & Risau, W. Platelet-derived growth factor receptor-beta is induced during tumor development and upregulated during tumor progression in endothelial cells in human gliomas. *Lab Invest* **67**, 529-534 (1992).

8 Levine, A. J., Momand, J. & Finlay, C. A. The p53 tumour suppressor gene. *Nature* **351**, 453-456, doi:10.1038/351453a0 (1991).

9 Kleihues, P. & Ohgaki, H. Primary and secondary glioblastomas: from concept to clinical diagnosis. *Neuro Oncol* **1**, 44-51, doi:10.1093/neuonc/1.1.44 (1999).

10 Thakkar, J. P. *et al.* Epidemiologic and molecular prognostic review of glioblastoma. *Cancer Epidemiol Biomarkers Prev* **23**, 1985-1996, doi:10.1158/1055-9965.EPI-14-0275 (2014).

11 Westphal, M. & Lamszus, K. The neurobiology of gliomas: from cell biology to the development of therapeutic approaches. *Nat Rev Neurosci* **12**, 495-508, doi:10.1038/nrn3060 (2011).

12 Paolillo, M., Boselli, C. & Schinelli, S. Glioblastoma under Siege: An Overview of Current Therapeutic Strategies. *Brain Sci* **8**, doi:10.3390/brainsci8010015 (2018).

13 Wilson, T. A., Karajannis, M. A. & Harter, D. H. Glioblastoma multiforme: State of the art and future therapeutics. *Surg Neurol Int* **5**, 64, doi:10.4103/2152-7806.132138 (2014).

14 Esteller, M. *et al.* Inactivation of the DNA-repair gene MGMT and the clinical response of gliomas to alkylating agents. *N Engl J Med* **343**, 1350-1354, doi:10.1056/NEJM200011093431901 (2000).

15 Stupp, R. *et al.* Radiotherapy plus concomitant and adjuvant temozolomide for glioblastoma. *N Engl J Med* **352**, 987-996, doi:10.1056/NEJMoa043330 (2005).

16 Stupp, R. *et al.* Maintenance Therapy With Tumor-Treating Fields Plus Temozolomide vs Temozolomide Alone for Glioblastoma: A Randomized Clinical Trial. *JAMA* **314**, 2535-2543, doi:10.1001/jama.2015.16669 (2015).

17 Wang, Y., Pandey, M. & Ballo, M. T. Integration of Tumor-Treating Fields into the Multidisciplinary Management of Patients with Solid Malignancies. *Oncologist*, doi:10.1634/theoncologist.2017-0603 (2019).

18 Davis, M. E. Tumor treating fields - an emerging cancer treatment modality. *Clin J Oncol Nurs* **17**, 441-443, doi:10.1188/13.CJON.441-443 (2013).

19 Nabors, L. B. *et al.* Central Nervous System Cancers, Version 1.2015. *J Natl Compr Canc Netw* **13**, 1191-1202, doi:10.6004/jnccn.2015.0148 (2015).

20 Yi, Y., Hsieh, I. Y., Huang, X., Li, J. & Zhao, W. Glioblastoma Stem-Like Cells: Characteristics, Microenvironment, and Therapy. *Front Pharmacol* **7**, 477, doi:10.3389/fphar.2016.00477 (2016).

21 Potten, C. S. & Loeffler, M. Stem cells: attributes, cycles, spirals, pitfalls and uncertainties. Lessons for and from the crypt. *Development* **110**, 1001-1020 (1990).

22 Vescovi, A. L., Galli, R. & Reynolds, B. A. Brain tumour stem cells. *Nat Rev Cancer* **6**, 425-436, doi:10.1038/nrc1889 (2006).

23 Singh, H. Two decades with dimorphic Chloride Intracellular Channels (CLICs). *FEBS Lett* **584**, 2112-2121, doi:10.1016/j.febslet.2010.03.013 (2010).

24 Ignatova, T. N. *et al.* Human cortical glial tumors contain neural stem-like cells expressing astroglial and neuronal markers in vitro. *Glia* **39**, 193-206, doi:10.1002/glia.10094 (2002).

25 Galli, R. *et al.* Isolation and characterization of tumorigenic, stem-like neural precursors from human glioblastoma. *Cancer Res* **64**, 7011-7021, doi:10.1158/0008-5472.CAN-04-1364 (2004).

26 Denysenko, T. *et al.* Glioblastoma cancer stem cells: heterogeneity, microenvironment and related therapeutic strategies. *Cell Biochem Funct* **28**, 343-351, doi:10.1002/cbf.1666 (2010).

27 Bayin, N. S., Modrek, A. S. & Placantonakis, D. G. Glioblastoma stem cells: Molecular characteristics and therapeutic implications. *World J Stem Cells* **6**, 230-238, doi:10.4252/wjsc.v6.i2.230 (2014).

28 Nowell, P. C. The clonal evolution of tumor cell populations. *Science* **194**, 23-28, doi:10.1126/science.959840 (1976).

29 Cabioglu, N. *et al.* Increased lymph node positivity in multifocal and multicentric breast cancer. *J Am Coll Surg* **208**, 67-74, doi:10.1016/j.jamcollsurg.2008.09.001 (2009).
30 Nguyen-Khac, F. *et al.* Chromosomal abnormalities in transformed Ph-negative myeloproliferative neoplasms are associated to the transformation subtype and independent of JAK2 and the TET2 mutations. *Genes Chromosomes Cancer* **49**, 919-927, doi:10.1002/gcc.20802 (2010).
31 Shackleton, M., Quintana, E., Fearon, E. R. & Morrison, S. J. Heterogeneity in cancer: cancer stem cells versus clonal evolution. *Cell* **138**, 822-829, doi:10.1016/j.cell.2009.08.017 (2009).
32 Vermeulen, L., de Sousa e Melo, F., Richel, D. J. & Medema, J. P. The developing cancer stem-cell model: clinical challenges and opportunities. *Lancet Oncol* **13**, e83-89, doi:10.1016/S1470-2045(11)70257-1 (2012).
33 Xiang, D. *et al.* Nucleic acid aptamer-guided cancer therapeutics and diagnostics: the next generation of cancer medicine. *Theranostics* **5**, 23-42, doi:10.7150/thno.10202 (2015).
34 Scheel, C. *et al.* Paracrine and autocrine signals induce and maintain mesenchymal and stem cell states in the breast. *Cell* **145**, 926-940, doi:10.1016/j.cell.2011.04.029 (2011).
35 Lathia, J. D., Mack, S. C., Mulkearns-Hubert, E. E., Valentim, C. L. & Rich, J. N. Cancer stem cells in glioblastoma. *Genes Dev* **29**, 1203-1217, doi:10.1101/gad.261982.115 (2015).
36 Hemmati, H. D. *et al.* Cancerous stem cells can arise from pediatric brain tumors. *Proc Natl Acad Sci U S A* **100**, 15178-15183, doi:10.1073/pnas.2036535100 (2003).
37 Son, M. J., Woolard, K., Nam, D. H., Lee, J. & Fine, H. A. SSEA-1 is an enrichment marker for tumor-initiating cells in human glioblastoma. *Cell Stem Cell* **4**, 440-452, doi:10.1016/j.stem.2009.03.003 (2009).
38 Liu, G. *et al.* Analysis of gene expression and chemoresistance of CD133+ cancer stem cells in glioblastoma. *Mol Cancer* **5**, 67, doi:10.1186/1476-4598-5-67 (2006).
39 Bao, S. *et al.* Targeting cancer stem cells through L1CAM suppresses glioma growth. *Cancer Res* **68**, 6043-6048, doi:10.1158/0008-5472.CAN-08-1079 (2008).
40 Ogden, A. T. *et al.* Identification of A2B5+CD133- tumor-initiating cells in adult human gliomas. *Neurosurgery* **62**, 505-514; discussion 514-505, doi:10.1227/01.neu.0000316019.28421.95 (2008).
41 Kunzelmann, K. Ion channels and cancer. *J Membr Biol* **205**, 159-173, doi:10.1007/s00232-005-0781-4 (2005).
42 Prevarskaya, N., Skryma, R. & Shuba, Y. Ion channels and the hallmarks of cancer. *Trends Mol Med* **16**, 107-121, doi:10.1016/j.molmed.2010.01.005 (2010).
43 Cuddapah, V. A. & Sontheimer, H. Ion channels and transporters [corrected] in cancer. 2. Ion channels and the control of cancer cell migration. *Am J Physiol Cell Physiol* **301**, C541-549, doi:10.1152/ajpcell.00102.2011 (2011).
44 Yamaguchi, H. & Condeelis, J. Regulation of the actin cytoskeleton in cancer cell migration and invasion. *Biochim Biophys Acta* **1773**, 642-652, doi:10.1016/j.bbamcr.2006.07.001 (2007).
45 Litan, A. & Langhans, S. A. Cancer as a channelopathy: ion channels and pumps in tumor development and progression. *Front Cell Neurosci* **9**, 86, doi:10.3389/fncel.2015.00086 (2015).
46 Jiang, B. *et al.* Expression and roles of Cl- channel ClC-5 in cell cycles of myeloid cells. *Biochem Biophys Res Commun* **317**, 192-197, doi:10.1016/j.bbrc.2004.03.036 (2004).
47 Peretti, M. *et al.* Mutual Influence of ROS, pH, and CLIC1 Membrane Protein in the Regulation of G1-S Phase Progression in Human Glioblastoma Stem Cells. *Mol Cancer Ther* **17**, 2451-2461, doi:10.1158/1535-7163.MCT-17-1223 (2018).
48 Peretti, M. *et al.* Chloride channels in cancer: Focus on chloride intracellular channel 1 and 4 (CLIC1 AND CLIC4) proteins in tumor development and as novel therapeutic targets. *Biochim Biophys Acta* **1848**, 2523-2531, doi:10.1016/j.bbamem.2014.12.012 (2015).
49 Kobayashi, T. *et al.* Chloride intracellular channel 1 as a switch among tumor behaviors in human esophageal squamous cell carcinoma. *Oncotarget* **9**, 23237-23252, doi:10.18632/oncotarget.25296 (2018).
50 Singha, B. *et al.* CLIC1 and CLIC4 complement CA125 as a diagnostic biomarker panel for all subtypes of epithelial ovarian cancer. *Sci Rep* **8**, 14725, doi:10.1038/s41598-018-32885-2 (2018).
51 Liu, Y. *et al.* Chloride intracellular channel 1 regulates the antineoplastic effects of metformin in gallbladder cancer cells. *Cancer Sci* **108**, 1240-1252, doi:10.1111/cas.13248 (2017).
52 Xu, Y. *et al.* Expression of CLIC1 as a potential biomarker for oral squamous cell carcinoma: a preliminary study. *Onco Targets Ther* **11**, 8073-8081, doi:10.2147/OTT.S181936 (2018).
53 Littler, D. R. *et al.* The enigma of the CLIC proteins: Ion channels, redox proteins, enzymes, scaffolding proteins? *FEBS Lett* **584**, 2093-2101, doi:10.1016/j.febslet.2010.01.027 (2010).
54 Littler, D. R. *et al.* The intracellular chloride ion channel protein CLIC1 undergoes a redox-controlled structural transition. *J Biol Chem* **279**, 9298-9305, doi:10.1074/jbc.M308444200 (2004).
55 Murzin, A. G. Biochemistry. Metamorphic proteins. *Science* **320**, 1725-1726, doi:10.1126/science.1158868 (2008).
56 Averaimo, S., Milton, R. H., Duchen, M. R. & Mazzanti, M. Chloride intracellular channel 1 (CLIC1): Sensor and effector during oxidative stress. *FEBS Lett* **584**, 2076-2084, doi:10.1016/j.febslet.2010.02.073 (2010).

57 Liou, G. Y. & Storz, P. Reactive oxygen species in cancer. *Free Radic Res* **44**, 479-496, doi:10.3109/10715761003667554 (2010).
58 Panieri, E. & Santoro, M. M. ROS homeostasis and metabolism: a dangerous liason in cancer cells. *Cell Death Dis* **7**, e2253, doi:10.1038/cddis.2016.105 (2016).
59 Setti, M. *et al.* Functional role of CLIC1 ion channel in glioblastoma-derived stem/progenitor cells. *J Natl Cancer Inst* **105**, 1644-1655, doi:10.1093/jnci/djt278 (2013).
60 Peter, B., Ngubane, N. C., Fanucchi, S. & Dirr, H. W. Membrane mimetics induce helix formation and oligomerization of the chloride intracellular channel protein 1 transmembrane domain. *Biochemistry* **52**, 2739-2749, doi:10.1021/bi4002776 (2013).
61 Harrop, S. J. *et al.* Crystal structure of a soluble form of the intracellular chloride ion channel CLIC1 (NCC27) at 1.4-A resolution. *J Biol Chem* **276**, 44993-45000, doi:10.1074/jbc.M107804200 (2001).
62 Goodchild, S. C. *et al.* Oxidation promotes insertion of the CLIC1 chloride intracellular channel into the membrane. *Eur Biophys J* **39**, 129-138, doi:10.1007/s00249-009-0450-0 (2009).
63 Warton, K. *et al.* Recombinant CLIC1 (NCC27) assembles in lipid bilayers via a pH-dependent two-state process to form chloride ion channels with identical characteristics to those observed in Chinese hamster ovary cells expressing CLIC1. *J Biol Chem* **277**, 26003-26011, doi:10.1074/jbc.M203666200 (2002).
64 Achilonu, I., Fanucchi, S., Cross, M., Fernandes, M. & Dirr, H. W. Role of individual histidines in the pH-dependent global stability of human chloride intracellular channel 1. *Biochemistry* **51**, 995-1004, doi:10.1021/bi201541w (2012).
65 Tonini, R. *et al.* Functional characterization of the NCC27 nuclear protein in stable transfected CHO-K1 cells. *FASEB J* **14**, 1171-1178, doi:10.1096/fasebj.14.9.1171 (2000).
66 Averaimo, S. *et al.* Point mutations in the transmembrane region of the clic1 ion channel selectively modify its biophysical properties. *PLoS One* **8**, e74523, doi:10.1371/journal.pone.0074523 (2013).
67 Valenzuela, S. M. *et al.* The nuclear chloride ion channel NCC27 is involved in regulation of the cell cycle. *J Physiol* **529 Pt 3**, 541-552, doi:10.1111/j.1469-7793.2000.00541.x (2000).
68 Gritti, M. *et al.* Metformin repositioning as antitumoral agent: selective antiproliferative effects in human glioblastoma stem cells, via inhibition of CLIC1-mediated ion current. *Oncotarget* **5**, 11252-11268, doi:10.18632/oncotarget.2617 (2014).
69 Wulfkuhle, J. D. *et al.* Proteomics of human breast ductal carcinoma in situ. *Cancer Res* **62**, 6740-6749 (2002).
70 Chen, C. D. *et al.* Overexpression of CLIC1 in human gastric carcinoma and its clinicopathological significance. *Proteomics* **7**, 155-167, doi:10.1002/pmic.200600663 (2007).
71 Wang, J. W. *et al.* Identification of metastasis-associated proteins involved in gallbladder carcinoma metastasis by proteomic analysis and functional exploration of chloride intracellular channel 1. *Cancer Lett* **281**, 71-81, doi:10.1016/j.canlet.2009.02.020 (2009).
72 Petrova, D. T. *et al.* Expression of chloride intracellular channel protein 1 (CLIC1) and tumor protein D52 (TPD52) as potential biomarkers for colorectal cancer. *Clin Biochem* **41**, 1224-1236, doi:10.1016/j.clinbiochem.2008.07.012 (2008).
73 Chang, Y. H. *et al.* Cell secretome analysis using hollow fiber culture system leads to the discovery of CLIC1 protein as a novel plasma marker for nasopharyngeal carcinoma. *J Proteome Res* **8**, 5465-5474, doi:10.1021/pr900454e (2009).
74 Tang, H. Y. *et al.* A xenograft mouse model coupled with in-depth plasma proteome analysis facilitates identification of novel serum biomarkers for human ovarian cancer. *J Proteome Res* **11**, 678-691, doi:10.1021/pr200603h (2012).
75 Zhang, J. *et al.* Clic1 plays a role in mouse hepatocarcinoma via modulating Annexin A7 and Gelsolin in vitro and in vivo. *Biomed Pharmacother* **69**, 416-419, doi:10.1016/j.biopha.2014.11.019 (2015).
76 Wang, L. *et al.* Elevated expression of chloride intracellular channel 1 is correlated with poor prognosis in human gliomas. *J Exp Clin Cancer Res* **31**, 44, doi:10.1186/1756-9966-31-44 (2012).
77 Huang, J. S. *et al.* Diverse cellular transformation capability of overexpressed genes in human hepatocellular carcinoma. *Biochem Biophys Res Commun* **315**, 950-958, doi:10.1016/j.bbrc.2004.01.151 (2004).
78 Wang, P. *et al.* Regulation of colon cancer cell migration and invasion by CLIC1-mediated RVD. *Mol Cell Biochem* **365**, 313-321, doi:10.1007/s11010-012-1271-5 (2012).
79 Wang, P. *et al.* Chloride intracellular channel 1 regulates colon cancer cell migration and invasion through ROS/ERK pathway. *World J Gastroenterol* **20**, 2071-2078, doi:10.3748/wjg.v20.i8.2071 (2014).
80 Menon, S. G. & Goswami, P. C. A redox cycle within the cell cycle: ring in the old with the new. *Oncogene* **26**, 1101-1109, doi:10.1038/sj.onc.1209895 (2007).
81 Liu, Z., Zhou, T., Ziegler, A. C., Dimitrion, P. & Zuo, L. Oxidative Stress in Neurodegenerative Diseases: From Molecular Mechanisms to Clinical Applications. *Oxid Med Cell Longev* **2017**, 2525967, doi:10.1155/2017/2525967 (2017).
82 Mittal, M., Siddiqui, M. R., Tran, K., Reddy, S. P. & Malik, A. B. Reactive oxygen species in inflammation and tissue injury. *Antioxid Redox Signal* **20**, 1126-1167, doi:10.1089/ars.2012.5149 (2014).

83 Verbon, E. H., Post, J. A. & Boonstra, J. The influence of reactive oxygen species on cell cycle progression in mammalian cells. *Gene* **511**, 1-6, doi:10.1016/j.gene.2012.08.038 (2012).

84 Rojas, L. B. & Gomes, M. B. Metformin: an old but still the best treatment for type 2 diabetes. *Diabetol Metab Syndr* **5**, 6, doi:10.1186/1758-5996-5-6 (2013).

85 Nathan, D. M. *et al.* Medical management of hyperglycaemia in type 2 diabetes mellitus: a consensus algorithm for the initiation and adjustment of therapy: a consensus statement from the American Diabetes Association and the European Association for the Study of Diabetes. *Diabetologia* **52**, 17-30, doi:10.1007/s00125-008-1157-y (2009).

86 Rodbard, H. W. *et al.* Statement by an American Association of Clinical Endocrinologists/American College of Endocrinology consensus panel on type 2 diabetes mellitus: an algorithm for glycemic control. *Endocr Pract* **15**, 540-559, doi:10.4158/EP.15.6.540 (2009).

87 Effect of intensive blood-glucose control with metformin on complications in overweight patients with type 2 diabetes (UKPDS 34). UK Prospective Diabetes Study (UKPDS) Group. *Lancet* **352**, 854-865 (1998).

88 Bailey, C. J. & Day, C. Traditional plant medicines as treatments for diabetes. *Diabetes Care* **12**, 553-564, doi:10.2337/diacare.12.8.553 (1989).

89 Bailey, C. J. & Turner, R. C. Metformin. *N Engl J Med* **334**, 574-579, doi:10.1056/NEJM199602293340906 (1996).

90 Nattrass, M. & Alberti, K. G. Biguanides. *Diabetologia* **14**, 71-74, doi:10.1007/bf01263443 (1978).

91 Scheen, A. J. Clinical pharmacokinetics of metformin. *Clin Pharmacokinet* **30**, 359-371, doi:10.2165/00003088-199630050-00003 (1996).

92 Rena, G., Pearson, E. R. & Sakamoto, K. Molecular mechanism of action of metformin: old or new insights? *Diabetologia* **56**, 1898-1906, doi:10.1007/s00125-013-2991-0 (2013).

93 Davidoff, F. Effects of guanidine derivatives on mitochondrial function. 3. The mechanism of phenethylbiguanide accumulation and its relationship to in vitro respiratory inhibition. *J Biol Chem* **246**, 4017-4027 (1971).

94 Andrzejewski, S., Gravel, S. P., Pollak, M. & St-Pierre, J. Metformin directly acts on mitochondria to alter cellular bioenergetics. *Cancer Metab* **2**, 12, doi:10.1186/2049-3002-2-12 (2014).

95 Wheaton, W. W. *et al.* Metformin inhibits mitochondrial complex I of cancer cells to reduce tumorigenesis. *Elife* **3**, e02242, doi:10.7554/eLife.02242 (2014).

96 Shu, Y. *et al.* Effect of genetic variation in the organic cation transporter 1 (OCT1) on metformin action. *J Clin Invest* **117**, 1422-1431, doi:10.1172/JCI30558 (2007).

97 Viollet, B. *et al.* Cellular and molecular mechanisms of metformin: an overview. *Clin Sci (Lond)* **122**, 253-270, doi:10.1042/CS20110386 (2012).

98 Hawley, S. A., Gadalla, A. E., Olsen, G. S. & Hardie, D. G. The antidiabetic drug metformin activates the AMP-activated protein kinase cascade via an adenine nucleotide-independent mechanism. *Diabetes* **51**, 2420-2425, doi:10.2337/diabetes.51.8.2420 (2002).

99 Foretz, M. *et al.* Metformin inhibits hepatic gluconeogenesis in mice independently of the LKB1/AMPK pathway via a decrease in hepatic energy state. *J Clin Invest* **120**, 2355-2369, doi:10.1172/JCI40671 (2010).

100 Heckman-Stoddard, B. M. *et al.* Repurposing old drugs to chemoprevention: the case of metformin. *Semin Oncol* **43**, 123-133, doi:10.1053/j.seminoncol.2015.09.009 (2016).

101 Song, K. *et al.* Active glycolytic metabolism in CD133(+) hepatocellular cancer stem cells: regulation by MIR-122. *Oncotarget* **6**, 40822-40835, doi:10.18632/oncotarget.5812 (2015).

102 Garnier, D., Renoult, O., Alves-Guerra, M. C., Paris, F. & Pecqueur, C. Glioblastoma Stem-Like Cells, Metabolic Strategy to Kill a Challenging Target. *Front Oncol* **9**, 118, doi:10.3389/fonc.2019.00118 (2019).

103 Shibao, S. *et al.* Metabolic heterogeneity and plasticity of glioma stem cells in a mouse glioblastoma model. *Neuro Oncol* **20**, 343-354, doi:10.1093/neuonc/nox170 (2018).

104 Pelletier, S. J. & Cicchetti, F. Cellular and molecular mechanisms of action of transcranial direct current stimulation: evidence from in vitro and in vivo models. *Int J Neuropsychopharmacol* **18**, doi:10.1093/ijnp/pyu047 (2014).

105 Das, S., Holland, P., Frens, M. A. & Donchin, O. Impact of Transcranial Direct Current Stimulation (tDCS) on Neuronal Functions. *Front Neurosci* **10**, 550, doi:10.3389/fnins.2016.00550 (2016).

106 McCaig, C. D., Rajnicek, A. M., Song, B. & Zhao, M. Controlling cell behavior electrically: current views and future potential. *Physiol Rev* **85**, 943-978, doi:10.1152/physrev.00020.2004 (2005).

107 Sohn, M. K., Jee, S. J. & Kim, Y. W. Effect of transcranial direct current stimulation on postural stability and lower extremity strength in hemiplegic stroke patients. *Ann Rehabil Med* **37**, 759-765, doi:10.5535/arm.2013.37.6.759 (2013).

108 Boggio, P. S. *et al.* Temporal cortex direct current stimulation enhances performance on a visual recognition memory task in Alzheimer disease. *J Neurol Neurosurg Psychiatry* **80**, 444-447, doi:10.1136/jnnp.2007.141853 (2009).

109 Benninger, D. H. *et al.* Transcranial direct current stimulation for the treatment of Parkinson's disease. *J Neurol Neurosurg Psychiatry* **81**, 1105-1111, doi:10.1136/jnnp.2009.202556 (2010).

110 Andrade, C. Once- to twice-daily, 3-year domiciliary maintenance transcranial direct current stimulation for severe, disabling, clozapine-refractory continuous auditory hallucinations in schizophrenia. *J ECT* **29**, 239-242, doi:10.1097/YCT.0b013e3182843866 (2013).
111 Dell'Osso, B. *et al.* Transcranial direct current stimulation for the outpatient treatment of poor-responder depressed patients. *Eur Psychiatry* **27**, 513-517, doi:10.1016/j.eurpsy.2011.02.008 (2012).
112 Paulus, W. Transcranial direct current stimulation (tDCS). *Suppl Clin Neurophysiol* **56**, 249-254 (2003).
113 Nitsche, M. A. *et al.* Pharmacological modulation of cortical excitability shifts induced by transcranial direct current stimulation in humans. *J Physiol* **553**, 293-301, doi:10.1113/jphysiol.2003.049916 (2003).
114 Pelletier, S. J. *et al.* The morphological and molecular changes of brain cells exposed to direct current electric field stimulation. *Int J Neuropsychopharmacol* **18**, doi:10.1093/ijnp/pyu090 (2014).
115 Ferrucci, R. *et al.* Transcranial direct current stimulation improves recognition memory in Alzheimer disease. *Neurology* **71**, 493-498, doi:10.1212/01.wnl.0000317060.43722.a3 (2008).
116 Penolazzi, B. *et al.* Transcranial direct current stimulation and cognitive training in the rehabilitation of Alzheimer disease: A case study. *Neuropsychol Rehabil* **25**, 799-817, doi:10.1080/09602011.2014.977301 (2015).
117 Yang, M. & Brackenbury, W. J. Membrane potential and cancer progression. *Front Physiol* **4**, 185, doi:10.3389/fphys.2013.00185 (2013).
118 Barker, A. T., Jalinous, R. & Freeston, I. L. Non-invasive magnetic stimulation of human motor cortex. *Lancet* **1**, 1106-1107, doi:10.1016/s0140-6736(85)92413-4 (1985).
119 Merton, P. A. & Morton, H. B. Stimulation of the cerebral cortex in the intact human subject. *Nature* **285**, 227, doi:10.1038/285227a0 (1980).
120 Mills, K. R. Magnetic brain stimulation: a review after 10 years experience. *Electroencephalogr Clin Neurophysiol Suppl* **49**, 239-244 (1999).
121 Rossini, P. M. & Rossi, S. Clinical applications of motor evoked potentials. *Electroencephalogr Clin Neurophysiol* **106**, 180-194, doi:10.1016/s0013-4694(97)00097-7 (1998).
122 Gugino, L. D. *et al.* Transcranial magnetic stimulation coregistered with MRI: a comparison of a guided versus blind stimulation technique and its effect on evoked compound muscle action potentials. *Clin Neurophysiol* **112**, 1781-1792 (2001).
123 Krings, T. *et al.* Functional magnetic resonance imaging and transcranial magnetic stimulation: complementary approaches in the evaluation of cortical motor function. *Neurology* **48**, 1406-1416, doi:10.1212/wnl.48.5.1406 (1997).
124 Krings, T. *et al.* Stereotactic transcranial magnetic stimulation: correlation with direct electrical cortical stimulation. *Neurosurgery* **41**, 1319-1325; discussion 1325-1316, doi:10.1097/00006123-199712000-00016 (1997).
125 Rossini, P. M. *et al.* Non-invasive electrical and magnetic stimulation of the brain, spinal cord and roots: basic principles and procedures for routine clinical application. Report of an IFCN committee. *Electroencephalogr Clin Neurophysiol* **91**, 79-92, doi:10.1016/0013-4694(94)90029-9 (1994).
126 Ziemann, U., Lonnecker, S., Steinhoff, B. J. & Paulus, W. Effects of antiepileptic drugs on motor cortex excitability in humans: a transcranial magnetic stimulation study. *Ann Neurol* **40**, 367-378, doi:10.1002/ana.410400306 (1996).
127 Davey, N. J. *et al.* Responses of thenar muscles to transcranial magnetic stimulation of the motor cortex in patients with incomplete spinal cord injury. *J Neurol Neurosurg Psychiatry* **65**, 80-87, doi:10.1136/jnnp.65.1.80 (1998).
128 Chistyakov, A. V. *et al.* Excitatory and inhibitory corticospinal responses to transcranial magnetic stimulation in patients with minor to moderate head injury. *J Neurol Neurosurg Psychiatry* **70**, 580-587, doi:10.1136/jnnp.70.5.580 (2001).
129 Boniface, S. J., Mills, K. R. & Schubert, M. Responses of single spinal motoneurons to magnetic brain stimulation in healthy subjects and patients with multiple sclerosis. *Brain* **114 (Pt 1B)**, 643-662, doi:10.1093/brain/114.1.643 (1991).
130 Boniface, S. J., Schubert, M. & Mills, K. R. Suppression and long latency excitation of single spinal motoneurons by transcranial magnetic stimulation in health, multiple sclerosis, and stroke. *Muscle Nerve* **17**, 642-646, doi:10.1002/mus.880170612 (1994).
131 Maeda, F., Keenan, J. P., Tormos, J. M., Topka, H. & Pascual-Leone, A. Modulation of corticospinal excitability by repetitive transcranial magnetic stimulation. *Clin Neurophysiol* **111**, 800-805 (2000).
132 Pascual-Leone, A. *et al.* Study and modulation of human cortical excitability with transcranial magnetic stimulation. *J Clin Neurophysiol* **15**, 333-343 (1998).
133 Pascual-Leone, A., Valls-Sole, J., Wassermann, E. M. & Hallett, M. Responses to rapid-rate transcranial magnetic stimulation of the human motor cortex. *Brain* **117 (Pt 4)**, 847-858, doi:10.1093/brain/117.4.847 (1994).
134 Chen, R. *et al.* Depression of motor cortex excitability by low-frequency transcranial magnetic stimulation. *Neurology* **48**, 1398-1403, doi:10.1212/wnl.48.5.1398 (1997).

135 Maeda, F., Keenan, J. P., Tormos, J. M., Topka, H. & Pascual-Leone, A. Interindividual variability of the modulatory effects of repetitive transcranial magnetic stimulation on cortical excitability. *Exp Brain Res* **133**, 425-430, doi:10.1007/s002210000432 (2000).
136 Berardelli, A. *et al.* Facilitation of muscle evoked responses after repetitive cortical stimulation in man. *Exp Brain Res* **122**, 79-84, doi:10.1007/s002210050493 (1998).
137 Gangitano, M. *et al.* Modulation of input-output curves by low and high frequency repetitive transcranial magnetic stimulation of the motor cortex. *Clin Neurophysiol* **113**, 1249-1257 (2002).
138 Siebner, H. R. *et al.* Imaging brain activation induced by long trains of repetitive transcranial magnetic stimulation. *Neuroreport* **9**, 943-948, doi:10.1097/00001756-199803300-00033 (1998).
139 Fox, P. *et al.* Imaging human intra-cerebral connectivity by PET during TMS. *Neuroreport* **8**, 2787-2791, doi:10.1097/00001756-199708180-00027 (1997).
140 Paus, T. *et al.* Transcranial magnetic stimulation during positron emission tomography: a new method for studying connectivity of the human cerebral cortex. *J Neurosci* **17**, 3178-3184 (1997).
141 Kimbrell, T. A. *et al.* Frequency dependence of antidepressant response to left prefrontal repetitive transcranial magnetic stimulation (rTMS) as a function of baseline cerebral glucose metabolism. *Biol Psychiatry* **46**, 1603-1613, doi:10.1016/s0006-3223(99)00195-x (1999).
142 Ilmoniemi, R. J. *et al.* Neuronal responses to magnetic stimulation reveal cortical reactivity and connectivity. *Neuroreport* **8**, 3537-3540, doi:10.1097/00001756-199711100-00024 (1997).
143 Strafella, A. P., Paus, T., Barrett, J. & Dagher, A. Repetitive transcranial magnetic stimulation of the human prefrontal cortex induces dopamine release in the caudate nucleus. *J Neurosci* **21**, RC157 (2001).
144 Gustafsson, B. & Wigstrom, H. Physiological mechanisms underlying long-term potentiation. *Trends Neurosci* **11**, 156-162, doi:10.1016/0166-2236(88)90142-7 (1988).
145 Christie, B. R., Kerr, D. S. & Abraham, W. C. Flip side of synaptic plasticity: long-term depression mechanisms in the hippocampus. *Hippocampus* **4**, 127-135, doi:10.1002/hipo.450040203 (1994).
146 Ben-Shachar, D., Belmaker, R. H., Grisaru, N. & Klein, E. Transcranial magnetic stimulation induces alterations in brain monoamines. *J Neural Transm (Vienna)* **104**, 191-197, doi:10.1007/BF01273180 (1997).
147 Keck, M. E. *et al.* Acute transcranial magnetic stimulation of frontal brain regions selectively modulates the release of vasopressin, biogenic amines and amino acids in the rat brain. *Eur J Neurosci* **12**, 3713-3720, doi:10.1046/j.1460-9568.2000.00243.x (2000).
148 Hausmann, A., Weis, C., Marksteiner, J., Hinterhuber, H. & Humpel, C. Chronic repetitive transcranial magnetic stimulation enhances c-fos in the parietal cortex and hippocampus. *Brain Res Mol Brain Res* **76**, 355-362, doi:10.1016/s0169-328x(00)00024-3 (2000).
149 Ji, R. R. *et al.* Repetitive transcranial magnetic stimulation activates specific regions in rat brain. *Proc Natl Acad Sci U S A* **95**, 15635-15640, doi:10.1073/pnas.95.26.15635 (1998).
150 Kosslyn, S. M. *et al.* The role of area 17 in visual imagery: convergent evidence from PET and rTMS. *Science* **284**, 167-170, doi:10.1126/science.284.5411.167 (1999).
151 Mottaghy, F. M., Gangitano, M., Sparing, R., Krause, B. J. & Pascual-Leone, A. Segregation of areas related to visual working memory in the prefrontal cortex revealed by rTMS. *Cereb Cortex* **12**, 369-375, doi:10.1093/cercor/12.4.369 (2002).
152 Hilgetag, C. C., Theoret, H. & Pascual-Leone, A. Enhanced visual spatial attention ipsilateral to rTMS-induced 'virtual lesions' of human parietal cortex. *Nat Neurosci* **4**, 953-957, doi:10.1038/nn0901-953 (2001).
153 Theoret, H., Haque, J. & Pascual-Leone, A. Increased variability of paced finger tapping accuracy following repetitive magnetic stimulation of the cerebellum in humans. *Neurosci Lett* **306**, 29-32, doi:10.1016/s0304-3940(01)01860-2 (2001).
154 George, M. S. *et al.* A controlled trial of daily left prefrontal cortex TMS for treating depression. *Biol Psychiatry* **48**, 962-970, doi:10.1016/s0006-3223(00)01048-9 (2000).
155 Figiel, G. S. *et al.* The use of rapid-rate transcranial magnetic stimulation (rTMS) in refractory depressed patients. *J Neuropsychiatry Clin Neurosci* **10**, 20-25, doi:10.1176/jnp.10.1.20 (1998).
156 Fitzgerald, P. B., Brown, T. L. & Daskalakis, Z. J. The application of transcranial magnetic stimulation in psychiatry and neurosciences research. *Acta Psychiatr Scand* **105**, 324-340, doi:10.1034/j.1600-0447.2002.1r179.x (2002).
157 Pascual-Leone, A. *et al.* Akinesia in Parkinson's disease. II. Effects of subthreshold repetitive transcranial motor cortex stimulation. *Neurology* **44**, 892-898, doi:10.1212/wnl.44.5.892 (1994).
158 Ben-Shachar, D., Gazawi, H., Riboyad-Levin, J. & Klein, E. Chronic repetitive transcranial magnetic stimulation alters beta-adrenergic and 5-HT2 receptor characteristics in rat brain. *Brain Res* **816**, 78-83, doi:10.1016/s0006-8993(98)01119-6 (1999).
159 Mally, J. & Stone, T. W. Improvement in Parkinsonian symptoms after repetitive transcranial magnetic stimulation. *J Neurol Sci* **162**, 179-184, doi:10.1016/s0022-510x(98)00318-9 (1999).
160 Ghabra, M. B., Hallett, M. & Wassermann, E. M. Simultaneous repetitive transcranial magnetic stimulation does not speed fine movement in PD. *Neurology* **52**, 768-770, doi:10.1212/wnl.52.4.768 (1999).

161 Tergau, F., Wassermann, E. M., Paulus, W. & Ziemann, U. Lack of clinical improvement in patients with Parkinson's disease after low and high frequency repetitive transcranial magnetic stimulation. *Electroencephalogr Clin Neurophysiol Suppl* **51**, 281-288 (1999).
162 Hallett, M. Physiology of dystonia. *Adv Neurol* **78**, 11-18 (1998).
163 Siebner, H. R. *et al.* Low-frequency repetitive transcranial magnetic stimulation of the motor cortex in writer's cramp. *Neurology* **52**, 529-537, doi:10.1212/wnl.52.3.529 (1999).
164 Ziemann, U., Paulus, W. & Rothenberger, A. Decreased motor inhibition in Tourette's disorder: evidence from transcranial magnetic stimulation. *Am J Psychiatry* **154**, 1277-1284, doi:10.1176/ajp.154.9.1277 (1997).
165 Menkes, D. L. & Gruenthal, M. Slow-frequency repetitive transcranial magnetic stimulation in a patient with focal cortical dysplasia. *Epilepsia* **41**, 240-242, doi:10.1111/j.1528-1157.2000.tb00146.x (2000).
166 Tergau, F., Naumann, U., Paulus, W. & Steinhoff, B. J. Low-frequency repetitive transcranial magnetic stimulation improves intractable epilepsy. *Lancet* **353**, 2209, doi:10.1016/S0140-6736(99)01301-X (1999).
167 Cao, Y., D'Olhaberriague, L., Vikingstad, E. M., Levine, S. R. & Welch, K. M. Pilot study of functional MRI to assess cerebral activation of motor function after poststroke hemiparesis. *Stroke* **29**, 112-122, doi:10.1161/01.str.29.1.112 (1998).
168 Marshall, R. S. *et al.* Evolution of cortical activation during recovery from corticospinal tract infarction. *Stroke* **31**, 656-661, doi:10.1161/01.str.31.3.656 (2000).
169 Netz, J., Lammers, T. & Homberg, V. Reorganization of motor output in the non-affected hemisphere after stroke. *Brain* **120 (Pt 9)**, 1579-1586, doi:10.1093/brain/120.9.1579 (1997).
170 Oliveri, M. *et al.* rTMS of the unaffected hemisphere transiently reduces contralesional visuospatial hemineglect. *Neurology* **57**, 1338-1340, doi:10.1212/wnl.57.7.1338 (2001).
171 Naeser, M. A. *et al.* Transcranial magnetic stimulation and aphasia rehabilitation. *Arch Phys Med Rehabil* **93**, S26-34, doi:10.1016/j.apmr.2011.04.026 (2012).
172 Carter, M. E. & de Lecea, L. Optogenetic investigation of neural circuits in vivo. *Trends Mol Med* **17**, 197-206, doi:10.1016/j.molmed.2010.12.005 (2011).
173 Crick, F. The impact of molecular biology on neuroscience. *Philos Trans R Soc Lond B Biol Sci* **354**, 2021-2025, doi:10.1098/rstb.1999.0541 (1999).
174 Boyden, E. S., Zhang, F., Bamberg, E., Nagel, G. & Deisseroth, K. Millisecond-timescale, genetically targeted optical control of neural activity. *Nat Neurosci* **8**, 1263-1268, doi:10.1038/nn1525 (2005).
175 Jerome, J. & Heck, D. H. The age of enlightenment: evolving opportunities in brain research through optical manipulation of neuronal activity. *Front Syst Neurosci* **5**, 95, doi:10.3389/fnsys.2011.00095 (2011).
176 Airan, R. D., Thompson, K. R., Fenno, L. E., Bernstein, H. & Deisseroth, K. Temporally precise in vivo control of intracellular signalling. *Nature* **458**, 1025-1029, doi:10.1038/nature07926 (2009).
177 Wojtovich, A. P. & Foster, T. H. Optogenetic control of ROS production. *Redox Biol* **2**, 368-376, doi:10.1016/j.redox.2014.01.019 (2014).
178 Ingles-Prieto, A., Reichhart, E., Schelch, K., Janovjak, H. & Grusch, M. The optogenetic promise for oncology: Episode I. *Mol Cell Oncol* **1**, e964045, doi:10.4161/23723548.2014.964045 (2014).
179 Yang, F. *et al.* Light-controlled inhibition of malignant glioma by opsin gene transfer. *Cell Death Dis* **4**, e893, doi:10.1038/cddis.2013.425 (2013).
180 Guru, A., Post, R. J., Ho, Y. Y. & Warden, M. R. Making Sense of Optogenetics. *Int J Neuropsychopharmacol* **18**, pyv079, doi:10.1093/ijnp/pyv079 (2015).
181 Nagel, G. *et al.* Channelrhodopsin-2, a directly light-gated cation-selective membrane channel. *Proc Natl Acad Sci U S A* **100**, 13940-13945, doi:10.1073/pnas.1936192100 (2003).
182 Nagel, G. *et al.* Light activation of channelrhodopsin-2 in excitable cells of Caenorhabditis elegans triggers rapid behavioral responses. *Curr Biol* **15**, 2279-2284, doi:10.1016/j.cub.2005.11.032 (2005).
183 Aravanis, A. M. *et al.* An optical neural interface: in vivo control of rodent motor cortex with integrated fiberoptic and optogenetic technology. *J Neural Eng* **4**, S143-156, doi:10.1088/1741-2560/4/3/S02 (2007).
184 Rein, M. L. & Deussing, J. M. The optogenetic (r)evolution. *Mol Genet Genomics* **287**, 95-109, doi:10.1007/s00438-011-0663-7 (2012).
185 Bamann, C., Gueta, R., Kleinlogel, S., Nagel, G. & Bamberg, E. Structural guidance of the photocycle of channelrhodopsin-2 by an interhelical hydrogen bond. *Biochemistry* **49**, 267-278, doi:10.1021/bi901634p (2010).
186 Yizhar, O. *et al.* Neocortical excitation/inhibition balance in information processing and social dysfunction. *Nature* **477**, 171-178, doi:10.1038/nature10360 (2011).
187 Zhang, F. *et al.* Red-shifted optogenetic excitation: a tool for fast neural control derived from Volvox carteri. *Nat Neurosci* **11**, 631-633, doi:10.1038/nn.2120 (2008).
188 Lin, J. Y., Knutsen, P. M., Muller, A., Kleinfeld, D. & Tsien, R. Y. ReaChR: a red-shifted variant of channelrhodopsin enables deep transcranial optogenetic excitation. *Nat Neurosci* **16**, 1499-1508, doi:10.1038/nn.3502 (2013).

189 Klapoetke, N. C. *et al.* Independent optical excitation of distinct neural populations. *Nat Methods* **11**, 338-346, doi:10.1038/nmeth.2836 (2014).
190 Han, X. & Boyden, E. S. Multiple-color optical activation, silencing, and desynchronization of neural activity, with single-spike temporal resolution. *PLoS One* **2**, e299, doi:10.1371/journal.pone.0000299 (2007).
191 Gradinaru, V., Thompson, K. R. & Deisseroth, K. eNpHR: a Natronomonas halorhodopsin enhanced for optogenetic applications. *Brain Cell Biol* **36**, 129-139, doi:10.1007/s11068-008-9027-6 (2008).
192 Wietek, J. *et al.* Conversion of channelrhodopsin into a light-gated chloride channel. *Science* **344**, 409-412, doi:10.1126/science.1249375 (2014).
193 Chuong, A. S. *et al.* Noninvasive optical inhibition with a red-shifted microbial rhodopsin. *Nat Neurosci* **17**, 1123-1129, doi:10.1038/nn.3752 (2014).
194 Berglund, K., Birkner, E., Augustine, G. J. & Hochgeschwender, U. Light-emitting channelrhodopsins for combined optogenetic and chemical-genetic control of neurons. *PLoS One* **8**, e59759, doi:10.1371/journal.pone.0059759 (2013).
195 Tung, J. K., Gutekunst, C. A. & Gross, R. E. Inhibitory luminopsins: genetically-encoded bioluminescent opsins for versatile, scalable, and hardware-independent optogenetic inhibition. *Sci Rep* **5**, 14366, doi:10.1038/srep14366 (2015).
196 Warden, M. R., Cardin, J. A. & Deisseroth, K. Optical neural interfaces. *Annu Rev Biomed Eng* **16**, 103-129, doi:10.1146/annurev-bioeng-071813-104733 (2014).
197 Wykes, R. C., Kullmann, D. M., Pavlov, I. & Magloire, V. Optogenetic approaches to treat epilepsy. *J Neurosci Methods* **260**, 215-220, doi:10.1016/j.jneumeth.2015.06.004 (2016).
198 Tonnesen, J., Sorensen, A. T., Deisseroth, K., Lundberg, C. & Kokaia, M. Optogenetic control of epileptiform activity. *Proc Natl Acad Sci U S A* **106**, 12162-12167, doi:10.1073/pnas.0901915106 (2009).
199 Krook-Magnuson, E., Armstrong, C., Oijala, M. & Soltesz, I. On-demand optogenetic control of spontaneous seizures in temporal lobe epilepsy. *Nat Commun* **4**, 1376, doi:10.1038/ncomms2376 (2013).
200 Tye, K. M. *et al.* Dopamine neurons modulate neural encoding and expression of depression-related behaviour. *Nature* **493**, 537-541, doi:10.1038/nature11740 (2013).
201 Chen, Y., Xiong, M. & Zhang, S. C. Illuminating Parkinson's therapy with optogenetics. *Nat Biotechnol* **33**, 149-150, doi:10.1038/nbt.3140 (2015).
202 Tye, K. M. & Deisseroth, K. Optogenetic investigation of neural circuits underlying brain disease in animal models. *Nat Rev Neurosci* **13**, 251-266, doi:10.1038/nrn3171 (2012).
203 Chaudhury, D. *et al.* Rapid regulation of depression-related behaviours by control of midbrain dopamine neurons. *Nature* **493**, 532-536, doi:10.1038/nature11713 (2013).
204 Yamamoto, K. *et al.* Chronic optogenetic activation augments abeta pathology in a mouse model of Alzheimer disease. *Cell Rep* **11**, 859-865, doi:10.1016/j.celrep.2015.04.017 (2015).
205 Henriksen, B. S., Marc, R. E. & Bernstein, P. S. Optogenetics for retinal disorders. *J Ophthalmic Vis Res* **9**, 374-382, doi:10.4103/2008-322X.143379 (2014).
206 Lagali, P. S. *et al.* Light-activated channels targeted to ON bipolar cells restore visual function in retinal degeneration. *Nat Neurosci* **11**, 667-675, doi:10.1038/nn.2117 (2008).
207 Caporale, N. *et al.* LiGluR restores visual responses in rodent models of inherited blindness. *Mol Ther* **19**, 1212-1219, doi:10.1038/mt.2011.103 (2011).
208 Ahmad, A., Ashraf, S. & Komai, S. Optogenetics applications for treating spinal cord injury. *Asian Spine J* **9**, 299-305, doi:10.4184/asj.2015.9.2.299 (2015).
209 Barbieri, F. *et al.* Inhibition of Chloride Intracellular Channel 1 (CLIC1) as Biguanide Class-Effect to Impair Human Glioblastoma Stem Cell Viability. *Front Pharmacol* **9**, 899, doi:10.3389/fphar.2018.00899 (2018).